FZR - 94
June 1995

Annual Report 1994

Institute of Radiochemistry

Editor: Prof. Dr. H. Nitsche

Editorial staff: Dr. H.-J. Engelmann
Dr. G. Bernhard

Preface

The activities of the institute are focused on basic research related to the migration of radionuclides in the environment. Ultimately, the research results should help in risk assessment of radioactive contaminated sites and in the decision making for remediation and in the development of environmental decontamination and remediation strategies. Radioactive contaminations resulted from uranium mining and processing in the German states of Saxony and Thuringia, in the neighboring Czech Republic and from weapons production, testing and accidents of several former eastern and western block countries.

The institute's four research groups are administratively classified as Radioecology, Colloids and Aerosols, Organic Tracer Chemistry, and Application of Synchrotron Radiation. It is the philosophy of the institute to regard this division as purely administrative, and therefore, scientific problems are tackled by an integrated approach by which members of different groups work closely together. Initial results of this integrated problem-solving are reflected in the topical structure of this annual report in the following sections: Speciation and Migration of Radionuclides, Behavior of Colloids, Interaction of Radionuclides with Organic Matter, and Application of X-Ray Absorption Spectroscopy. Only the section on the Chemistry of the Heaviest Elements should be viewed as a stand-alone topic. It is planned, however, to investigate the intricacies of the aerosol jet with the methods that are currently being established by the Colloid and Aerosol Group.

During the past year, great efforts were made in establishing enhanced equipment capabilities. We completed the installation of a novel laser system for time-resolved fluorescence and for photoacoustic spectroscopy which uses a tunable optical parametric oscillator laser instead of the commonly-used dye laser. After thorough evaluation, a photon auto-correlation spectrometer was purchased for colloid research, and testing of the instrument is near completion.

In April 1994, a proposal was submitted to the European Synchrotron Radiation Facility (ESRF) in Grenoble, France, to establish a Rossendorf beam line (ROBL) for hard x-ray absorption spectroscopy (XAS). This proposal was developed together with the Institute for Ion Beam and Materials Research. The Radiochemistry Institute plans to establish an end station for XAS measurements on radioactive materials by placing a glove box in the synchrotron beam. Much time was spent during the year to satisfy regulatory constraints due to the handling of radioactivity at the ESRF.

Considerable efforts were necessary for planning the layout of our new Radiochemistry Building that is scheduled for construction and completion in 1995. Seventeen laboratory units will enable us then to expand our research to the actinide elements beyond uranium.

We particularly appreciate the ongoing collaborations with the following institutions: Glenn T. Seaborg Institute at the Lawrence Livermore National Laboratory, Livermore, California, U.S.A.; The Actinide Group of the Lawrence Berkeley Laboratory, Berkeley, California, U.S.A.; Stanford Synchrotron Radiation Laboratory, Stanford, California,

U.S.A.; Deutsches Elektronen-Synchrotron Hamburg; Institut für Radiochemie, Technische Universität München; Institut für Nukleare Entsorgungstechnik, Forschungszentrum Karlsruhe; Institut für Anorganische und Analytische Chemie, Friedrich-Schiller-Universität Jena; TU Bergakademie Freiberg; Fraunhofer-Institut für Grenzflächen- und Bioverfahrenstechnik Stuttgart; Joint Institute of Nuclear Research, Dubna, Russia; Paul Scherrer Institute, Villigen, Switzerland; Institut für Kernchemie, Universität Mainz; Institute for Experimental Botany and Institute for Microbiology, Academy of Sciences, Prague, Czech Republic; Medical Faculty, Charles University, Prague, Czech Republic.

During 1994, we were able to initiate collaborations with the following institutions: Kurnakov Institute for General and Inorganic Chemistry, Russian Academy of Sciences, Moscow, Russia; Kurchatov Institute, Russian Research Center, Moscow, Russia; Severtsov Institute of Evolutionary Morphology and Ecology of Animals, Russian Academy of Sciences, Moscow, Russia.

We would like to thank the many visitors, German and international, for their interest in our research and for their participation in the institute's seminars.

Rossendorf, June 1995 Prof. Dr. Heino Nitsche

CONTENTS

I. SCIENTIFIC CONTRIBUTIONS

Speciation and Migration of Radionuclides

SORPTION OF URANIUM ON ROCK MATERIALS

G. Geipel

Forschungszentrum Rossendorf e.V., Institute of Radiochemistry

The saxonian mine tailing piles contain many radionuclides. For instance the mine tailing pile 250 in Schlema had a uranium inventory of about 100 tons. Due to the weathering processes, these radionuclides were mobilized and transported through the pile. To modell the radionuclides' transport process in a tailing pile, it is necessary to know distribution ratios and loading capacities of the rock materials. Several minerals that are formed by the weathering process can act as natural ion exchangers. These materials can absord radionuclides from the seepage waters.
Uranium has the highest concentration of all radionuclides present in the seepage waters. It is necessary to know if and how it is absorbed on the rock material.
To elucidate this question, sorption experiments were carried out in with and without external pH control.

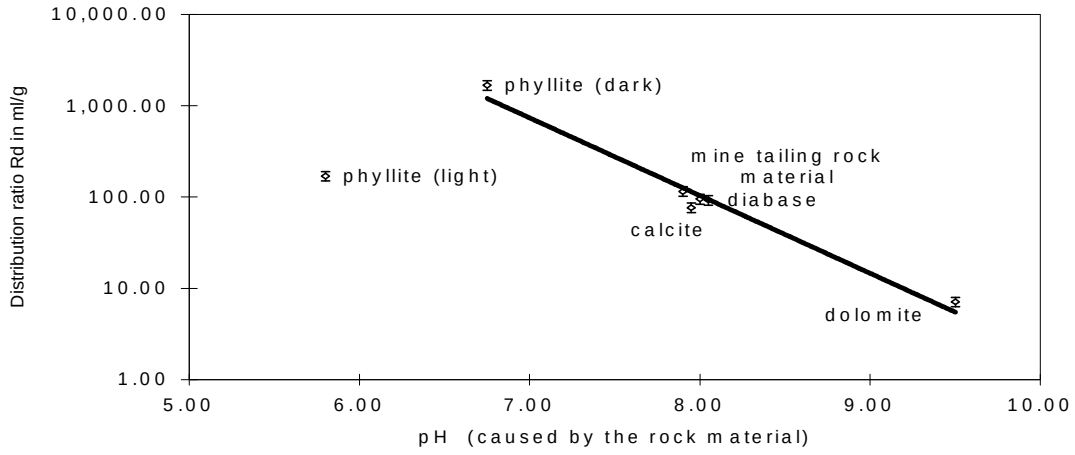

Fig. 1.: Dependence of the distribution ratio of Uranylions on the pH on several rock materials (grain size < 0.063 mm)

In the first series of experiments, the pH of the solution was controlled by the properties of the rock material and reached a characteristic value for each rock material. The initial uranyl perchlorate solution was contacted for 48 h with the rock material and then the solid and solution were separated. The rock material was washed with deionized water. The uranium content of the solution was determined by ICP-MS. The uranium sorbed on the rock material was calculated as the difference between the uranium content before and after the sorption process. Fig. 1 shows the distribution ratios for uranium as a function the pH for several different rock materials.
In the second series of experiments, the pH of the solution was controlled by an automatic titrator (Schott TPC 2000). The rock material was contacted with the solution for 20 hours and after phase separation, the uranium content was analyzed for as above. Fig. 2 shows the distribution ratios as a function of the solution pH for two sieved fractions of rock material from a mill tailing pile.

Because the rock material contains initially uranium that can leach when the material is suspended in 0.1 M Sodium perchlorate solution, it was necesssry to determine this amount which was then taken into account when the uranium was added for the sorption experiments /1/.

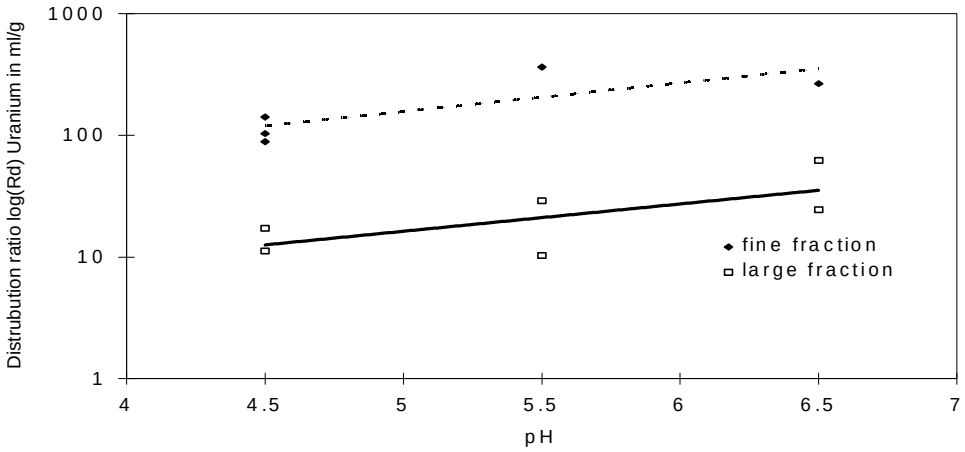

Fig. 2.: Dependence of the distribution ratio of Uranylions on the pH on rock material from a mill tailing pile

The sorption behavior is very different than for the systems shown in Fig. 1. Due to a change in the soprtion reaction, we found that the sorption behavior cahnges with changing pH /2/. The change of the sorption mechanism depends on the change of the uranium speciation in the solution. For positively charged uranyl species, which are dominant at lower pH, hydrogen ions take part in the sorption mechanism. The chemical reaction can be described as an ion exchange reaction between the uranyl species and hydrogen ions. At higher pH, negatively charged uranyl species are dominant and hydroxyl ions will take part in the sorption reaction [2].

Acknowledgements:

This work was supported by the Bundesminister für Forschung und Technologie under contract no. 02 S 7433.

References:

[1] M. Thieme, Sorption of Thorium on Granodiorite and Rockpile Material, this report, p. 3

[2] K.H. Lieser et. al., Sorption of the Uranyl Ions on Hydrous Silicon Dioxide, Radiochim. Acta 57, (1992), 45

SORPTION OF THORIUM ON GRANODIORITE AND ROCK PILE MATERIAL

M. Thieme
Forschungszentrum Rossendorf e.V., Institute of Radiochemistry

Although uranium represents the element with the highest concentration among the radioactive contaminants that are being emitted from uranium-mining residues, the behaviour of other members of the radioactive chains is also of radiological interest. The present contribution focusses on thorium, which has the relatively stable isotope ^{232}Th, and several less stable isotopes ^{234}Th, ^{230}Th, ^{231}Th and ^{227}Th that are being produced with the uranium decay series.

Batch-type sorption of thorium was studied using two fractions of a granodiorite (Demitz-Thumitz, Lausitz) and of rock pile material (rock pile no. 250, Schlema, Erzgebirge), respectively. The experiments, that were carried out in duplicate involved one loading and two elution steps under anoxic conditions and ambient temperature. The starting parameters of loading were 100-0.1 mg dm^{-3} Th(IV) and 0.01 mol dm^{-3} H^+. Elution was accomplished using 0.1 and 1 mol dm^{-3} HNO_3. The pH was followed on line, because it is a crucial parameter for sorption /1/.

The solution concentrations of Th in the respective starting and final states were determined by ICP-MS (designated by 0, end, lo, el) following acid addition and filtering. The calculation of the distribution ratios for loading and elution, respectively, involved blank values (bl) which take extraction effects into account. The latter were obtained with no thorium addition in the loading treatment.

$$R_{d,lo} = \left(\frac{c_{lo,0} - c_{lo,bl}}{c_{lo,end}} - 1\right)\frac{V}{m} \qquad R_{d,el} = \left(\frac{c_{lo,0} - c_{lo,end} - c_{lo,bl} - c_{el,bl}}{c_{el,end}} - 1\right)\frac{V}{m}$$

The obtained loading results confirm the generally high sorption tendency of Th(IV) /2/. Within the usual duration of 24 h the interaction with rock pile material gave distribution ratios that increased monotonically from $R_{d,lo}$. 10^4 to 10^6 cm^3 g^{-1} with growing starting concentration. Drastical shifts were observed in pH_{lo} (2 6 6.5-8.5). In the case of elution, $R_{d,el}$ was in the range 10 to 1 cm^3 g^{-1}. The recoveries were generally less than 90%.

As Fig. 1 shows for the system with granodiorite, the sorption was high even at low pH_{lo}, which changed only by a few tenths due to the different mineralogical composition of this rock. The slight dependence of pH_{lo} on $c_{lo,0}$ can be explained by competing effects between H^+ and Th^{4+} ions in the interaction with the solid.

It should be noted that the hydrolysis of Th^{4+} starts in the same pH region of about 2.5 /3/. The diagram reflects the sufficient reproducibility of the duplicate experiments. At the starting concentration $c_{lo,0}$ = 100 mg dm^{-3} a sharp decrease in $R_{d,lo}$ occurred. This finding points to oversaturation in the binding capacity. Assuming surface complexation as the mechanism of binding, the experimental conditions may be utilised to gain information of the mean binding site density for thorium ions. The consideration is based on the equation:

$$2 = \frac{c_{so}(M)}{c_{site}} = \frac{y\ (c_{lo,0} - c_{lo,eq})\ V\ N_L\ /\ m}{d_{site}\ a_s}$$

where 2 - coverage of the total surface, c_{so}(Th) - equivalent concentration of sorbed Th(IV), c_{site} - total concentration of the binding sites, y - stoichiometric number in the complex $(S\text{-}O)_yM^{(z-y)+}$ (y = 4 for pH_{lo} = 2.3), V - volume of the solution, N_L - Loschmidt number, m - mass of the rock, a_S - specific area according to BET (fraction 0.125/0.5 mm: 0.6 $m^2\ g^{-1}$ for granodiorite, 9.1 $m^2\ g^{-1}$ for rock pile material).

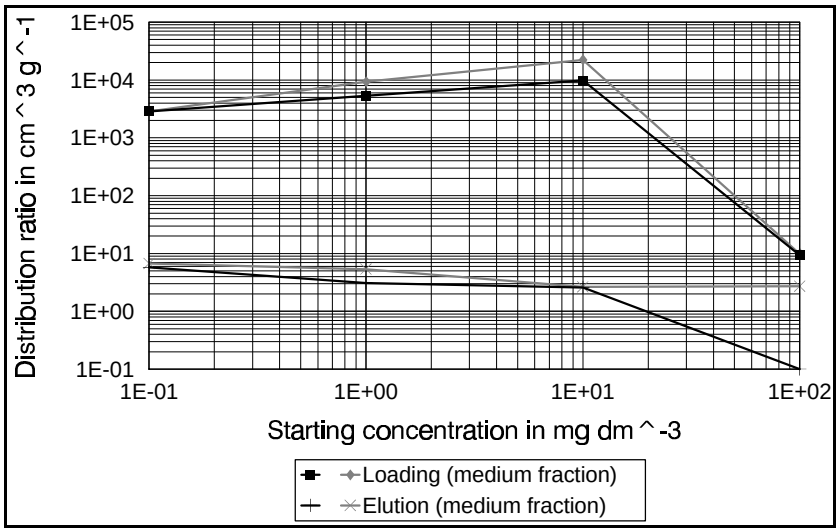

Fig.1: Plot of distribution ratios determined in the system granodiorite (0.2/0.63 mm) / Th(IV) in the loading and elution steps, resp., *vs.* the starting concentration of Th(IV)

From the actual conditions follows $d_{site,\ exp} \approx 8.6\ nm^{-2}$. This approximate value agrees fairly well with the figure of 6 nm^{-2} given without further specifications /1/. Contrarily, for the analog case of rock pile material (medium fraction), a coverage of only 13% is assessed, assuming a tetradentate complexation of the Th(IV) ions.
Discussing the behaviour of Th(IV) in these systems, a number of features may be outlined:

- The high valency of the metal ions (Lewis acid) promotes the binding strength. For comparison, the sorption of uranyl ions to rockpile material was characterised by distribution ratios more than three orders of magnitude less /4/.

- The diminished acidity in the rockpile system causes to a decrease of the concentration of the free metal ions, corresponding to the predictions of the concept of surface complexation /1/.

- Macroscopic data of BET measurements can be correlated with binding phenomena on an atomic scale. However, it should be noted that the sorption on rock will not uniformly proceed. Microradiographic studies following the loading of granite with $^{233}U(VI)$ in a slightly basic solution revealed that the sorption was quite heterogenous /5/.

The results concerning the sorption behaviour of thorium predict a very low mobility of this element in the geosphere. However, the situation in the surroundings of the mining rock piles may be modified by the influence of the radioactive decay involving radioelements with higher mobilities.

Acknowledgements

The sorption experiments were performed by H. Neubert. Support was given by W. Wiesener and U. Schaefer (ICP-MS) and G. Schuster (BET).
The work was financially supported by BMFT under contract no. 02 S 7533.

References

/1/ W. Stumm, Chemistry of the Solid-Water Interface,
New York: Wiley, 1992, pp. 13.

/2/ J. J. W. Higgo, Radionuclide Interactions with Marine Sediments,
Report NSS/R142, Sept.1987.

/3/ T. Nakashima, E. Zimmer, Hydrolysis of $Th(NO_3)_4$ and Its Extractability by TBP,
Radiochimica Acta 37 (1984) 165.

/4/ M. Thieme in: Institut of Radiochemistry, Annual Report 1993, FZR-43, June 1994, p.14.

/5/ J. R. Smyth, J. Thompson, K. Wolfsberg, Microradioautographic Studies of the Sorption of U and Am on Natural Rock Samples,
Radioact. Waste Managem. 1 (1980) 13.

DETERMINATION OF CARBON IN ROCK MATERIAL OF THE MINE TAILING PILE NO. 250 SCHLEMA (DEPTH PROFILE)

G. Schuster, G. Geipel

Forschungszentrum Rossendorf e.V., Institute of Radiochemistry

We determined that dolomite and calcite are major mineral components with inorganic carbon in mine tailing piles in the mining region of Schlema. With this study we want to determine (a) the total carbon content of the rock material and (b) the depth distribution of U-238 and other radionuclides from a core from the mine tailing pile no. 38 in Schlema. We used thermogravimetry and nuclear counting techniques.

Experimental

The samples were slowly oxidized in the LECO carbon hydrogen analyzer RC 412 in an oxygen stream. The thermic heating program is shown in table 1. The different Table 1: Thermic program for determination of organic and inorganic carbon.

starting temperature [°C]	end point temperature [°C]	heating speed [°C/min]	waiting time [sec]
60	975	10	600

carbon components react at different temperatures generating CO_2. This temperature and therefore time dependent release makes it possible to quantitatively determine the individual fractions. In addition to the CO_2, water will be released due to sample oxidation. Both gases are quantitatively determined in the analyzer by measuring the IR spectra.

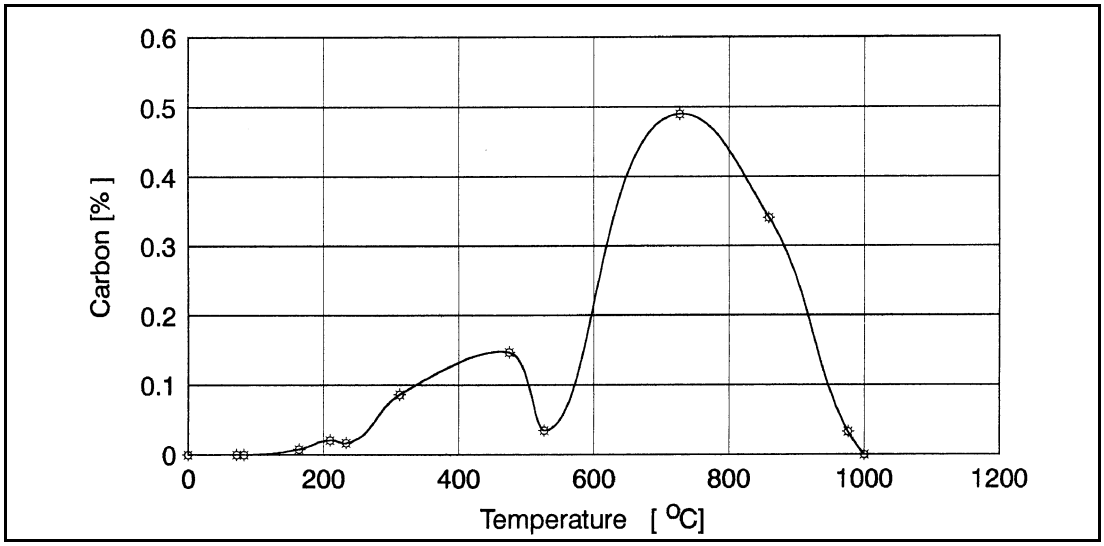

Fig. 1: CO_2-emission at the thermal handling of mill tailing pile material (sample 8.3-8.8 m)

Table 2: Determination of carbon on rock material of the mine tailing pile no. 250 in Schlema (depth profile)

sample	content of carbon [%]		
sampling depth [m]	C_{total} (TC)	$C_{inorg.}$ (TIC)	$C_{org.}$ (TOC)
<1.5	1.19	1.04	0.15
1.5-2.5	0.85	0.61	0.24
8.3-8.8	1.04	0.64	0.42
11-12	0.47	0.36	0.11
14.8-15.8	0.53	0.35	0.18
18-19	0.47	0,36	0,10
23-24	0.1	0,08	0,03

Table 3: Determination of carbon in samples with grain sizes <200µm.

sample	Content of Carbon [%]		
sampling depth [m]	C_{total}	$C_{inorg.}$	$C_{org.}$
8.3-8.8 <200µm	1.43	1.1	0.37
8.3-8.8 <200µm HCl beh.	0.45	0.06	0.37

Fig. 1 shows a CO_2 - release profile as a function of increasing temperature for a drill core coming from a depth of 8.3 to 8.8 meters.

The temperature that separates total inorganic carbon (TIC) and total organic carbon (TOC) is found between 550 and 600°C.
The radionuclide concentrations were determined with a HPGe-detector (EG&G) using Spectrum Master and software program Gammavison. The samples of about 600 g were measured in Marinelli beakers. The measuring time was 7200 s.

Results

The depth profile for TIC, TOC and TC (total carbon) are shown in Fig.2. The TOC concentration at the surface is very low. With incresing depth, TOC shows a maximum at about 5 m. The TIC decreases with the depth.

The samples are polydispersic powders with grain sizes between <100 µm and 3 mm. Considering that the larger particles do not react completely under the measuring conditions, we crushed two samples to a grain size of < 200 µm. The results of these samples are given in table 3. Additionally, the completeness of the thermic separation between TIC and TOC was checked. Crushed samples were treated with 3 ml diluted HCl at 50°C and then analyzed. The results are also given in table 3.
The results show a higher carbon content in the crushed samples. The samples which were treated with hydrochloric acid show nearly the same results than the thermic separation. This means that the inorganic carbon is quantitatively removed by the acidic treatment.

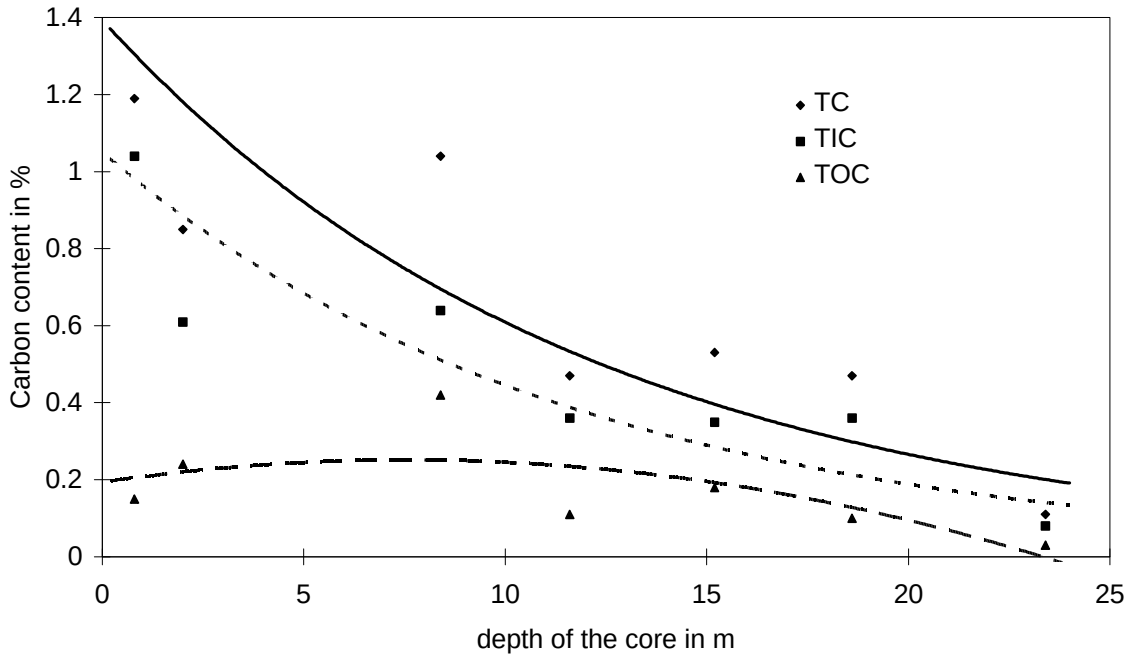

Fig. 2: Depth profile of the core for the carbon content

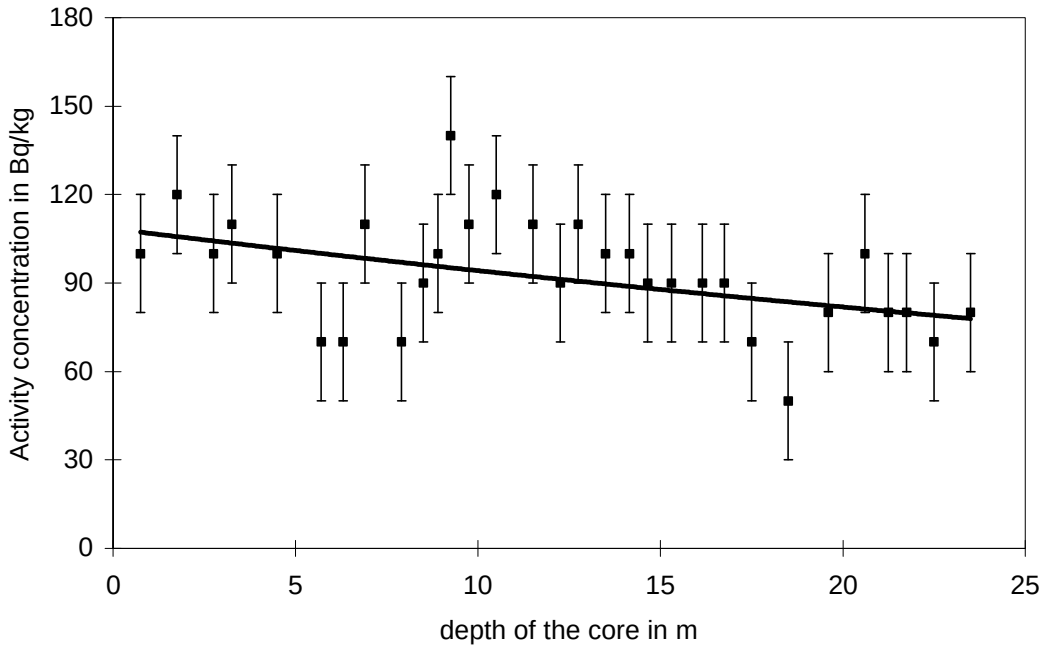

Fig. 3: Activity concentration of U-238 (Th-234) in the core from mine tailing pile no.38

For the same core we have determined the radionuclide concentration as a function of depth. Fig. 3 gives for an example of a depth profile for U-238, which is calculated from the Th-234 gamma lines. This is possible assuming that these two radioactive isotopes are in equilibrium. The other radionuclides (Ra-226, Pb- and Bi-Isotopes) show nearly the same depth profile.

We found a change in distrubution between inorganic and organic carbon with increasing depth. The concentrations of U-238 and inorganic carbon decreased with increasing depth. There is a correlation between the TIC and the uranium concentration but a influence of the TOC (humic acids) cannot be excluded. Possibly the humic acid transports some of uranium from higher to deeper layers. Further investigations are in progress.

DETERMINATION OF SULPHUR ISOTOPES FOR ELUCIDATING THE ORIGIN OF SULPHATE IN SEEPAGE FLUIDS OF URANIUM-MINING ROCK PILES

M. Thieme, M. Tichomirova[1]
Forschungszentrum Rossendorf e.V., Institute of Radiochemistry
[1] Technische Universität Bergakademie Freiberg, Institute of Mineralogy

The determination of the isotopic composition is a useful tool for obtaining information of the origin and the pathway of elements in geomedia /1/. This study focusses on sulphate that is contained in seepage fluids of uranium-mining rock piles with relatively high concentrations. There are two potential sources, i) the sulphur of sulphide or sulphate minerals, deposited in rock piles (contents of less than 1%), and ii) the sulphuric acid as a component of the atmosphere and the rain, which ingresses into the rock pile body.

The isotopic composition of sulphur was measured in the following phases:

- rain water collected in Carlsfeld, western Erzgebirge, altitude 940 m, in the interval 4 May - 1 June 1994; pH = 4.5-4.9, SO_4^{2-} ca. 7 mg dm^{-3};
- crystals of sulphides and baryte prepared from rock material of the piles 66 and 38old, Schlema, western Erzgebirge;
- seepage fluid sampled from the rock pile 38new, Schlema, 30 Sept 1993 and 10 June 1994; pH . 8, SO_4^{2-} 1.7-2.0 g dm^{-3}.

The samples were chemically transformed into SO_2 as the measuring gas. A delta E Gas Isotope Ratio Mass Spectrometer (Finnigan MAT) was used.

The results are compiled in Table 1.

Type of sample	$*^{34}S$ / ‰
Rain water, 3 samples	4.4, 5.7, 5.9
Sulphide minerals, 3 crystals	1.1, 3.3, 1.1
Baryte	15.7
Seepage fluid, 2 samples	1.9, -4.1

Table 1: Isotopic compositions of sulphur in different sample types referring to the CDT standard (Cañon-Diablo meteorite, Troilite phase); reproducibility within ±0.2‰ including sample preparation.

The data are characterised by a relatively wide range of the $^{32}S/^{34}S$ composition. They indicate unambiguously that there are significant differences in the isotopic compositions of the rain water samples or the baryte on the one hand and that of the seepage on the other. Contrarily, the data of the sulphides show an overlapping with at least

one of the values for the seepage. Thus, the conclusion seems to be justified that the oxidation of sulphide minerals in the interior of the rock pile represents the major source for the sulphate dissolved in the effluent. Isotopic effects are not expected to be very large for this reaction, because the oxidation will be far from equilibrium.

Taking pyrite as an example, the overall reaction in neutral medium may be

$$4\ FeS_2 + 15\ O_2 + 10\ H_2O\ 6\ 4\ FeOOH + 8\ H_2SO_4\ ,$$

with sulphuric acid being neutralised afterwards by interaction with silicate and carbonate minerals. However, the oxidation mechanism proved to be rather complicated /2/.

Acknowledgements

This work was supported by the BMBF under contract no. 02 S 7533.

The experimental support of H. Lux (TU Dresden, Institut für Pflanzen- und Holzchemie), A. Brachmann (FZ Rossendorf, Institut für Radiochemie) and F. Haubrich (TU Bergakademie Freiberg, Institut für Mineralogie) is gratefully acknowledged.

References

/1/ P. Möller, Anorganische Geochemie, Springer-Verlag, Berlin 1986, pp. 243.

/2/ S. Karthe, R. Szargan, E. Suoninen, Oxidation of Pyrite Surfaces - a Photoelectron Spectroscopic Study, Appl. Surf. Sci. 72 (1993) 157.

A NEW HYDROTHERMAL SYNTHESIS AND CHARACTERIZATION OF HYDROUS URANYL SILICATE, $(UO_2)_2SiO_4 \bullet 2H_2O$

H. Moll, G. Schuster[1], G. Bernhard, H. Nitsche
Forschungszentrum Rossendorf e.V., Institute of Radiochemistry, [1] WIP TU Dresden

The aim of this work was to explore a reproducible synthesis of $(UO_2)_2SiO_4 \bullet 2H_2O$ and to accuratly characterize the reaction products with several different analytical methods /1/. Such well characterized material can be used as model substance for solubility and speciation investigations e.g. the environmental behavior of uranium in laboratory experiments. A new method was developed for the synthesis of uranyl orthosilicate that was derived from the procedure described by Legros et al. /2/.

Aqueous solutions (0.1M) of uranyl acetate (p.A. MERCK) and sodium metasilicate (p.A. J.T. Baker) were combined in a teflon vessel and transferred to a Parr bomb. The pH of the resulting solution was 5.0. After 3 days, the Parr bomb was heated to 383 K for about 10 days. Then it was slowly cooled down. The resulting fine-crystalline yellow precipitate was filtered (0.45µm) and washed several times with boiling deionized water to remove any excess reactants. The isolated products were dried at 383 K for 24 h and then homogenized. The yields was 82±2%; the excess uranium was recoverd in the filtrate. The yield indicates a good reproducibility of the developed synthesis. Kuznetsov et al. /3/ reported yields of 60 to 70%. The reaction time strongly influences the yields. Upon decreasing the reaction time to about 5 days, the yields increased from 0±2% to the value of 82±2%. When a 1M sodium metasilicate solution was used, the yields were only 40±10%.

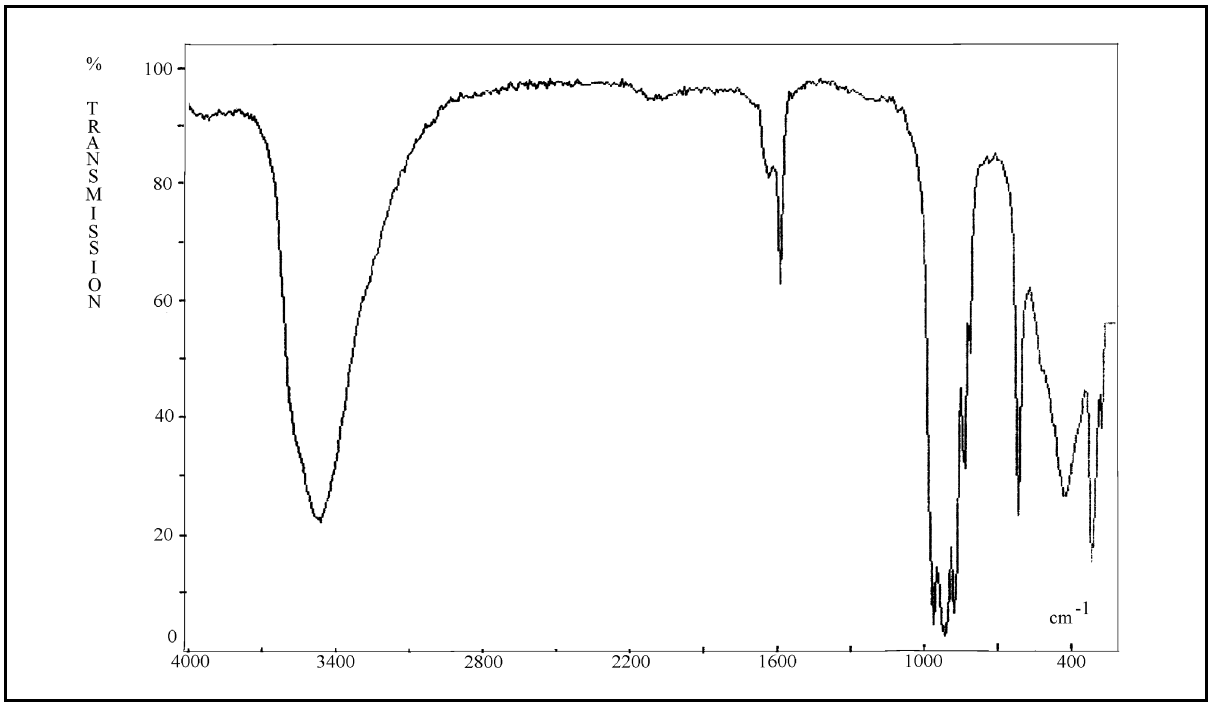

Fig. 1: IR spectrum of $(UO_2)_2SiO_4 \bullet 2H_2O$.

Uranyl silicate with the proposed formula of $(UO_2)_2SiO_4 \bullet 2H_2O$ theoretically contains 71.2% uranium, 4.2% silicon and 5.39% crystal water and has a stoichiometric ratio n(U)/n(Si) = 2. ICP-MS investigations showed that the prepared samples contain 69.4±1% U and 4.2±0.2% Si. The U and Si contents were determined using an inductively coupled plasma (Ar-plasma) mass spectrometer (ELAN-5000, Perkin Elmer, Überlingen). The samples were dissolved in 0.1M $HClO_4$ (suprapur, MERCK). Taking into consideration the measured adhered moisture of 0.9±0.2%, the recalculated contents (U: 70.35±0.9%, Si: 4.22±0.1%) better agree with the theoretical data. The synthetic soddyite has a stoichiometric ratio n(U)/n(Si) = 1.94±0.06.

The samples synthesized with 1M Na_2SiO_3 solution contain a smaller amount of uranium (66 ± 1%) and a larger amount of silicon (4.8 ± 0.1%). In these products, a sodium impurity of 1.57 ± 0.005% was measured. It is possible that these products contain amorphous Si-O-structures and additionally condensed sodium silicates.

The infrared investigations were carried out with a double-beam Infrared-Spectrometer (M80, JENOPTIC CARL-ZEISS-JENA GmbH). The spectra were measured from 4000 to 200cm^{-1}. Samples were mixed with KBr. The infrared spectrum of our synthetic soddyite is shown in Fig. 1.

The experimental results are in good agreement with the results of Legros /2/ and Plesko /4/. Phases other than uranyl silicate were not detected. The uranyl silicates synthesized are composed structurally of UO_2^{2+}-groups and SiO_4^{4-}-tetrahedra. Si-OH groups were not detected, as indicated by the lack of an absorption band at 3100cm^{-1} /2/. The sharp absorption bands at 963cm^{-1} and 878cm^{-1} show that the SiO_4-tetrahedra

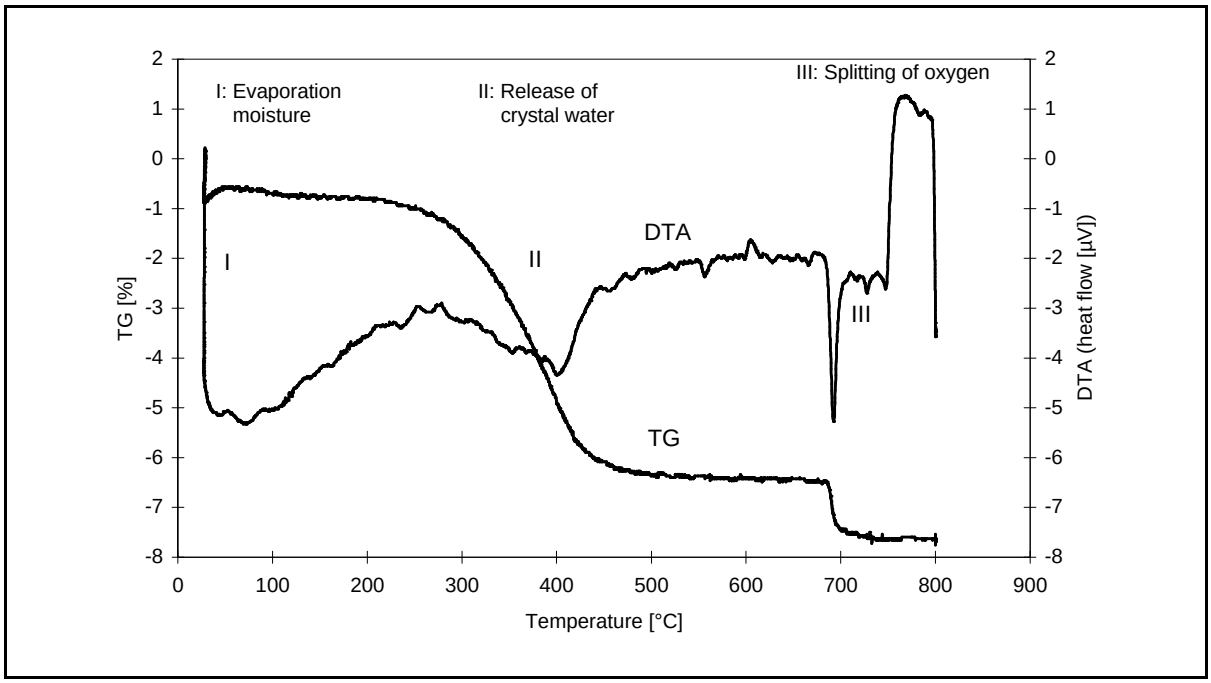

Fig. 2: Thermoanalytical diagram of thermal gravimetry (TG) and differential thermoanalysis (DTA) of uranyl silicate (5°/min, oxygen)

in these compounds are isolated and unpolymerized /4/. ^{29}Si-MAS-NMR investigations confirmed this result.

Using a thermoanalyser (STA 92, Seteram, France) thermographimetric (TG), differential-thermographimetric (DTG) and differential-thermoanalytical (DTA) measurements were made in a temperature range of 25 to 800°C with a heating rate of 5°C/min in an atmosphere of humic oxygen (3l/h).

The TG and DTA curves for our synthetic soddyite are shown in Fig. 2. No differences were visible between our samples and the comparative samples prepared according to Legros /2/. The water adsorbed on the surface with a mass loss of 0.9 ± 0.2% was released in the temperature region from 25 to 213°C (first broad peak of the DTA curve in Fig. 2). The endothermal release of structural water occurs from 213 to 527°C (second peak of the DTA curve in Fig. 2).

The decomposition according to the reaction $(UO_2)_2SiO_4 \bullet 2H_2O$ 6 $2UO_3 + SiO_2 + 2H_2O$ (1), shows that the release of structural water occurs simultaneously with the release of UO_3 and SiO_2 and therefore cannot be distinguished in the DTA curve. The endothermal oxygen release according to the reaction $3UO_3$ 6 $U_3O_8 + 0{,}5O_2$ (2) was observed from 679 to 726°C (third sharp peak of the DTA curve in Fig. 2).

The structural water content was 5.51 ± 0.08%. The formula index 2.06 ± 0.03 agrees better with the theoretical value than that of Legros /2/. The oxygen release for reaction (2) is associated with a theoretical mass loss of 1.6%. For reaction (2) a mass loss of 1.26 ± 0.09% was measured for both synthesized samples and the comparative samples prepared according to Legros et al. /2/. A reason for this difference in weight loss may be the nonstoichiometry of uranium oxides in reaction (2). For example, after one hour oxidation at 800°C, a oxygen-to-uranium ratio of 2.642 in U_3O_8 was obtained. The theoretical value 2.667 was not reached /5/.

The samples synthesized with 1M Na_2SiO_3 solution contain a smaller amount of structural water ( )m of 4.0 ± 0.4%). Typical for these samples was the incomplete reaction (2). This reaction was even absent in some samples ( )m of 0.26 ± 0.01%). The drying of this substance can be done up to 150 °C without any loss of crystal water.

This study shows that $(UO_2)_2SiO_4 \bullet 2H_2O$ can be reproducibly synthesized with a high phase purity by the developed hydrothermal synthesis.

Acknowledgement

The authors thank Mrs. W. Wiesener for the ICP-MS and AAS measurements, Mrs. R. Nicolai for the infrared analysis and Mrs. E. Brendler (TU Bergakademie Freiberg) for the ^{29}Si-MAS-NMR measurements.

References

/1/ H. Moll, T. Reich, W. Matz, G. Bernhard, D.K. Shuh, J.J. Bucher, N. Kaltsoyannis, N.M. Edelstein, A. Scholz
Structural analysis of $(UO_2)_2SiO_4 \bullet 2H_2O$ by XRD and EXAFS
this report.

/2/ J.P. Legros, R. Legros, E. Masdupuy
Sur un Silicate d'Uranyl Isomere du Germanate d'Uranyl
Bull. Soc. Chim. France 8, 3051 (1972).

/3/ L.M. Kuznetsov, A.N. Tsvigunov, E.S. Makarov
Hydrothermal synthesis and physics-chemical study of the synthetic analog of soddyite
Geochimiya 10, 1493 (1981).

/4/ P.E. Plesko, B.E. Scheetz, W.B. White
Infrared vibrational characterization and synthesis of a family of hydrous alkali uranyl silicates and hydrous uranyl silicate minerals
Amer. Mineral 77, 431 (1992).

/5/ G. Schuster, G. Braun, K. Henkel
Fehlerbetrachtung zur gravimetrischen O/U Bestimmungsmethode
ZfK-Report 489, (1981).

UV/VIS SPECTROSCOPIC STUDY OF Bi^{3+} HYDROLYSIS

A. Brachmann, G. Geipel, G.Bernhard, H. Nitsche
Forschungszentrum Rossendorf e.V., Institute of Radiochemistry

The mine tailing piles located in the uranium mining region of Saxony and Thuringia contain bismuth. The bismuth stems from two sources: the Bi-Co-Ni-Ag-U paragenesis and the radioactive decay of natural uranium producing several different bismuth isotopes (e.g. ^{209}Bi, ^{210}Bi,^{214}Bi). It was shown, that some of the bismuth leaves from the mine tailing piles one the influence of rain and surface waters and is transported by the seepage waters to the environment. Because the seepage waters' pH range varies between 3 and 7, the bismuth speciation can change by the formation of different hydrolysis products.
Although bismuth hydrolysis was investigated by several research groups, the studies used indirect determination methods or direct methods with high concentrations of bismuth /1-3/. At high concentrations polynuclear bismuth hydrolytic species can form and dominate the system. At relatively low environmental concentrations, as they were observed in the mine tailing seepage waters, monomeric hydrolysis species may form. This study investigated the hydrolysis of bismuth at low concentrations by optical spectroscopy.
To determine the progress of the hydrolysis as a function of pH, a set of solutions with increasing pH value was prepared. The total Bi^{3+} concentration of each sample was $5*10^{-5}$ mol/L. Atmospheric carbon dioxide was not excluded in these experiments because no significant amount of carbonate can form in the solution at the acidic pH that was used for the study.
The UV/VIS absorption spectrum of each solution was recorded in the wavelength range from 190 nm to 800 nm.
The free ion has an absorption band with a maximum at 223 nm due to the electronic transition $^1S_0$ -- $^3P_1$ /5/. At pH ~ 0 the existence of any hydrolysed species can be excluded and the molar extinktion coefficient was calculated ($10800 M^{-1}*cm^{-1}$). With increasing pH, the longer wavelength flank shifts to higher wavelengths. In the pH range from 1 to 2, a pair of isosbestic points at 212 nm and 238 nm can be observed, wich is clear evidence for the formation of the first hydrolysed species without any further changes in the system (Fig. 1). Provided that the bandshapes of the different species could be approximated by gaussian profiles, the peak deconvolution of the spectra resulting from coexisting species is possible. This allows the calculation of molar extinction coefficients and finally of the concentrations of all present species.
A certain relation of absorption bands and species was only possible at low pH values. By increasing pH the spectra became more and more complex. The arising influence of carbonate - and possibly polynucleare species prevents the quantitative evaluation of the spectra. Due to this, the calculation of the speciation is limited only to the low pH range. The following stability constants were calculated:

	log ß		log ß
$[Bi(OH)^{2+}]/[Bi^{3+}][OH^-]$	11,6 ± 0,5	$[Bi(OH)_2^+]/[Bi^{3+}][OH^-]^2$	22,9 ± 0,6

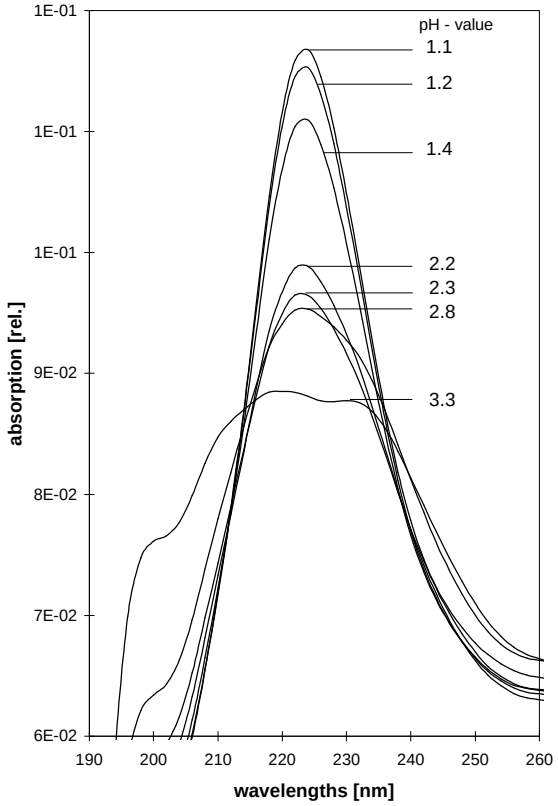

Fig.1: Absorption spectra in the pH - range 1.1 - 3.3

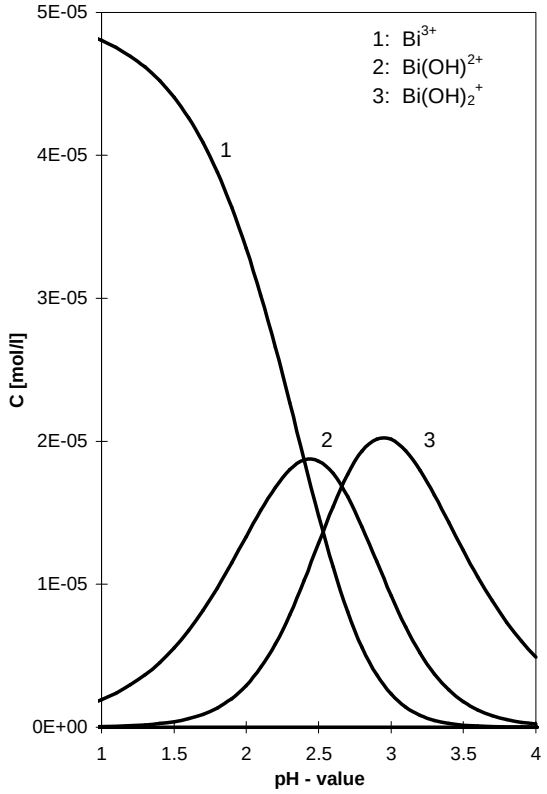

Fig.2: Speciation model of Bi^{3+} using the stability constants obtained in this work

(Fig. 2 by using the progam "RAMESES" provided from B. W. DARVELL, University of Hong Kong)

The resultes are in good agreement with complexation constants obtained by other methods (e.g. /1/-/3/). The speciation is graphically presented in Fig.2.
In addition to the evaluation by peak deconvolution, the statistical procedure of evolving factor analysis was used to validate the number of coexisting species (e.g. /6/). The starting point of this method is a matrix A (MxW) which is constructed by the set of recorded spectra, where M is the absorption in relation to wavelength and W is the spectrum in dependence of the pH value. All from zero significant different eigenvalues of the matrix $Y = A^tA$ are representative for one species. By successive calculation of the eigenvalues of the submatrices A_i, constructed by the 1,2,...,i spectra, one obtains a set of rising values. The analogous procedure started from the "last" spectrum also resultes in a set of rising eigenvalues. The grapical presentation of these "sets" of eigenvalues as a function of pH is shown in Fig. 3. For each species one obtains two crossing lines. The cutting points are representative for the maximum concentration of one species. This method, however, proved not to be as successful as we expected. Thereby we do not use it for speciation, but as a basis to generate speciation models. In our case, we see the statistical evidence for three existing species (Bi^{3+}, $Bi(OH)^{2+}$, $Bi(OH)^{+}_{2}$) and also the same general species distribution as obtained from peak deconvolution.

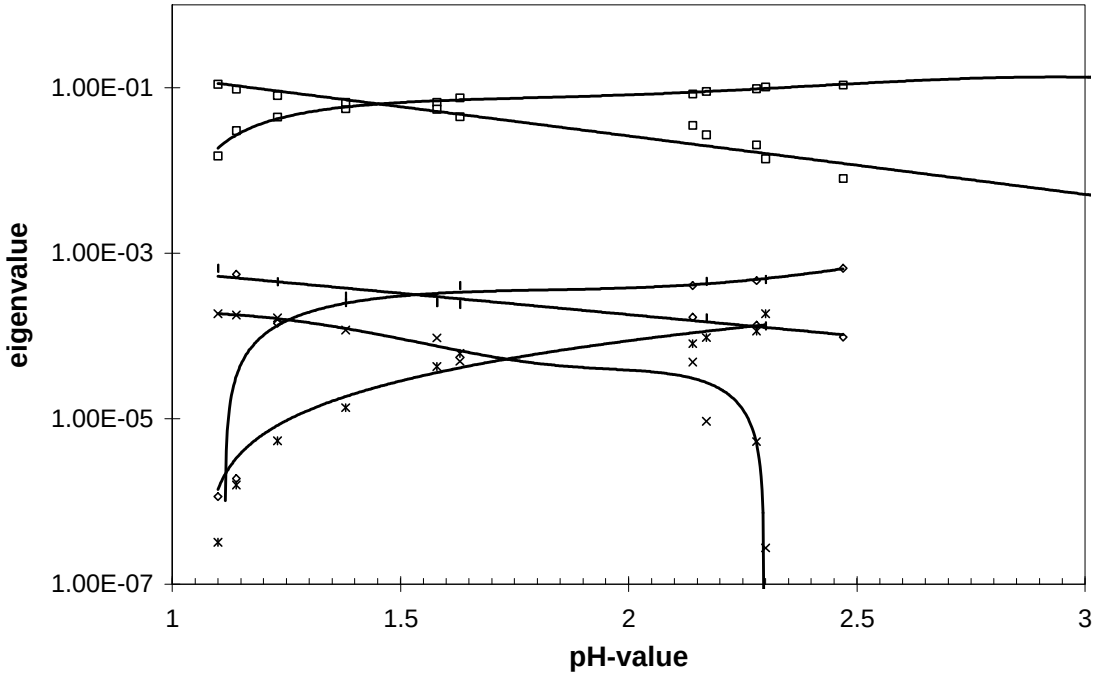

Fig. 3: Graphical presentation of the results of evolving factor analysis

References

/1/ P.I. Artyukhin, D.V. Andreev, V.I. Malkova,
Determination of formation constants of monomeric bismuth(III) hydroxo complexes according to the data on bismuth-207 on glass
Radiokhimia 32, 54 (1990)

/2/ T.F. Bidleman
Bismuth-Dithizone Equlibria and Hydrolysis of Bismuth Ion in Aqueous Solution
Anal. Chim. Acta 56, 221 (1971)

/3/ Hataye, H. Suganuma, H. Ikegami, T. Kuchiki
Solvent Extraction Study on the Hydrolysis of tracer Concentrations of Bismuth(III) in Perchlorate and Nitrate Solutions
Bull. Chem. Soc. Jpn. 55, 1475 (1982)

/4/ C. Dragulescu, A. Nimara, I. Julean
Contributions to the bismuth hydrolysis study. II Spectrophotometric and polarographic investigations on bismuthyl perchlorate hydrolysis
Revue Roummaine de Chimie 7, 1181 (1972)

/5/ C.K. Jorgensen
Oxidation numbers and oxidation states
Springer Verlag, Berlin, Heidelberg, New York (1969)

/6/ M. Maeder, A.D. Zuberbühler
The resolution of overlapping chromatographic peaks by evolving factor analysis
Anal. Chim. Acta 181, 287 (1986)

TIME-RESOLVED LASER-INDUCED FLUORESCENCE STUDIES (TRLFS) - EXPERIENCIES WITH A NEW LASER SYSTEM

G. Geipel

Forschungszentrum Rossendorf e.V., Institute of Radiochemisrty

A new time-resolved laser-induced fluorescence measuring system was installed at the institute. The system consists of a Nd-YAG pump laser and an Optical Parametrical Oscillator (OPO) Laser. The OPO replaces the Dye Laser of older conventional systems and has the capability of continously scanning a wide wave-length range. Fig. 1 shows the layout of the system.

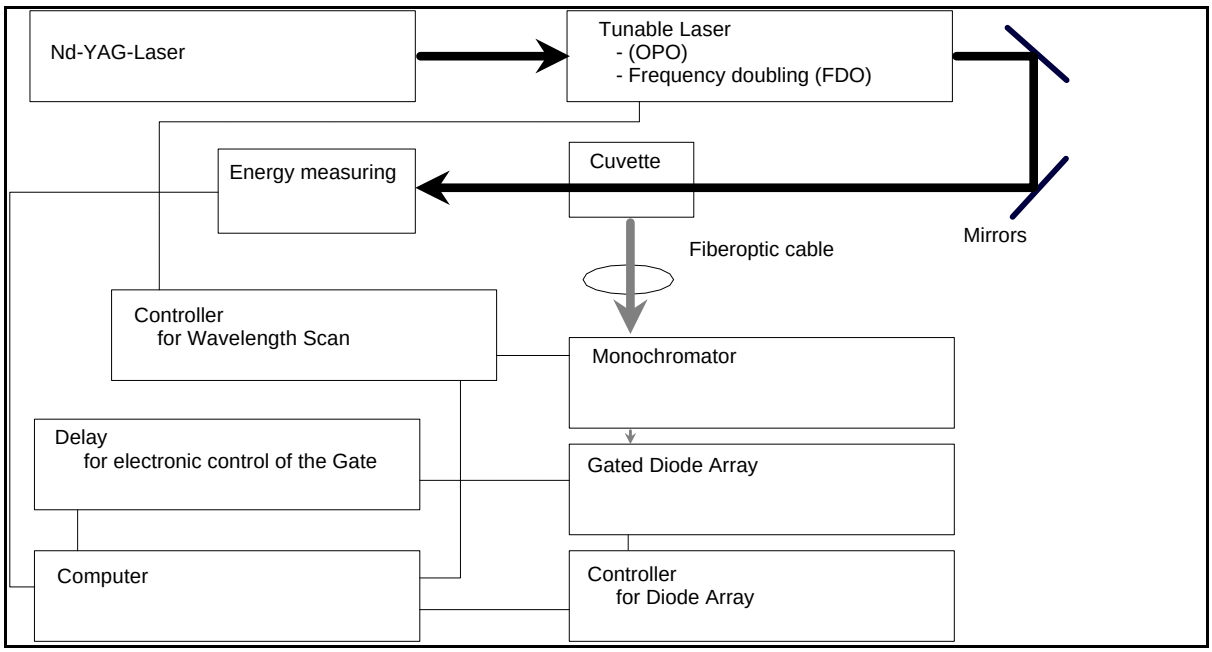

Fig.1: Design of the fluorescence measurement system

The Nd-YAG Laser (GCR-190, Spectra Physics) has a repetition rate of 10 Hz and a power of 1 J per pulse at 1064 nm. The third harmonic of this laser at 355 nm has a pulse power of 320 mJ per pulse and is used for pumping the OPO-System (MOPO-730, Spectra Physics). The MOPO-730 has a bandwith of 0.2 cm^{-1} and an spectral range from 440 nm to 690 nm and 730 nm to 1800 nm. With a frequency doubling system (FDO), which is a stand-alone unit that is not yet incorporated in the MOPO, we reach a wavelength of 260 nm. The laser power is about 30 mJ per pulse in the range 450 to 680 nm and with the FDO a laser power between 2 and 6 mJ per pulse is obtained in the range 260 nm to 340 nm.
For measuring the fluorescence of the samples, we use a special cuvette holder. In the back of this holder, a fast silicon photodiode is located for measuring the actual laser power. Rectangular to the laser beam, a fiber optic is arranged to collect the fluorescence light and send it to the monochromator (EG&G 1235 with three gratings).

From the monochromator, the spectral light is measured with a gated diode array system (EG&G 1255). The delay time and the gate width is controlled with a delay generator (EG&G 9650). The measured signals are read with by detector interface (EG&G 1471A). All devices are connected via IEEE 488 to a personal computer. This computer is used for experiment control and data storage using home-made software. This progam corrects for background effects and correlates the signal to the laser power.

For testing of the system, a 10^{-5} M uranyl perchlorate solution at several different pH values was used.
As an example Fig. 2 shows the time dependence of the spectra of a uranyl perchlorate solution at pH 2.16. The band maxima are given in table 1. There is very good agreement with the data of Kato [1] and Czerwinski [2]. For the life time of the uranylion we calculated 1.57 +/- 0.07 µs, which is between the values of 1.9 +/- 0.2 given by Kato for 0.1 M $HClO_4$ and 0.9 +/- 0.3 µs for the free uranylion [1].

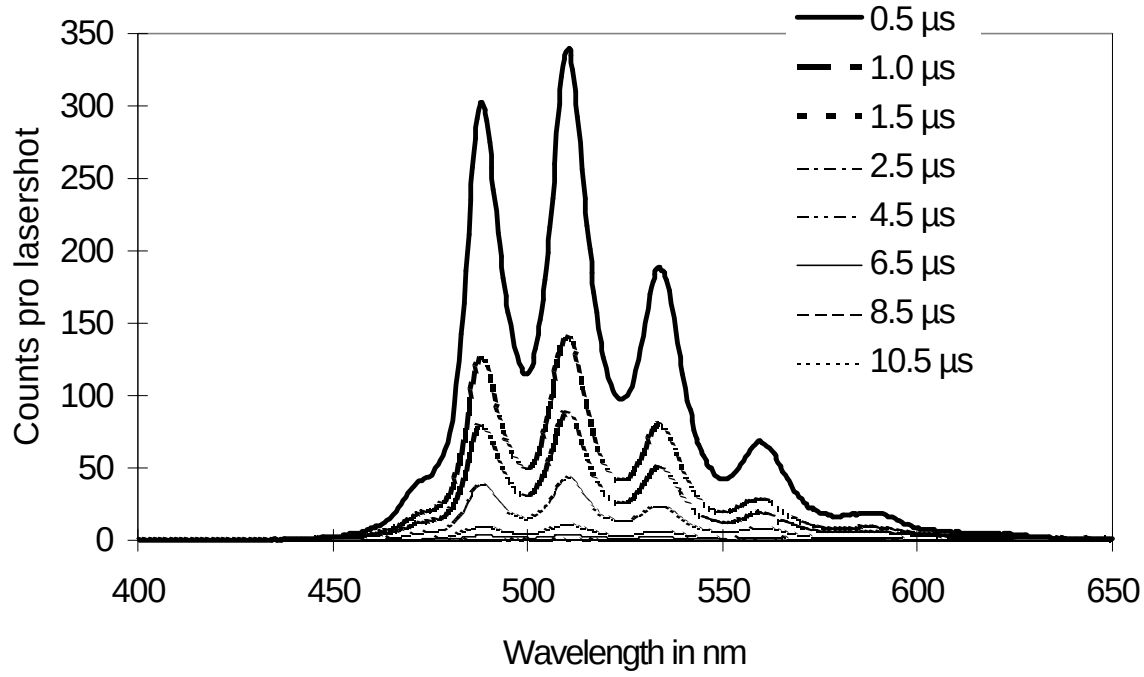

Fig. 2: Time depending spectra of the uranyl ion in 0.1 M ClO_4^- -media at pH 2.16

The measurements of the lifetime of the free uranyl ions and the agreement of the centers of the band maxima show that our design for TRLIFS-measurements produces the same results, than literature data.

Table 1: Centers of the fluorescence band maxima for the uranylion in several media (in nm)

Y. Kato et al. [1]	K.Czerwinski et. al. [2]	This work		
ClO_4^-	ClO_4^-	ClO_4^-; pH 2.16	SO_4^{--}; pH 2.16	SO_4^{--}; pH 3.13
473.0		473.6	482.7	484.7
488.0	490.0	488.1	492.8	493.9
509.0	511.0	510.4	514.9	515.5
534.0	535.0	534.0	538.2	538.6
560.0	560.0	558.6	562.9	563.9
588.0	588.0	586.2	587.7	592.5

For further test of the system, a solution of 10^{-5} M uranyl ions in 0.05 M sulfuric acid at pH 2.16 and 3.13 was measured. The maxima of the fluorescence bands are also given in table 1. The measured lifetimes are 1.57 µs for the free uranyl ions and 4.1 +/- 0.06 µs for the first uranyl sulphate complex. The measurements demonstrate that the new laser system is well suited for highly sensitive fluorescence spectroscopy.

References:

[1] Y. Kato, et. al., A Study of U(VI) Hydrolysis and Carbonate Complexation by Time-Resolved Laser-Induced Fluorescence Spectroscopy (TRLIFS) Radiochim. Acta 64, (1994), 107

[2] K. R. Czerwinski, et. al., Complexation of the Uranyl Ion with Aquatic Humic Acid, Radiochim. Acta 65, (1994), 111

THE DETERMINATION OF URANIUM IN URANYLNITRATE-SOLUTION BY THE SOLID-ELECTROLYTE METHOD COMBINED WITH MASS SPECTROSCOPY

C. Nebelung
Forschungszentrum Rossendorf e.V., Institute of Radiochemistry

A practicable method for the determination of the uranium concentration in $UO_2(NO_3)_2$-solution is the solid-electrolyte-coulometry combined with mass spectroscopy. The solid-electrolyte method is described in /1,2/. The measuring principle is shown in Fig.1.

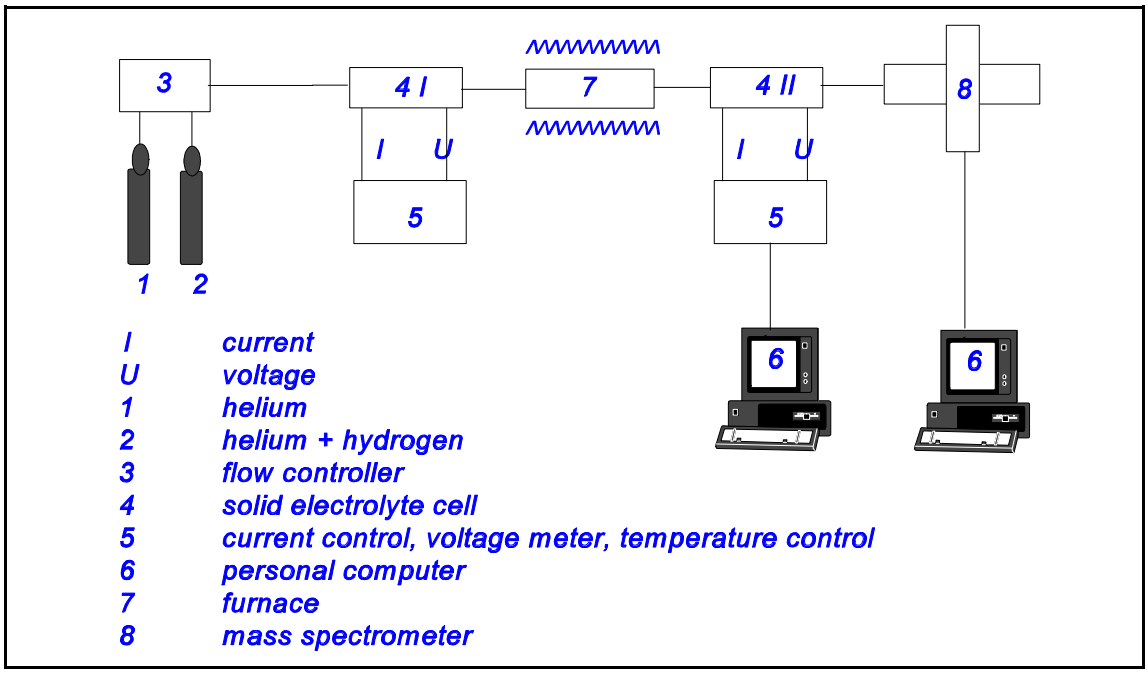

Fig. 1: Measuring principle

The carrier gas is measured in the first potentiometric working solid-electrolyte cell (4I). The sample reacts with the gas in the furnace (7). During this reaction, the gas is examined if oxygen is released or consumed. The change of the oxygen concentration is determined in the second cell (4II) by coulometric titration /1/. The components of the gas are measured subsequently by a quadrupol-mass-spectrometer (8) with a heated capillary gas-inlet.

The carrier gas is helium with $8.63 \cdot 10^{-4}$ atm hydrogen (cell potential of -1100 mV at 700°C). The partial free enthalpy of oxygen changes due to the temperature changes in the furnace. In the second cell, oxygen is pumped up to a partial pressure of $1.4 \cdot 10^{-5}$ atm (cell potential of -200 mV). To calculate the uranylnitrate concentration, it is necessary to know what kind of the possible reaction (1) to (5) takes place in the furnace:

$UO_2(NO_3)_2 + 2\,H_2 \rightarrow UO_2 + 2\,H_2O + 2\,NO_2$ (1)
$UO_2(NO_3)_2 + 3\,H_2 \rightarrow UO_2 + 3\,H_2O + 2\,N_2O_3$ (2)
$UO_2(NO_3)_2 + 4\,H_2 \rightarrow UO_2 + 4\,H_2O + 2\,NO$ (3)
$UO_2(NO_3)_2 + 5\,H_2 \rightarrow UO_2 + 5\,H_2O + N_2O$ (4)
$UO_2(NO_3)_2 + 6\,H_2 \rightarrow UO_2 + 6\,H_2O + N_2$ (5)

Fig. 2 shows the dependence of the partial molar free enthalpy on the temperature of this nitrogen-oxygen-reactions calculated by /3/ and the curves of the carrier gas.

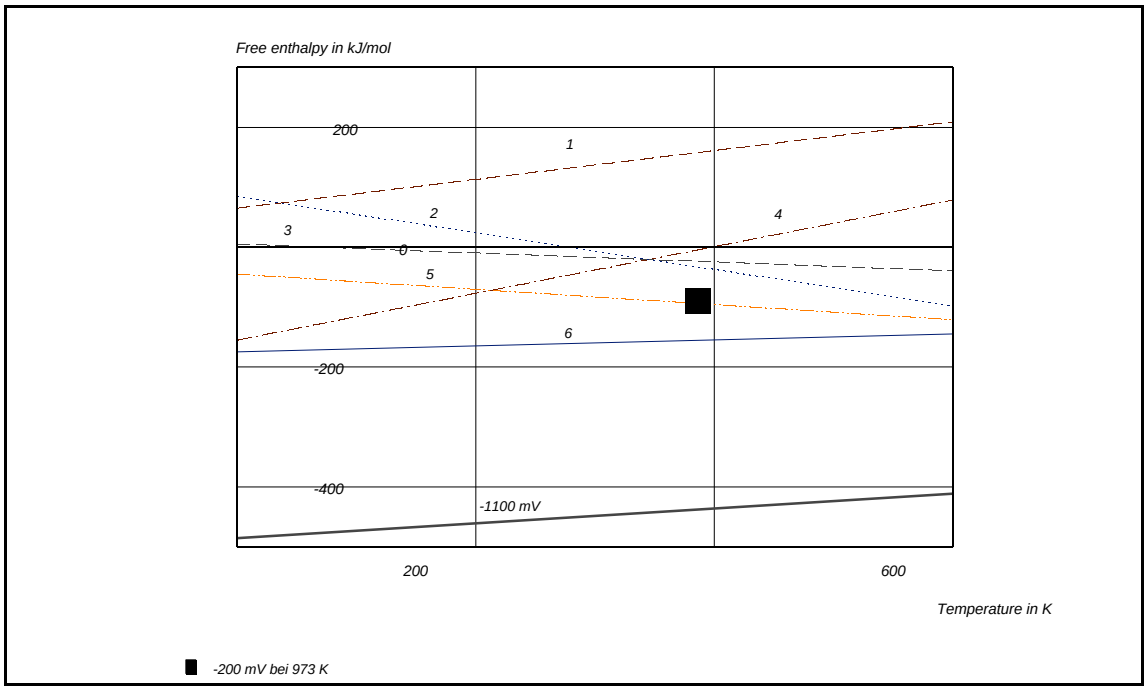

Fig. 2: Partial molar free enthalpy - temperature - dependence of nitrogen and nitrogen oxide - oxygen reactions

1: $2\ NO_2 \times 2\ N_2O_3 + O_2$ 2: $2\ NO_2 \times 2\ NO + O_2$
3: $4/3\ NO_2 \times 2/3\ N_2O + O_2$ 4: $4\ NO \times 2\ N_2O + O_2$
5: $NO_2 \times 1/2\ N_2 + O_2$ 6: $2\ NO \times N_2 + O_2$

According to the thermodynamic calculation of the nitrogen-oxygen reaction (Fig. 2) N_2 can be expected in the first cell and in the furnace, and NO in the second cell (-200 mV at 973 K) after the reaction in the furnace.
The U(VI) is reduced to U(IV) at the oxygen partial pressure of the used gas /4,5/.

The uranylnitrate solution (between 0.1 and 10 ml) was evaporated in the furnace in the gas-stream at room temperature. The dried sample is heated up to 900°C. Fig. 3a shows the titration current - time - dependence with a large reduction peak at 340°C and a smaller peak at 680°C. The mass spectrometer only shows significant changes of the partial pressure of the mass 30 = NO (Fig. 3b) at the same temperatures. Changes of the partial pressures of the other nitrogen oxides or N_2 are not observed. This shows that the reaction (3) takes place only.

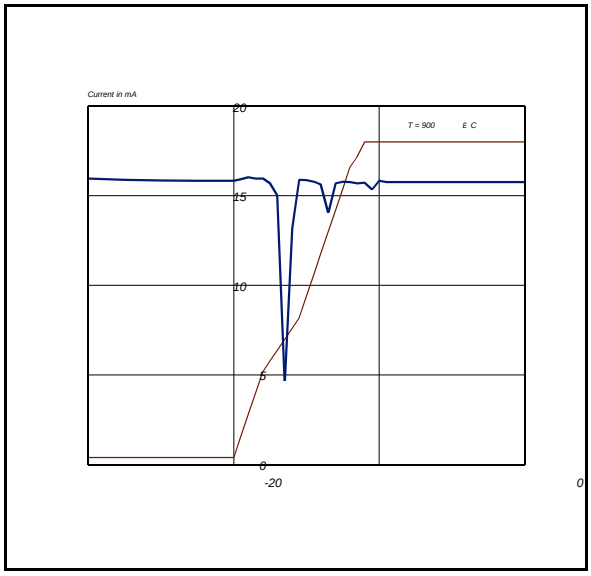

Fig. 3a: Titration current-time-dependence of the reduction of uranylnitrate in the solid electrolyte cell

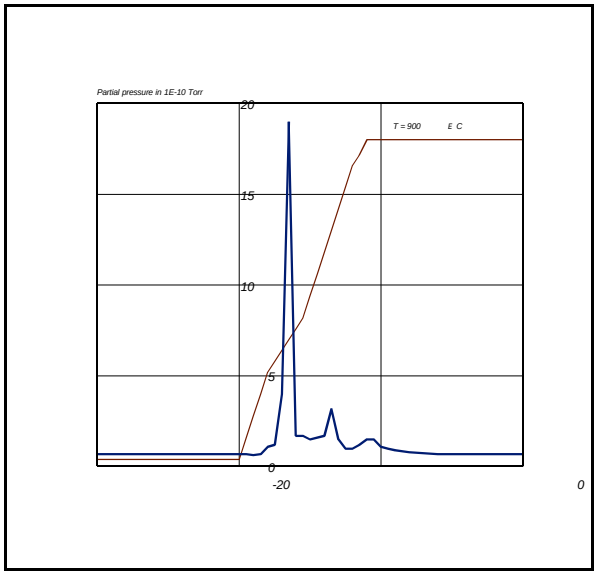

Fig. 3b: Partial pressure of NO - time dependence mass spectrometry

Seven measurements (between 0.1 and 10ml) of a 10^{-2} m $UO_2(NO_3)$ revealed only (88.1 $\pm$ 3.9) % of the expected hydrogen consumption (according to reduction equation (3)).
This difference to the expected concentration can be caused by the design of the experiment: it is possible that at the beginning of the reaction equation (1) takes place. During the drying of uranyl nitrate, the total partial pressure is very high. During this time, changes of the partial pressures (i.e. NO_2) cannot be measured in the mass spectrometer.

A second possibility to determine the uraniums concentration was also tested. After the first reduction of the uranyl nitrate, the samples are oxidized in air at 450°C to U_3O_8 /6/ and reduced at 900°C in the helium-hydrogen gas-stream.
The reduction of U_3O_8 is measured and calculated from the coulometric titration according to the reaction:

$$U_3O_8 + 2\,H_2 \rightarrow 3\,UO_2 + 2\,H_2O \qquad (6)$$

The uranium content was determined by 10 measurements of 10 ml of a 10^{-2} m $UO_2(NO_3)_2$-solution.
The uranium content measured corresponds to a (0.010045 $\pm$ 0.000054) molar solution (error of 0.5%).

In Fig. 4 the typical current-time-curve for the reaction (6) is described.

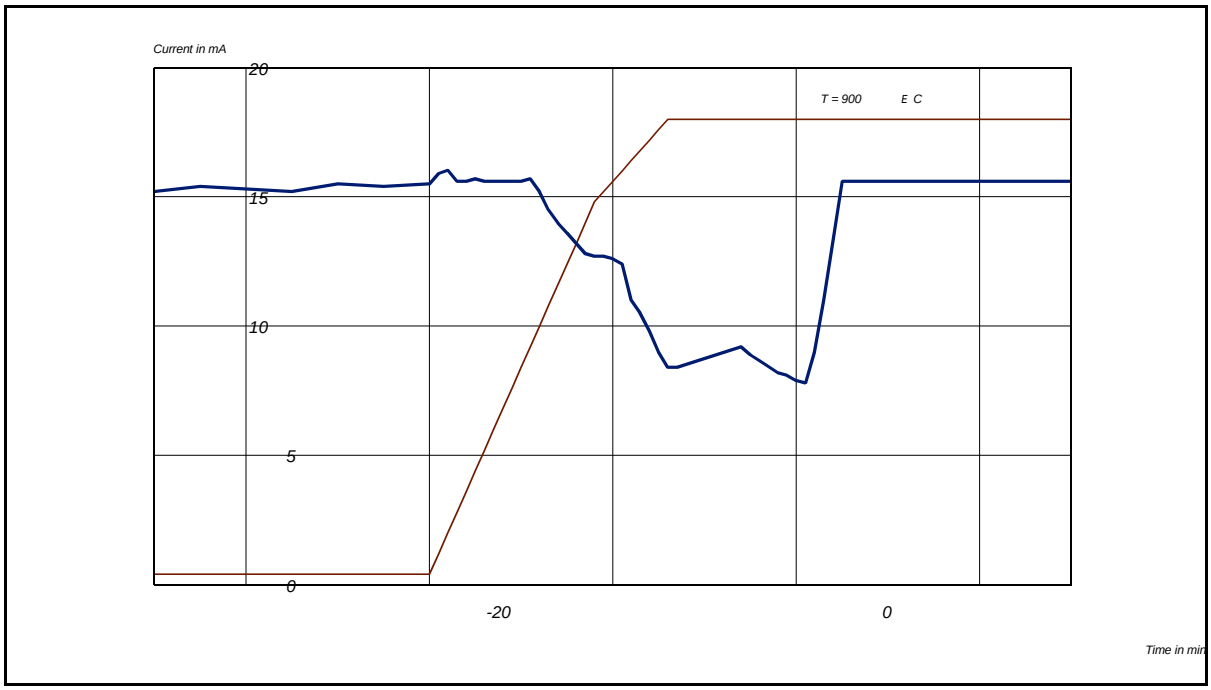

Fig. 4: Current - time dependence for the U_3O_8 reduction

The direct coulometric reduction of uranylnitrate does not exact results. The coulometric titration with a solid electrolyte cell at the second reduction (after the oxidation in air at 450°C) is a very exact method to determine the uranium content in an $UO_2(NO_3)$-solution. In comparison with the automatic potentiometric titration (± 3 %) /7/, ICPMS (± 6 %) or spectrophotometry (± 2 %) the solid electrolyte coulometry with a tolerance of ± 0.5 % seems to be superior.

References

/1/ Gerätebeschreibung OXYLYT-Meßgerät zur Analyse von Gasen und Festkörpern, ZfK Rossendorf (1991)

/2/ K. Teske, W. Gläser
Microchimia acta 1, 653 (1975)

/3/ O. Knacke, O. Kubaschewski, K. Hesselmann
Thermodynamical Properties of Inorganic Substances
Springer Verlag 1991

/4/ C. Nebelung
Materials Science Forum 76, 289 (1991)

/5/ T. B. Lindemer, T. M. Besman
J. Nucl. Mat. 130, 473 (1985)

/6/ C. Nebelung, K. Teske
Report ZfK-544 (1984) S. 116

/7/ J. Slania, F. Bakker, A.J.P. Groen, W.A. Lingerak
Fresenius Z. Anal. Chem. 289, 102 (1978)

ACOUSTOPHORETIC MEASUREMENTS ON FINELY GROUND ROCK SAMPLES

R. Herbig[1], G. Hüttig
Forschungszentrum Rossendorf e.V., Institute of Radiochemistry
[1] TU Bergakademie Freiberg, Institute of Ceramic Materials

Electro-acoustic effect in suspensions

Contacting a liquid phase, finely ground materials may develop a net-charge on its surface. The charge can arise from a variety of mechanisms such as ionization of surface chemical groups, adsorption of ions, or unequal dissolution of ions from an ionic crystal lattice. The net charge on the surface is balanced by an equal and opposite charge of ions which surround the surface of the particle as a diffuse cloud. The charged surface and the surrounding counterions establish an electrical double-layer. The electrical potential at or near the beginning of the diffuse layer is termed the zeta potential and controls the electrostatic interaction forces between the particles. Properties of a suspension, like their rheology, mobility of the particles and stability toward coagulation are governed by the zeta potential. The electrokinetic behaviour of a solid in a suspension is clearly characterized by the pH depending "zeta-potential-profile." Zeta potential and isoelectric point characterize the surface activity of a solid.

The Electrokinetic Sonic Amplitude (ESA) - measurement is based on an electrokinetic effect in disperse systems. When an alternating electric field is applied to a colloidal dispersion the particles will move in the electric field because of their surface electrical charge. If there is a density difference between the particles and the liquid, this oscillatory motion of the particles will result in the transfer of momentum to the liquid and the development of an acoustic wave. This effect has been termed ESA /1/. ESA is the pressure amplitude generated by the suspension per unit electric field strength and has SI units of pascals per volt per metre.

Up to concentrations of 10 volume percent, the ESA unit is linearly proportional to the concentration. ESA is analogous to the electrophoretic mobility that is represented in terms of velocity normalized by the strength of the applied electric field. In cases where the zeta potential must be known, electro-acoustic measurements up to 10 volume percent concentrations are far superior to traditional microelectrophoresis measurements that require dilution to the part per million ranges. It means ESA-measurements are more realistic than other methods.

The pH-depending ESA profile and the phase angle between electric field and acoustic response allow conclusions on the surface-depending properties and reactions. In mineral samples, these reactions may be manifold because of their complex composition.

ESA measurements of aqueous suspensions of mineral samples

The measurements should give a first impression on the different pH-dependent behaviour of the minerals diabase, granodiorite, and dump rock. The results, shown in

figures 1 - 3, should be valuated regarding the low volume concentration (4.5 wt.%) and the high grain-size (d_{100}= 63 µm). But nevertheless, the colloidal behaviour will also be expressed phenomenologically in the behaviour of a suspension of not so finely ground particles.

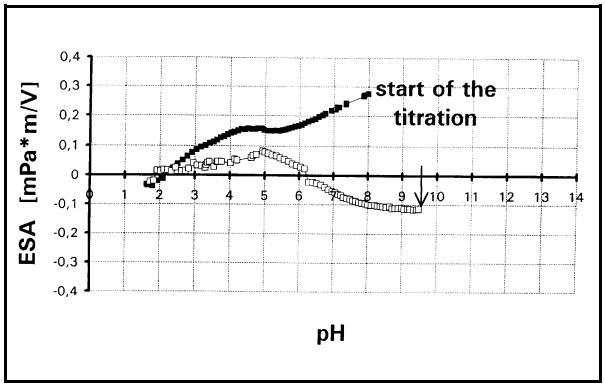

Fig. 1a: ESA of an aqueous diabas suspension

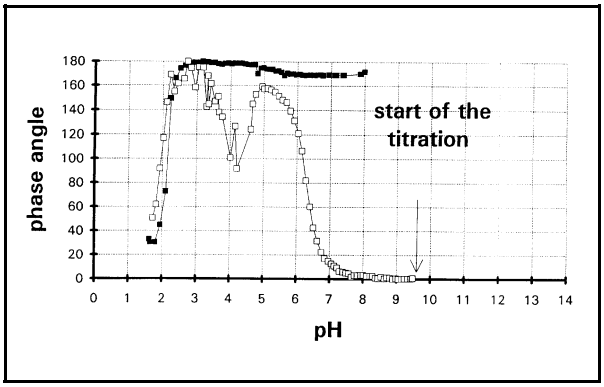

Fig. 1b: Change of the phase angle

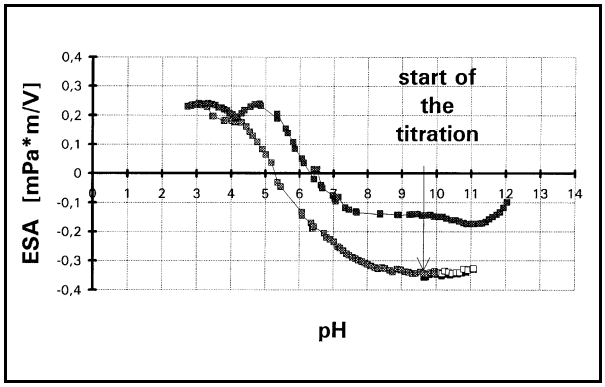

Fig. 2a: ESA of an aqueous granodiorit suspension

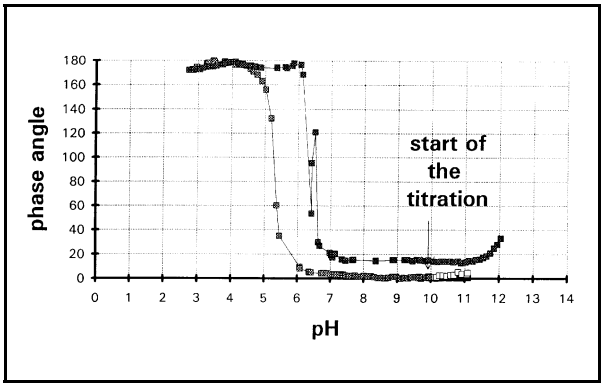

Fig. 2b: Change of the phase angle

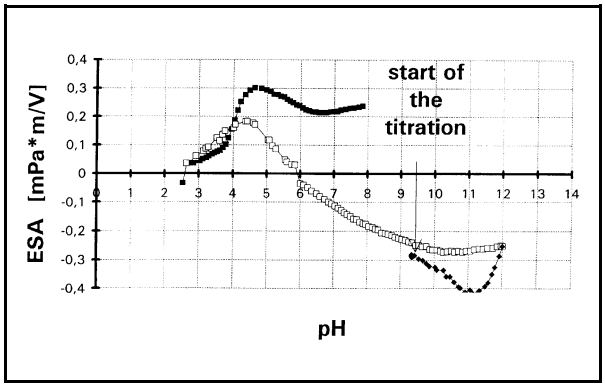

Fig. 3a: ESA of an aqueous dump rock suspension

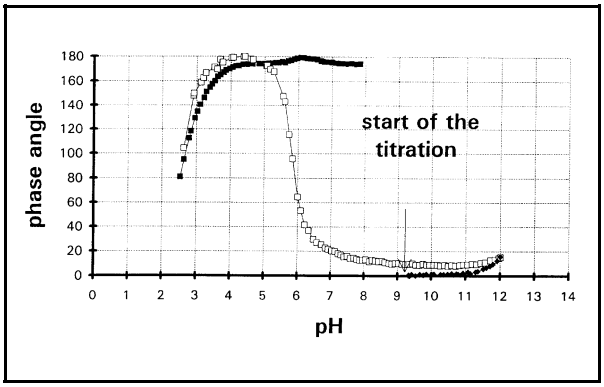

Fig. 3b: Change of the phase angle

The starting pH values become alkaline for all cases, after suspension of the material in destilled water: Dump rock pH 9, diabase pH 9.5, and granodiorite pH 9.7. The pH depending ESA measurement was carried out with 1M HNO_3 and 1M NaOH. At first, a pH of ~11 for granodiorite and for dump rock ~ 12 was adjusted.

With increasing hydrogen ion concentration, the ESA values decrease up to the isoelectric point. The isoelectric point (i.e.p.) - the point of zero mobility - corresponds with the point of ESA = 0. For diabase and dump rock the i.e.p. is near pH 6 (fig. 1, 3) and for granodiorite (fig. 2) near 5. At this point the surface is reloaded, characterized by a sharp 180E- change of the phase angle. The smeared increase of the phase angle (fig. 1b, 2b, 3b) may characterize a chemical surface reaction or is a result of the phase mixture in the samples with different i.e.p. of the constituents. Diabase shows surface reactions from pH region 2 to 6 (fig. 1b) and dump rock (fig. 3b) from pH 2 to 4 that develop a second i.e.p. at higher H^+. According these surface reactions at increasing OH^-, reloading of the surface can not occur.

The behaviour of granodiorite differs markedly (fig. 2a, 2b). Due possibly a surface reaction, the i.e.p. at increasing OH^- is shifted to higher pH values, but the i.e.p. is reached near pH 6.

Dump rock in contrast to granodiorite and even diabase shows a weak surface reaction near the pH 11(fig. 3a, 3b), resulting in a decrease of the ESA and the mobility accordingly.

Discussion

Although the ESA measurement are insufficient to determine the reaction kinetics, the pH dependent surface effects and reactions are clearly shown.
The behaviour of the rock samples differs markedly. Dump rock shows similarity to diabas at acidic pH. Surface reactions change the pH depending electrophoretic behaviour.
For more information the starting conditions - composition, density, physical and chemical surface conditions, grain size - should be determined exactly. The grain size should be decreased near to colloidal dimensions.
The reagents for the pH depending measurements should be selected according determined conditions and models.
Future investigations will focus on the influence of the physical and chemical state of the particle surface on the colloidal properties of aqueous suspensions. This is necessary to interpret the "zeta potential/ESA - pH value profile" of colloidal suspensions, and to control and to manipulate the interparticle forces.

References

/1/ Cannon, D.W.
Dissertation, Brown University, Providence, R.I., 1989

LOW-LEVEL MEASUREMENT OF ALPHA-ACTIVE NUCLIDES IN CONCRETE

C. Nebelung, S. Hübener, G. Bernhard
Forschungszentrum Rossendorf e.V., Institute of Radiochemistry

In the course decommissioning of nuclear power plants much of the concrete can be reused, recycled or deposited on dumps. These materials may be released from the regulatory control regime, if the content of nuclear material is lower than the clearance level which is for most of the alpha-active nuclides 0.5 Bq/g /1/ or 0.3 Bq/g /2/.

The measuring method has to meet the following requirements:

- result available after a short time (< 1 d)
- low detection limit (< 0.025 Bq/g)
- nuclide specific result
- large sample throughput

The measurements should allow to decide wether or not the contamination of the concrete building debris with the nuclides Th, U, Np, Pu and Am is higher than the clearance level.
Two different methods were tested: (1) direct alpha-spectroscopic measurement of thin layer sources prepared without chemical processing and (2) the measurement of sources prepared after separation by chlorination and thermochromatography.

The direct method consists of the following steps /3/:

- grinding the sample material to grain diameters $\leq$ 1 mm
- wet milling to grain diameters $\leq$ 2 µm
- preparation of thin layer sources
- alpha-spectrometric measurements

The chlorination consists of the following steps:

- reaction of the concrete with chlorine or a CCl_4/Cl_2 mixture at 1300 K and thermochromatography
- hydrolysis and source preparation by evaporation

Large area passivated ion-implanted planar silicon (PIPS) detectors and a gridded ionization chamber (GIC) are used as detectors in the alpha-spectrometric measurements. The PIPS detectors used, have a diameter of 80 mm and offer in measurements of reference sources prepared by electrodeposition a detection efficiency of about 25 % and a resolution of 55 keV (FWHM). The GIC can accommodate sources with 200 mm diameter. A detection efficiency of 50 % and a resolution of 60 keV (FWHM) has been achieved.

Concrete sources of various thickness with a known concentration of alpha-emitters were measured to calibrate the alpha-spectrometric measurement of thin layer sources as shown in Fig. 1.

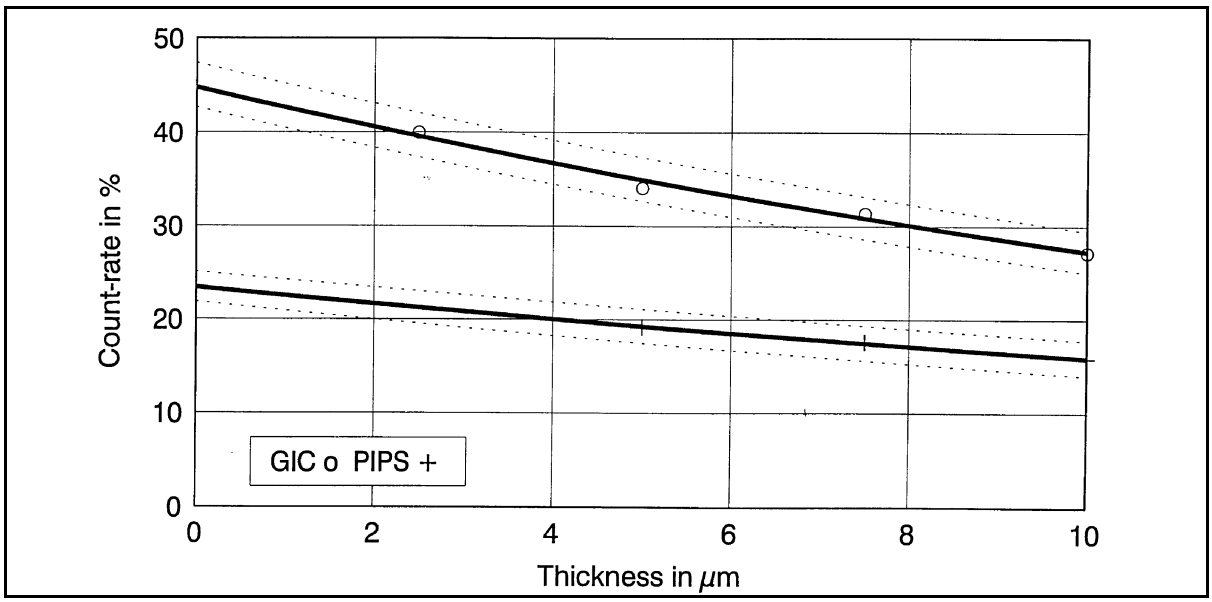

Fig. 1: Count rate - layer thickness dependence

Some typical spectra of concrete are presented in Fig. 2a and 2b.

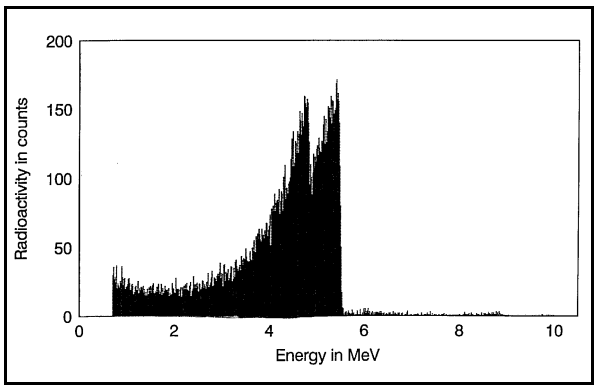

Fig. 2a: GIC spectrum of concrete RBB 4.8 µm, ^{241}Am, ^{233}U, ^{238}Pu (5,3 Bq) 6 h measuring time

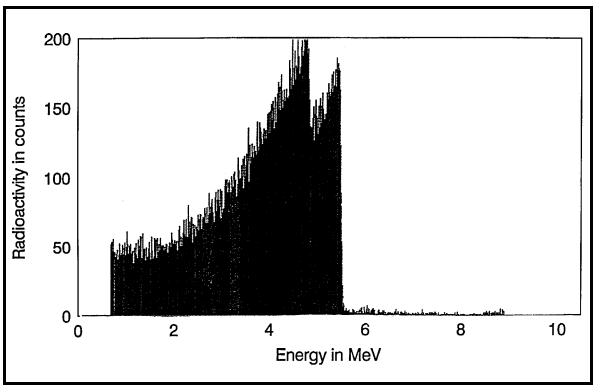

Fig. 2b: GIC spectrum of concrete RBB 9.5 µm, ^{241}Am, ^{233}U, ^{238}Pu (10,7 Bq), 6 h measuring time

The nuclide identification based on such spectra is possible but limited to simple cases. The evaluation of the spectra with the computer code ALPS /4/ was tested. The (^{238}Pu + ^{241}Am) / ^{233}U ratio of a source 4.8 µm was determined with a standard deviation of about 20 %. The evaluation of the spectra of a thicker 9.5 µm sources gave incorrect results.

From the calibration function the total alpha-radioactivity of various concrete samples can be determined.

Fig. 3 shows spectra of "inactive" concretes.

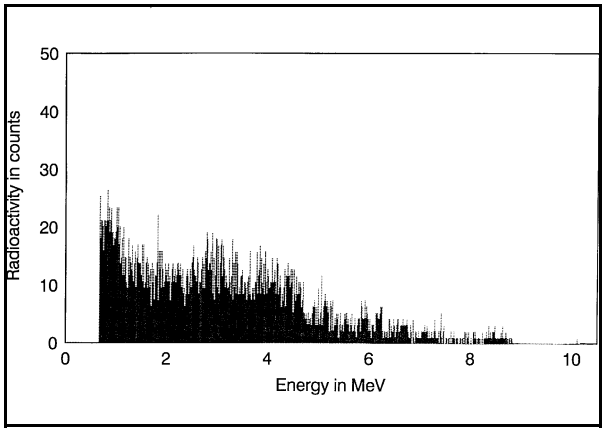

Fig. 3a: GIC spectrum for concrete WAK 7.5 µm, 20 h measuring time

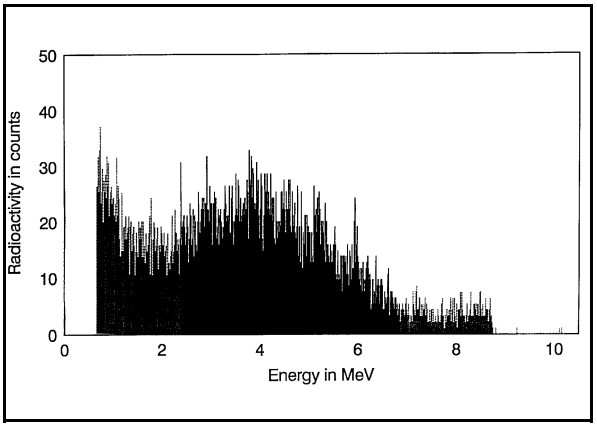

Fig. 3b: GIC spectrum for concrete DB2 7.5 µm, 20 h measuring time

Table 1 summarizes the results of direct measurements of various concrete samples.

concrete	GIC specific radioactivity	PIPS specific radioactivity
WAK	0.24 ± 0.03 Bq/g	0.22 ± 0.02 Bq/g
RBB	0.40 ± 0.03 Bq/g	0.36 ± 0.02 Bq/g
KKN	0.14 ± 0.02 Bq/g	0.11 ± 0.02 Bq/g
DB1	0.28 ± 0.03 Bq/g	
DB2	0.77 ± 0.03 Bq/g	

WAK "inactive" concrete from "Wiederaufarbeitungsanlage Karlsruhe"
RBB "inactive" concrete from Rossendorf
KKN "inactive" concrete from nuclear power station Niederaichbach

Table 1: Total alpha-radioactivity of various "inactive" concretes

Preliminary results of chlorination/thermochromatography studies indicate a separation of actinides from the concrete bulk. Sources for alpha-spectrometry can be prepared from the volatile fractions by dissolution in water or diluted acids and simple evaporation on stainless-steel supports.

The resolution of the spectra depicted in Fig. 4 allows to identify the radionuclide composition.

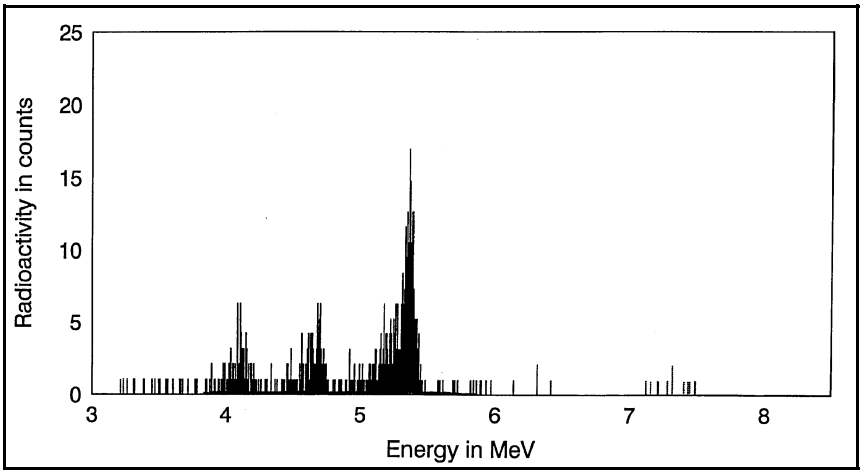

Fig. 4: Volatile fraction after chlorination PIPS-spectrum of concrete RBB + ^{241}Am, 20 h measuring time

The results indicate that the chlorination/thermochromatograhpy method is that compare well with those obtained from direct measurement of thin-layer sources.
The direct measurement method is relativley easy to use giving reliable and reproducible quantitative results. The chlorination/thermochromatography method can be used for additional qualitative nuclide identification.

Acknowledgement

These studies under the title "Methodenentwicklung zur Freimessung von Bauschutt auf alpha-aktive Nuklide" are supported by the BMFT under the contract number 02 S 7442 2.

References

/1/ Strahlenschutzverordnung 1989
3., aktualisierte Auflage, § 4 Abs. 4 Satz 1 Nr. 2 Buchstabe e, § 83
Bundesanzeiger, 1992

/2/ E. Warnecke
Recommended Clearance Levels for Radionuclides in Solid Materials
Report IAEA 8783y, Draft, Dec. 1993

/3/ S. Hübener, C. Nebelung, G. Bernhard
Bestimmung von Actiniden in Bauschutt auf alpha-aktive Nuklide
GDCh Vortragstagung, Fachgruppe Nuklearchemie, Berlin, 5. - 7.9.94

/4/ W. Westmeier, J. v. Aarle
PC-based high precision spectrometry
Nucl. Instr. Meth. A 439 (1990)

SPECIATION MODELLING: SOFTWARE EVALUATION

V.Brendler, H.Funke, H.Nitsche
Forschungszentrum Rossendorf e.V., Institute of Radiochemistry

In the past two decades software packages became an increasingly common tool for the modelling of complex environmental scenarios down to simple speciation problems. They can be divided into two main groups: A) Programs to compute speciations with given thermodynamic parameters, and B) programs to iterate such parameters starting from experimental data sets, most often obtained by spectrophotometric, potentiometric or extraction techniques. The second type of software necessarily contains also subroutines for the determination of species distributions, thus there is a strong relation between both types. Moreover, there is a second link between the two groups: the data bases used for modelling by group A are based on experiments by group B. Sometimes these databases come with their own management and retrieval software. There are so many different programs in use, often with high learning efforts, that it is hard for the potential end-user to judge: Which is the proper approach to solve my special application problem? To ease such decisions, the scope of this work is to determine major criteria for evaluations and to apply them to some representative software packages. We will work out their strengths and weaknesses and give recommendations as to their application.

The following programs have been available at the Institute of Radiochemistry since the end of 1994, they are listed according to the above subdivision:

A)	MTDATA /1/	VICTORIA /2/	EQ3/6 /3/	HYDRAQL /4/
	RAMESES /5/	C-HALTAFALL /6/	PHREEQE /7/	HARPHRQ /8/
	CHEMTARD /9/			
B)	SQUAD /10/	MINIQUAD85 /11/	C-LETAGROP /12/	FITEQL /13/
	PKAS /14/			

Features to be considered when evaluating speciation modelling software are:

- **!** Is the program capable of handling redox reactions, kinetic rate laws, adsorption, multiple phase equilibria ?
- **!** Which activity coefficient models are included ?
- **!** Which mathematical methods, especially minimization approaches, are applied?
- **!** How is the performance of computational speed & numerical robustness ?
- **!** Does the user have access to an internal database ? If so: Is it possible to introduce changes, exclusions, additions via input file options ?
- **!** Does the software provide graphical output or other postprocessing tools ?
- **!** Which operating system and programming language is necessary ?
- **!** Are manual and/or source code available, how can support be obtained?

Additionally, there are further features important for calculation: upper concentration limit, charge balance check, initial values, ability to cope with changes in volume,

temperature or pressure etc. Other questions arise especially for parameter iteration programs:

- What is the maximal dimension of the problem (number of species & reactions)?
- What kind of experimental data can be processed: spectrometry, potentiometry, solubility experiments, extraction, coulometry, NMR, ... ?
- Which parameters are adjustable: electrode potential, liquid junction potential, electrode drift, initial concentrations ?
- Which statistics are applied to allow judgement of the final parameter set, to determine the iteration stop criteria and to test for local minima ? And: How are uncertainties computed ?

	MTDATA	VICTORIA	EQ3/6	HYDRAQL	RAMESES	HALTAFALL	PHREEQE	CHEMTARD
Manual	X	X	X	X	X	X	-	X
Source Code	-	X	X	(X)	-	X	(X)	X
Solid Phases	X	X	X	X	(X)	X	X	X
Activity Coefficients	X	X	X	X	-	X	X	X
Adsorption	-	X	-	X	-	X	-	X
Redox	X	-	X	X	-	X	X	X
Kinetics	-	(X)	X	-	-	-	-	X
Transport	X	X	-	-	-	-	-	X
Database	X	X	X	X	-	-	(X)	-
Graphics	X	(X)	-	-	X	-	-	-
Operating System	UINX, DOS	UNIX	UNIX, DOS	DOS	DOS	UNIX,DOS	DOS	UNIX
Language	FORTRAN	FORTRAN	FORTRAN	FORTRAN	BASIC	C	FORTRAN	FORTRAN
Support	X	X	X	X	X	X	-	X

Remarks: There are other versions of the above programs available, the comparison focuses just on the software readily accessible at the Institute of Radiochemistry.

Table 1. General Comparison of Speciation Modelling Programs

A short summary for each program with regard to the research fields in radiochemistry follows, but one thing all have in common: they suffer from improper activity coefficient models for medium concentrated solutions (approx. > 0.2 molal).

- *VICTORIA* is designed for thermochemical applications with aerosol and gas specific phenomena, but not suited for aqueous solutions.
- *EQ3/6* and *HYDRAQL* can be recommended, especially for larger problems and higher precision. The actual choice will be determined by whether or not kinetics, redox reactions, surface complexation or temperature changes are important.

- **!** *C-HALTAFALL* seems to have no advantage over these programs, but it is more difficult to handle.
- **!** *RAMESES* does a good job in "quick & dirty" calculations, and is well suited for simple aqueous systems without redox aspects and solid phases.
- **!** *CHEMTARD* is the most comprehensive and powerful software, covering nearly all areas of interest, but also with a high degree of complexity and learning effort.
- **!** *MTDATA* is mainly focussed on thermochemical problems, but has a wide variety of databases (e.g. SGTE) also enabling aqueous solutions applications. With its extensive graphics capabilities it is a valuable tool too.
- **!** *PHREEQE* and *HARPHRQ* seem to be similar in scope to e.g. EQ3/6. But to judge them correctly more experience is necessary.

As for the time being, the recommended programs to evaluate stability constants from spectrophotometric and potentiometric experiments are *SQUAD* and *C-LETAGROP*, respectively. But definitely there is a need to test more programs in both fields. *EQ3/6* and *HYDRAQL* come with usable databases, but should be handled very carefully. If possible, one should check all the data entries relevant for one´s specific calculation. Errors and inconsistency are the main problems. The following conclusions are drawn:

- **!** There is neither an ideal program nor a perfect database !
- **!** The actual choice of software strongly depends of course on the kind of problem to be solved, but also on the weights of several other factors:
  - complexity of the problem
  - access to hard- and software
  - acceptable learning efforts
  - intended result postprocessing (graphics, tables etc.)
  - need for code modifications
- **!** The range of speciation computing programs is sufficient, and most of these programs are still under development. Contact has been established to the people responsible for these enhancements.
- **!** It is essential to widen the set of parameter iteration programs.
- **!** Data base evaluation should be continued and lead to an own trustworthy version, based maybe on a merging of parts of the NEA, EQ3/6, HYDRAQL and HATCHES data bases and others.

References

/1/ Davies, R.H., Dinsdale, A.T. et al.
MTDATA Handbook
National Physical Laboratory, UK, Documentation for NPL Database for Metallurgical Thermochemistry, ISSN 0143-7313, January 1989

/2/ Heames, T.J. et al.
VICTORIA : A Mechanistic Model of Radionuclide Behavior in the Reactor Coolant System Under Severe Accident Conditions
Report NUREG/CR-5545, SAND 90-0756, R3, R4, Rev1; Sandia Nat. Lab., Albuquerque, Sept. 1992

/3/ Wolery, T.J.
EQ3/6, A software package for the geochemical modeling of aqueous systems
UCRL-MA-110662 Part I, Lawrence Livermore National Laboratory, 1992
/4/ Papelis, Ch.; Hayes, K.F. and Leckie, L.O.
HYDRAQL: A program for the computation of chemical equilibrium composition of aqueous batch systems including surface-complexation modeling of ion adsorption at the oxide/solution interface
Dept. Civil Engineering, Stanford Univ., Technical Report 306, Stanford, 1988
/5/ Leung, V.W.-H.; Darvell, B.W. and Chan, A.P.-C.
A rapid algorithm for solution of the equations of multiple equilibrium systems - RAMESES
Talanta 35(1988)9,713-718
/6/ Östhols, E.
The C-Haltafall program system for equilibrium speciation calculations. Version 1.7
Royal Inst. Technology Report, TRITA-OOK-2062, Stockholm, 1994
/7/ Parkhurst, D.L.; Thorstenson, D.C. and Plummer, L.N.
PHREEQE - A computer program for geochemical calculations
U.S. Geological Survey Water-Resources Investigations 80-96, 1980
/8/ Brown, P.L.; Haworth, A.; Sharland, S.M. and Tweed, C.J.
HARPHRQ - A geochemical speciation program based on PHREEQE
UK Nirex Ltd., Nirex Safety Studies Report NSS/R188
/9/ Bennett, D.G.; Liew, S.K.; Mawbey, C.S. and Read, D.
CHEMTARD theoretical overview
DOE Technical Report TR-WSA-48, 1992
/10/ Leggett, D.J.
SQUAD: Stability quotients from absorbance data
in: Computational methods for the determination of formation constants, 159-173, Leggett,D.J. (ed.), Plenum Press, New York, 1985
/11/ Vacca, A. and Sabatini, A.
MINIQUAD and MIQUV: Two approaches for the computation of formation constants from potentiometric data
in: Computational methods for the determination of formation constants, 99-110, Leggett,D.J. (ed.), Plenum Press, New York, 1985
/12/ Östhols, E.
The C-Letagrop program system. Version 1.4
Royal Inst. Technology Report, TRITA-OOK-2051, Stockholm, 1994
/13/ Westall, J.C.
FITEQL - A computer program for determination of chemical equilibrium constants from experimental data
Dept. Chemistry, Oregon State University, Report 82-02, Corvallis, 1982
/14/ Martell, A.E. and Motekaitis, R.J.
Determination and use of stability constants
VCH, 2nd ed., New York, 1992

URANIUM SPECIATION MODELLING FOR SEEPAGE WATER

V.Brendler, M.Thieme, G.Geipel
Forschungszentrum Rossendorf e.V., Institute of Radiochemistry

We used speciation modelling to achieve a more detailed knowledge of the uranium speciation in natural waters leaching from rock piles in the former mining area in Saxony and Thuringia. In the framework of a BMFT project /1/, studies focus on the transport behaviour of radiotoxic pollutants found in rock piles and on the development of better concepts for their remediation. This work deals with the results of different model assumptions on the speciation of uranium in seepage waters. Special attention is paid to the effects of ionic strength and mineral precipitation.
Numerous samples of seepage waters from several rock piles near Schlema were analyzed for anions and cations. Table 1 summarizes the composition of a typical solution, here from rock pile 250 (pH = 7.75):

Cation	µmol / l	Anion	µmol / l
Mg^{2+}	21028	SO_4^{2-}	30208
Ca^{2+}	9850	CO_3^{2-}	2000
Na^{+}	909	Cl^{-}	310
K^{+}	410	SiO_3^{2-}	61
Li^{+}	49	NO_3^{-}	16
Fe^{3+}	47	AsO_4^{3-}	12
UO_2^{2+}	6		

Table 1: Ionic composition of representative seepage water

Two changes of the above analytical composition proved to be necessary for the modelling:

- **!** The given composition showed a charge imbalance of about 1.5 %, this was compensated by a slight adjustment of the major anion, sulphate, to 30388 µmol/l.

- **!** The reported iron content is much too high, maybe due to the presence of colloidal iron that was not removed and therefore was included in the analysis for dissolved iron. For this reason, all calculations set Fe^{+++} as to be limited by its equilibrium with Hematite Y [Fe^{+++}] = 3.617E-10 mol/l.

The ***EQ3/6*** software package /2/ was used to compute the speciation. Several different chemical models were tested to investigate the main factors controlling speciation and precipitation in the investigated aqueous solution. Fig 1. shows the uranium speciation (at thermodynamic equilibrium conditions) and the stability ranges for the precipitating minerals. A pH range from 3.5 to 9.5 was modelled by adding acid or base with pH 2 and 12, respectively. The following conclusions can be drawn from the modelling calculations:

! With decreasing acidity the following mineral paragenesis should be observed

pH 4.35 Soddyite precipitates
pH 6.69 Dolomite precipitates
pH 7.59 Talc precipitates
pH 7.81 Talc is converted into Antigorite (layered Mg silicate)
pH 7.95 Soddyite is converted into $CaUO_4$(s)
pH 9.35 Brucite precipitates (Mg hydroxide modification)

! The solution was supersaturated with respect to Dolomite and Soddyite. This can not be explained by assuming an analytical uncertainty of 10% for the appropriate carbonate or silicate contents. But definitely both minerals are not present in the actual solution, which can only be due to kinetic restraints, e.g. it is known that Dolomite is formed only during metamorphosis processes from other minerals. A total precipitation would result in a pH of 6.75.

! The solution shows a great buffer capacity, pH > 9 is hardly reachable.

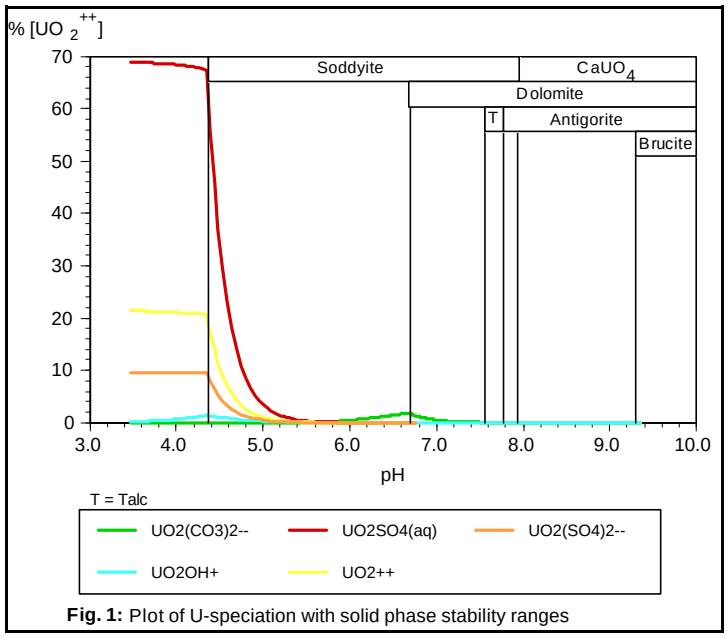

Fig. 1: Plot of U-speciation with solid phase stability ranges

In a second computation series all mineral precipitation was suppressed to obtain also the metastable uranium distribution in this seepage water. These results are shown in Fig.2 (calculated with activity coefficients according to the true ionic strength) and Fig.3 (zero ionic strength assumed).

! The proper consideration of the ionic strength is very essential. Neglecting that effect changes speciation drastically. In our calculations the DAVIES equation was applied. It is valid up to

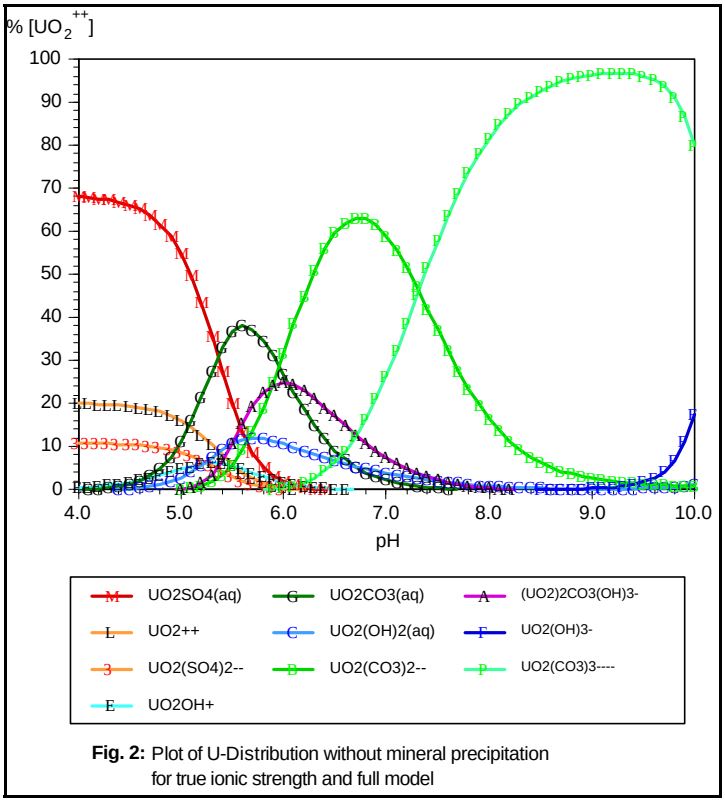

Fig. 2: Plot of U-Distribution without mineral precipitation for true ionic strength and full model

ionic strengths of 0.2 molal, the true ionic strength of the model solution (at 0.1244) lies well below that limit.

! Less critical is a reduction of the chemical model to a set only comprising the ions SO_4^{--}, UO_2^{++}, CO_3^{--} and OH . A comparison with Fig. 2 in /3/ shows that the uranium speciation is not altered significantly. Especially in the pH region of interest (6-9) this simplification gives a very good approximation of the original model containing all the other additional ions.

The existence of a reliable analytical data set is essential for speciation investigations and modelling. Further samples should be analyzed immediately after or even better during sampling because the pH, the redox state, the carbonate content and possible colloidal components are most sensitive to temperature changes and to air. They may substantially change with time. All colloidal components should be removed carefully prior to composition analysis and investigated separately. Fractions of the sample solution should be observed for a long time (under "original" T and p) to see whether they are stable toward precipitation.

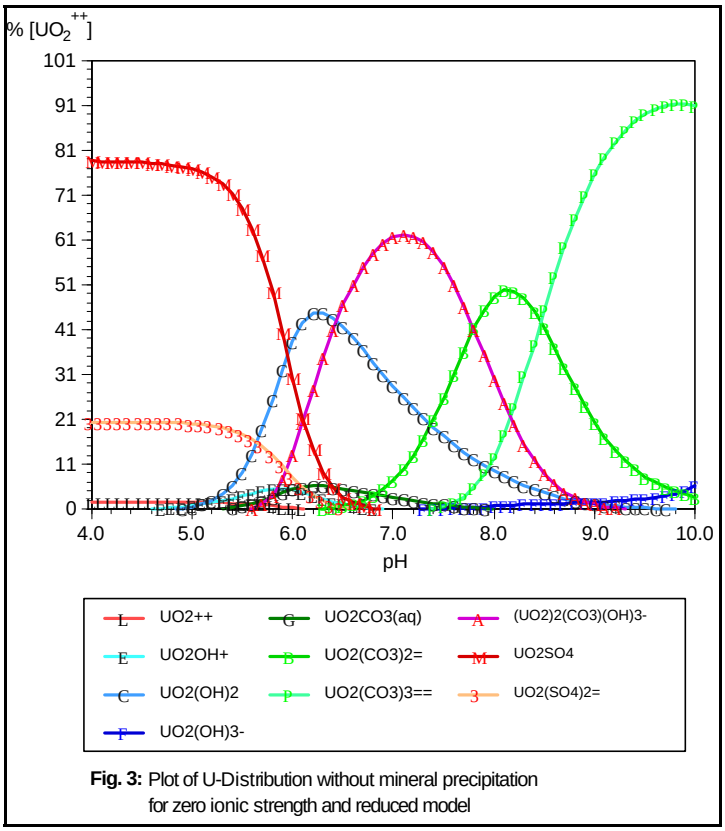

Fig. 3: Plot of U-Distribution without mineral precipitation for zero ionic strength and reduced model

An internally consistent set of thermodynamic data considering all relevant reactions is most important for successful modelling. Future modelling will also include redox reactions and adsorption processes.

References

/1/ Geipel, G.; Thieme, M. and Bernhard, G.
Untersuchungen zum Verhalten radiotoxischer Schadstoffe in Hinterlassenschaften des Uranbergbaus als Grundlage für Sanierungskonzepte.
BMFT Project 02 S 7533, Final Report, FZR, Inst. Radiochemistry, 1994

/2/ Wolery, T.J.
EQ3/6, A software package for geochemical modeling of aqueous systems
UCRL-MA-110662, Lawrence Livermore National Laboratory,1992

/3/ Thieme, M.; Nitzsche, H. and Geipel, G.
Distribution of stable isotopes of hydrogen, carbon, and oxygen in uranium-mining rock pile material and in seepage liquid.
Report FZR 43, Inst. Radiochemistry, 1993

Behavior of Colloids

DEVELOPMENT OF FILTRATION TECHNIQUES FOR THE CHARACTERIZATION OF HUMIC ACID COLLOIDS

H. Zänker, D. Wruck[1], S.I. Martin[2]
Forschungszentrum Rossendorf e.V., Institute of Radiochemistry
[1]Lawrence Livermore National Laboratory, Seaborg Institute of Transuranium Science
[2]Lawrence Livermore National Laboratory, Department of Earth Sciences

The behaviour of humic acids in aqueous solutions lies at the borderline between the behaviour of genuine physical solutions and that of colloidal solutions. The particle size distribution of humic acids has been investigated by a number of techniques, including size exclusion chromatography /1/, ultracentrifugation /2/, flow field-flow fractionation (Flow FFF) /3/, scanning electron microscopy (SEM) /4/, photon correlation spectroscopy (PCS) /4/, and ultrafiltration /5/, The results range from 200 to 100,000 Daltons for the molecular weights of the non-aggregated macromolecules. A programme to characterize humic acid particles in aqueous solutions of varying composition and to study the colloidal nature of such solutions was started at the Institute of Radiochemistry.

Particle populations of three types should be expected in a suspension of humic acid made by resuspension of dry powdered humic acid in water: the elementary particles (which are the macromolecules of the humic acid), 'micelle-like' aggregates formed by association of the dissolved macromolecules, and particles of undissolved humic acid material. As a first step, we are developing filtration techniques for the investigation of the humic acid particles. In the experiments reported here, we used polycarbonate screen filters of various pore sizes (Nuclepore Corp.; Altech Associates, Inc.) and ultrafilters of a nominal pore size of 4.1nm corresponding to a nominal molecular weight cutoff of 30,000 Daltons (Centricon-30, Amicon, Inc.). The former should retain undissolved material and possibly dissolved aggregates, the latter should also remove elementary particles of higher molecular weights. The filtrates were investigated for their contents of humic acid and submitted to other methods of particle size characterization (scanning electron microscopy, photon correlation spectroscopy).

The test material was a sample of humic acid powder made in the group of Organic Tracer Chemistry of our institute (internal label R19). Subsamples were obtained by dilution of the stock solution and filtration according to the scheme in Table 1.
The fractions of humic acid passing through the filters were determined by three methods. First, the filtrates were tested for their contents of total organic carbon (TOC) using a Model 700 O.I. Corporation TOC analyzer. The results are given in Table 2.

Then the UV light absorbances at 200nm, 210nm, and 220nm were determined by means of a 9420 UV-Visible Spectrometer, IBM Instruments, Inc. Third, the visible light absorbances were measured with a Model 200 Optical Waveguide Spectrum Analyzer from Guided Wave, Inc. (the following discussion is based on the absorbances at 450nm and 550nm).

Pore Size / Type of Filter	Concentration [mg/l]			
	0,2	2	20	400
Unfiltered	R19-0.2u	R19-2u	R19-20u	R19-400u
5000nm (Nuclepore)	R19-0.2 <5000	R19-2 <5000	R19-20 <5000	R19-400 <5000
450nm (Altech)	-	R19-2 <450	R19-20 <450	R19-400 <450
100nm (Nuclepore)	-	R19-2 <100	R19-20 <100	R19-400 <100
4.1nm (Centricon-30, Amicon, Inc.)	-	R19-2 <4.1	R19-20 <4.1	R19-400 <4.1

Table 1: Scheme of Obtaining Subsamples and of the Labels of Subsamples

Sample	TOC
R19-0.2<5000	about 0.2ppm
R19-0.2u	about 0.1ppm
R19-2<100	0.70ppm±20%
R19-2<450	1.05ppm±20%
R19-2<5000	0.70ppm±20%
R19-2u	0.85ppm±20%
R19-20<4.1	disturbed
R19-20<100	6ppm±20%
R19-20<450	6.3ppm±20%
R19-20<5000	6.5ppm±20%
R19-20u	6.5ppm±20%
R19-400	100ppm±20%

Table 2: Content of Organic Carbon

Table 3 provides a comparison of the fractions of humic acid that are still in the filtrate after the filtration through the different filters for the 20mg/l sample R19-20. The fractions are given in the form of percentages with the unfiltered sample as the "100% reference".

As it can be seen from this table, the humic acid concentrations in the filtrates decrease with decreasing filter pore size. According to the TOC analyses, as well as to the UV absorbances, the polycarbonate screen filters should remove only minor amounts of humic acid. Only the 4.1nm ultra filter seems to separate a significant fraction of the humic acid according to the UV absorbances (however, more than 60% pass even through the ultra filter according to our determination method for humic acid concentration).

Sample	Concentration [%]					
	TOC	UV Absorbance			Visible Absorbance	
		200nm	210nm	220nm	450nm	550nm
R19-20u	100	100	100	100	100	100
R19-20 <5000	100±20	99±10	99±10	98±10	91±10	88±10
R19-20 <450	97±20	100±10	98±10	96±10	73±10	60±10
R19-20 <100	92±20	94±10	90±10	88±10	61±10	44±10
R19-20 <4.1	disturbed	72±10	66±10	62±10	36±10	28±10

Table 3: Percentages of the Original Concentration of Humic Acid in the Filtrates of R19-20 After the Fitration Steps; Reference Concentration: R19-20u

The concentration determination by using the visible absorbances indicates a higher retention of the humic acid by all the filters compared to the concentration determination by using the UV absorbance. It appeares especially high for the filters of the smallest pore sizes. These different values from the UV absorbances and from the TOC results may rather be due to the well-known increase of the absorbance ratios:

$$A_{\text{lower wavelength}} / A_{\text{higher wavelength}}$$

with decreasing of the humic acid particle size /6/ than to the real retention behaviour of the humic acid.

From the TOC and the UV absorbance data can be concluded that the humic acid particles are smaller than 100 nm and that more than 60% are even smaller than 4.1 nm. This agrees with estimates in the literature assuming that the size of humic acid molecules is less than 10 nm /7/. Even 'micelle-like' aggregates have average diameters of only about 75 nm /4/.

However, the results obtained here as well as the amounts of scattered light observed during the photon correlation spectroscopic measurements that are reported in the next article /8/ indicate that small amounts of humic acid were present as bigger particles. This was confirmed by the colour of the filter membranes after the filtrations and also by scanning electron microscopic (SEM) micrographs.

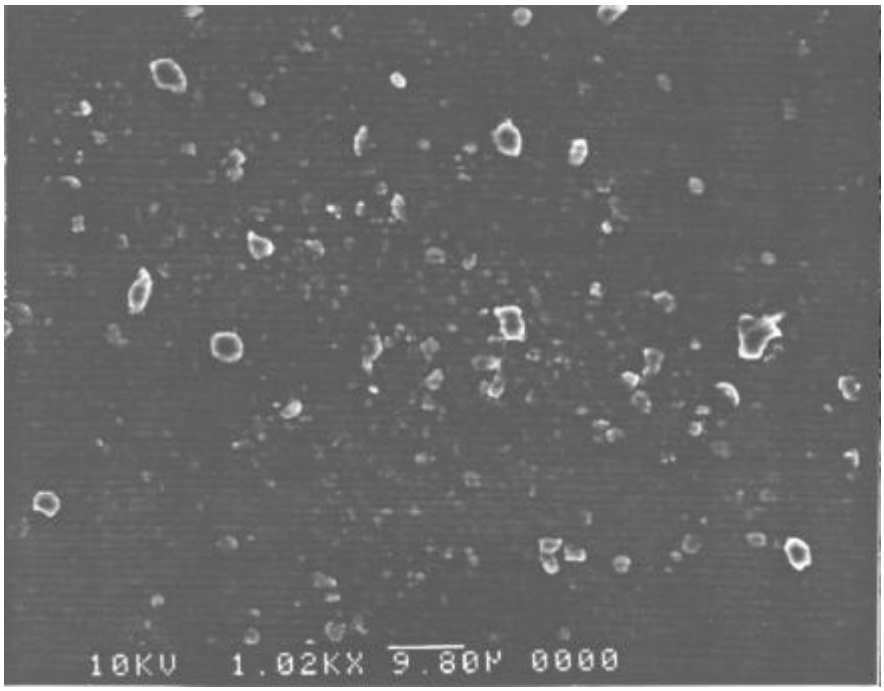

Fig. 1: SEM Micrograph of Sample R19-20<5000>100 (particles on poly-carbonate screen filter membrane) at a magnification of 1:1020

Figure 1 gives an example of an SEM micrograph. Here, subsample R19-20 was filtered through a 5000 nm filter. The filtrate was filtered through a 100 nm filter that was coated with carbon and submitted to SEM. The micrograph makes it plausible that all particle sizes between 100 and 5000 nanometers are present on the filter membrane. At least the presence of particles of sizes between about 300 nm and 5000 nm is unambiguous from the micrograph. The bigger particles are presumably rather residues of undissolved humic acid than aggregates of dissolved macromolecules.
Much experience was gained with the filtration of humic acid colloids and related techniques such as TOC analysis, UV and visible spectroscopy, and SEM. These

methods are now available in our institute and can be applied to real ecologcal systems.

References

/1/ C.J. Miles, P.L. Brezonik
High-Performance Size Exclusion Chromatography of Aquatic Humic Substances
J. Chromatogr. 259, 499 (1983)

/2/ P.M. Reid, A.E. Wilkinson, E. Tipping, M.N. Jones
Determination of Molecular Weights of Humic Substances by Analytica (UV Scanning) Ultracentrifugation
Geochim. Cosmochim. Acta 54, 131 (1990)

/3/ R. Beckett, Zhang Jue, J.C. Giddings
Determination of Molecular Weight Distributions of Fulvic and Humic Acids Using Flow Field-Flow Fractionation
Environ. Sci. Technol. 21, 289 (1987)

/4/ M.S. Caceci, A. Billon
Evidence of Large Organic Scatteres (50-200nm) in Humic Acid Samples
Org. Geochem. 15, 335 (1990)

/5/ J. Buffle, P. Deladoey, W. Haerdi
The Use of Ultrafiltration for the Separation and Fractionation of Organic Ligands in Fresh Waters
Anal. Chim. Acta 101, 339 (1978)

/6/ P. Burba and A. Abbatepaulo
Analytische Abtrennung und Anreicherung von aquatischen Huminstoffen an unterschiedlichen Kollektoren
Vom Wasser 75, 201 (1990)

/7/ R. Grauer
Zur Chemie von Kolloiden: Verfügbare Sorptionsmodelle und zur Frage der Kolloidhaftung.
Technischer Bericht 90-37.
Paul Scherrer Institut, Würenlingen und Villigen, Mai 1990

/8/ H. Zänker, D. Wruck, S.I. Martin
Testing a Photon Correlation Spectroscope Model 4700 from Malvern Instruments for the Investigation of Environmental Colloids.
This report

TESTING A MODEL 4700 PHOTON CORRELATION SPECTROSCOPE FROM MALVERN INSTRUMENTS FOR THE INVESTIGATION OF ENVIRONMENTAL COLLOIDS

H. Zänker, D. Wruck[1], S.I. Martin[2]
Forschungszentrum Rossendorf e.V., Institute of Radiochemistry
[1] Lawrence Livermore National Laboratory, Seaborg Institute of Transuranium Science
[2] Lawrence Livermore National Laboratory, Department of Earth Sciences

There are mainly three groups of colloids in natural waters: silicate colloids, oxide colloids, and colloids of humic substances. Environmental colloids with their particle concentrations of sometimes as little as a few tenths of a ppm and their particle size ranges from 1 nanometer to several microns are a special challenge to particle measuring techniques. One objective of the filtration experiments described in the previous article /1/ was to test the Malvern 4700 photon correlation spectroscope in combination with a 2W Innova 70 Argon Ion Laser (Coherent, Inc.) for its applicability in the investigation of humic acid colloids. Thus, all the subsamples described in Table 1 of /1/ were also submitted to photon correlation spectroscopy (PCS). The results of the filtering experiments in /1/ were taken as previous information for the PCS measurements.
Three parameters of the Malvern model 4700 can be varied by the operator that have influence on the results of the measurements:

(i) the laser power
(ii) the goniometer angle
(iii) the aperture of the photomultiplier.

The criterion for the selection of these device parameters is that the count rate of the scattered light shall not be too low or too high but in the so-called 'ideal' region. The

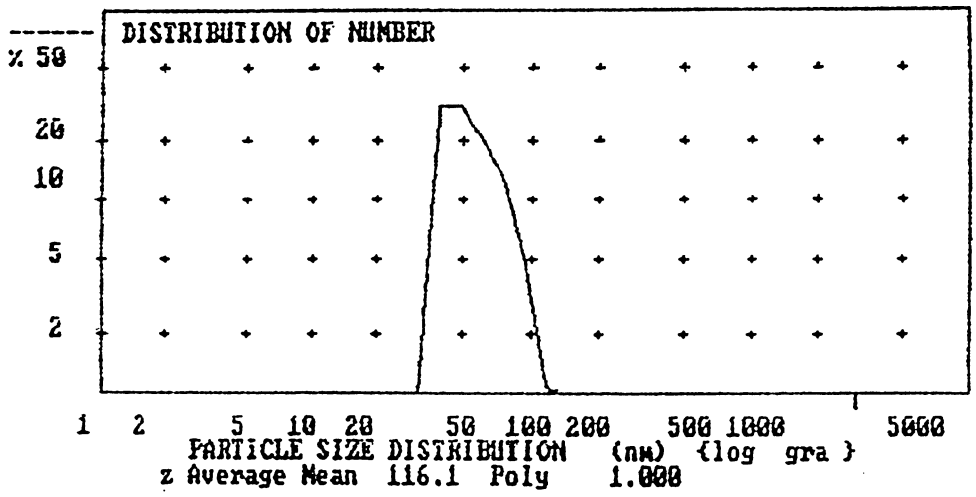

Fig. 1: Particle Size Distribution of Sample R19-400 u; Laser Power 1.6 W, Goniometer Angle 90 grd, Aperture 35 Microns

latter is indicated by the device. Thus, all parameter combinations are 'allowed' that do not result in count rates outside this 'ideal' region. The results are given in the form of histograms as shown in Figure 1 for the particle number distribution of sample R19-400u.

The results of our PCS measurements are summerized as follows:

Sample R19-400 (400 ppm of humic acid). The measurements with a high laser power (1.6 W) are more consistent than those with a lower laser power. The indicated particle size is always below 100nm for the measurements with the laser power of 1.6 W with two exceptions. There is a confusing dependence of the mean particle size on the goniometer angle in the 10 to 100 nanometer range. Not any peak in the histograms was found below 10 nm. (Most of the particles should be smaller than 10 nm according to our filtration experiments /1/.) After filtration through the 4.1 nm ultrafilter (sample R19-400<4.1), the count rate of scattered light was too low to yield meaningful results.

Sample R19-20 (20 ppm of humic acid). Here, the confusing dependence on the goniometer angle is even more distinct. The locations of the peaks in the histograms vary between 90 and 700 nm for the laser power of 1.6 W independently of the filter that was used. Not any peak was found below 90 nm. For both, the filtrates from the 4.1 nm filter and the filtrates from the 100 nm filter, the count rates of scattered light were too low at this level of humic acid concentration.

Sample R19-2 (2 ppm of humic acid). No useful amounts of scattered light could be detected for any filtrate at any laser power, goniometer angle and aperture of the photomultiplier.

Sample R19-0.2 (0.2 ppm of humic acid). No meaningful results obtainable under any condition.

The particle system submitted to PCS here, consisting of very small particles with a small portion of bigger particles of a broad particle size range, was certainly a difficult one. However, the filtration simplified the particle collective step by step. For testing the possibilities and limitations of the device, a difficult particle system is more desirable than a simple one. PCS with the Malvern Model 4700 is obviously senseless for samples of humic acid concentrations of 20 ppm or below and even for 400 ppm of humic acid the results were not conclusive. Despite the difficulties about the location of the peaks in the histograms , the most serious problem is undoubtless that the device fails at even high concentration levels.

Knowing this 'lower detection limit', we were not surprised about the results of our test measurements with more realistic environmental colloids. We investigated samples of ground water, mine water, seepage water, and river water. In such samples, colloids of all three types - silicates, oxides and humics - should be expected. Not any of these samples yielded amounts of scattered light that were high enough for obtaining correlograms (the count rate was far below the 'ideal' region).

Consequently, the Malvern 4700 can only be regarded as a useful device for measuring environmental colloids if a concentration step for the colloids is carried out before the measurement.
Such additional operations are undesirable because they are time-consuming and may alter the original system under investigation.

References

/1/ H. Zänker, D. Wruck, S.I. Martin
Development of Filtration Techniques for the Characterization of Humic Acids
This report

TESTING A MICROTRAC ULTRAFINE PARTICLE ANALYZER UPA-150 FROM LEEDS & NORTHRUP FOR THE INVESTIGATION OF ENVIRONMENTAL COLLOIDS

H. Zänker
Forschungszentrum Rossendorf e.V., Institute of Radiochemistry

As it was pointed out in the previous paper /1/, environmental colloids are an unusual challenge to any particle measuring method. Differently from more customary fields of colloid measurement as for instance those in the pharmaceutical industry, the cement industry or the food industry, the field of environmental colloids is characterized by very low particle concentrations and extremely broad ranges of particle size. Thus, the failure of Malvern 4700 described in /1/ is not too surprising.
At first glance, the Microtrac Ultrafine Particle Analyzer UPA-150 from Leeds & Northrup, which determines the Doppler shift of the scattered light (for a description see /2/), provided much more reasonable results than did the Malvern 4700 photon correlation spectroscope. A humic acid solution (sample R19, cf /1/) of a concentration of only 0.2 ppm gave a histogram with a single peak at 4 nanometers, which is well within the expected particle size range of the humic acid macromolecules of 1 to 10 nanometers /3/. At a concentration of 20 ppm, small further peaks at 12 nm, 150 nm and 250 nm were found in addition to the 4 nm peak of the macromolecules or "elementary particles". The existence of such minor rough fractions was known from our filtration experiments /4/. Thus, the results from the UPA-150 were very plausible. The only open question was the so-called 'loading index' of the UPA-150, which was extremly low for the two samples of humic acid and far away from the region recommended by the producer of the device. The 'loading index' is a measure of the intensity

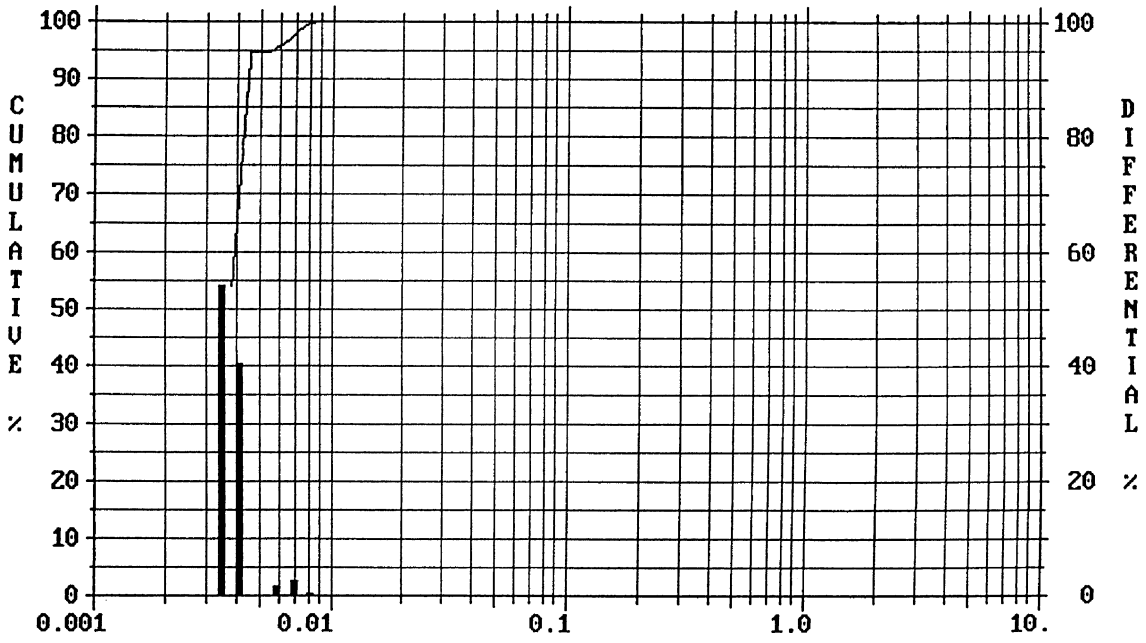

Fig. 1: Particle size distribution in a sample of Milli Q water (Particle size in µm)

of scattered light and thus for the particle concentration. It is similar to the 'count rate' of the Malvern 4700. In other words, also for the UPA-150 the question is crucial if it is capable of measuring low colloid concentrations. Therefore, the response of the UPA-150 to various colloids of low concentrations was tested.
First, Milli Q water (Millipore Corp.) was investigated to gain some experience about the behaviour of the device for waters that are really extremely low in particles. No scattering light photometer existing in the world should be able to find meaningful particle size distributions for extremely particle-free waters like Milli Q water. Figure 1 gives an example of the histograms obtained for Milli Q water. 14 consecutive measurements on samples of Milli Q water yielded the following results:

(i) all the 14 histograms show a large peak with a maximum between 3.5 and 6 nm

(ii) 10 of the histograms show a very small additional peak at 7 to 8 nm.

Surprisingly enough, the device produces peaks in the histograms even for the extremly particle-free Milli Q water. Very similar results were found for ordinary

Konzentration (ppm)	Number of Peaks	Location of Peaks (Nanometers)	
500	2	300	2500 (very small)
100	2	300	720 (very small)
50	2	300	6000 (very small)
10	2	300	3500 (very small)
5	2	500 (small)	3500
5	1	1000	
1	2	8 (very small)	450
0,5	3	7	400, 6000 (very small)
0,5	2	7	5000 (very small)
0,2	1	7	
0,2	1	1000	
0,1	1	5	
0,05	2	3,5	7 (very small)
0,01	2	3,5	7 (very small)

Table 1: Location of Peak Maxima in the Histograms for 304 nm Polystyrene Latex Particles

distilled water, which contains more particles than Milli Q water, but is still very low in particles. The 'loading index' was below 0,0008 for both, the samples of Milli Q water and the samples of distilled water.
Second, a population of standard particles (polystyrene latex particles of a diameter of 304 nm; Duke Scientific Corp.) of varying concentration was tested. The aim was to determine the lower concentration limit of reasonable response of the UPA-150 to particles of ideal properties (spherical, monodisperse etc.). This limit should be taken as a best-case approximation for the lower limit of reasonable response for the non-ideal environmental colloids (non-spherical, polydisperse, transparent etc.). A summary of the results is given in Table 1.
As it can be seen from this table, the particle size is nearly perfectly indicated by the device for particle concentrations of $ 10 ppm. Below this limit, the histograms become very contradictory. The 'loading index' at this borderline was about 0.0400.
Considering this 'limit of reasonable response' for standard particles, the histograms for real environmental colloids, which were obtained in a third step, were not too surprising. Samples of ground water, mine water, seepage water, humic acid of varying concentration and water of the river Elbe were tested (with filtration steps and without filtration). The 'loading index' was far below 0,0400 for all these samples. All the peaks found in the histograms had maxima below 10 nanometers. Figure 2 gives an example for seepage water. The similarity between this histogram and that of the Milli Q water (Figure 1) can be seen easily. All the peaks in the histograms of those low-concentrated samples are obviously phantom peaks. They seem to be produced by the data processing in the device and have nothing to do with the particles in the samples.

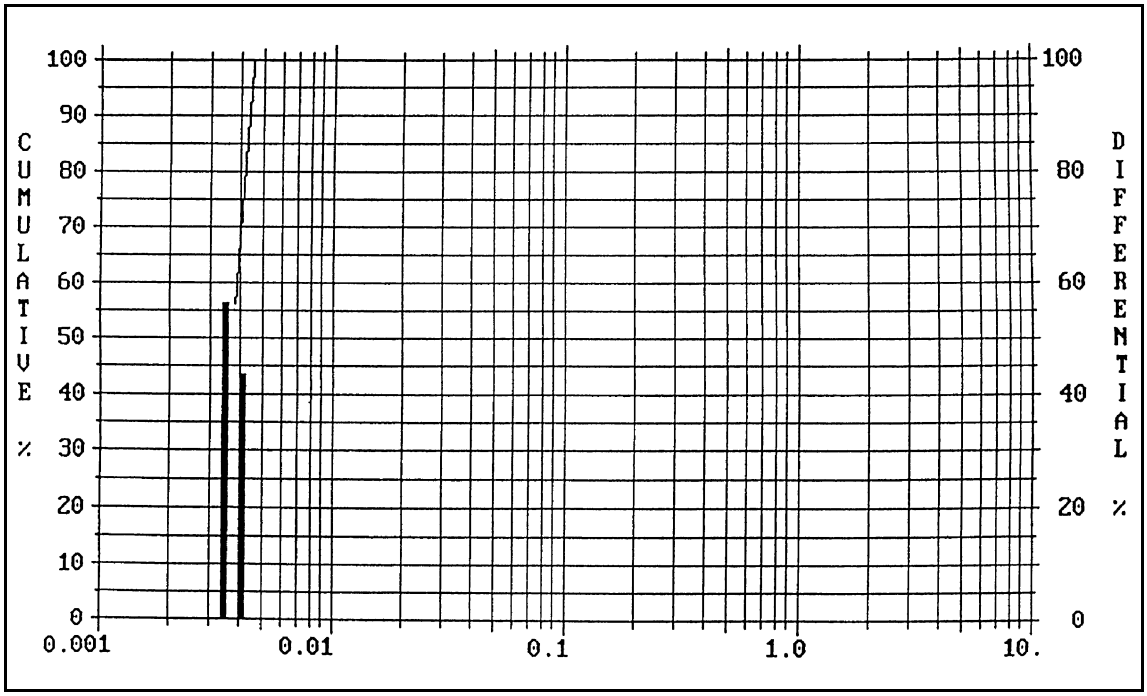

Fig.2: Particle Size Distribution in a Sample of Seepage Water
(Particle size in µm)

Thus, the UPA-150 does, like the Malvern 4700, not seem to be a useful device for the investigation of environmental colloids unless the disadvantages of concentrating the colloids before measurement are tolerated.

References

/1/ H. Zänker, D. Wruck, S.I. Martin
Testing a Model 4700 Photon Correlation Spectroscope from Malvern Instruments for the Investigation of Environmental Colloids.
This report

/2/ M. Weber
Betriebserfahrungen bei der Partikelgrößenmessung im Nanometerbereich mittels dynamischer Lichtstreuung,
Chem.-Ing.-Techn. 66, 707 (1994)

/3/ R. Grauer
Zur Chemie von Kolloiden: Verfügbare Sorptionsmodelle und zur Frage der Kolloidhaftung.
Technischer Bericht 90-37. Paul Scherrer Institut,
Würenlingen und Villigen, Mai 1990

/4/ H. Zänker, D. Wruck, S.I. Martin
Development of Filtration Techniques for the Characterization of Humic Acids.
This report

Interaction of Radionuclides with Organic Matter

ISOLATION OF MINE-WATER DISSOLVED ORGANIC SUBSTANCES

L. Baraniak, G. Schuster, G. Bernhard
Forschungszentrum Rossendorf e.V., Institute of Radiochemistry

Among the remediation activities in the uranium mining districts, the controlled flooding of the big mines plays an essential role. There is a long-term danger of contamination of neighboring and underlying groundwater tables by radioactivity (U, Th, Ra etc.) and toxic metals (As, Cr, Ni, Mn). To investigate the influence of organics on the chemical speciation of these contaminants, dissolved organic matter (DOC) was separated from flood water of the biggest uranium mine in the western part of the Erzgebirge /1/.

The separation and concentration of the DOC was carried out by a gentle chemical operation which ensures that the organic material is damaged as little as possible by the isolation procedure. Therefore, we selected the adsorption of the DOC from about 15 l acidified mine water (pH 2) on an exchange column (430x16 mm i.d.) that was filled with the hydrophobic, non-ionic ethylvinylbenzene-divinylbenzene copolymer Wofatit EP 61 (a macroporous /$20 nm/ Amberlite XAD analogon with a high specific surface: $600 m^2/g). The fractional desorption was carried out with diluted $NaClO_4$ and NaOH solutions (10 mMol/l). This treatment avoids the use of organic solvents and the disadvantageous polyelectrolyte lyophilization.

UV spectra at 220 and 254 nm showed that this DOC separation from the mine water has a yield of more than 85 per cent. The weakly adsorbed organic substances (about one third) were in the neutral $NaClO_4$ elution fraction (5x50 ml colourless and slightly iridescent solution). All the other stronger bound organics were in the NaOH fraction (6x50 ml light brown solution).

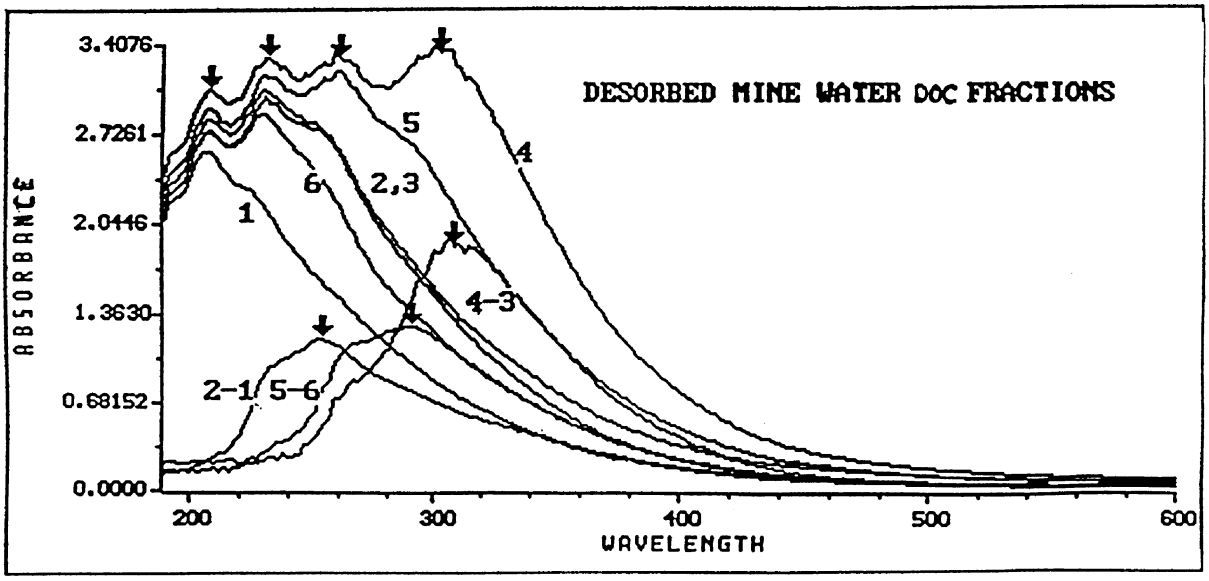

Fig. 1: Single and Difference UV Spectra of the Alkaline Eluent Fractions. The numbers at the spectra refer to the sample numbers of Tab. 1.

The spectra (Fig.1) revealed a successive appearance of 4 maxima at 208, 232, 260 and 302 nm. The comparison of the spectra with the DOC content (Tab.1) shows a proportionality between the band broadening and the DOC concentration. That is surprising because the characteristic change in the band shape should be attributed to different organic compounds.

Sample No.	1	2	3	4	5	6
DOC [ppm]	51	144	330	380	236	120
PEC [meq/g]	8	26	17	19	17	27

Tab.1: DOC Content and H^+ Exchange Capacity (PEC) of the Alkaline Eluent Fractions

The mean H^+-exchange capacity amounts to 19 meq/g, about 4 times as much as for aquatic humic acids /2/.

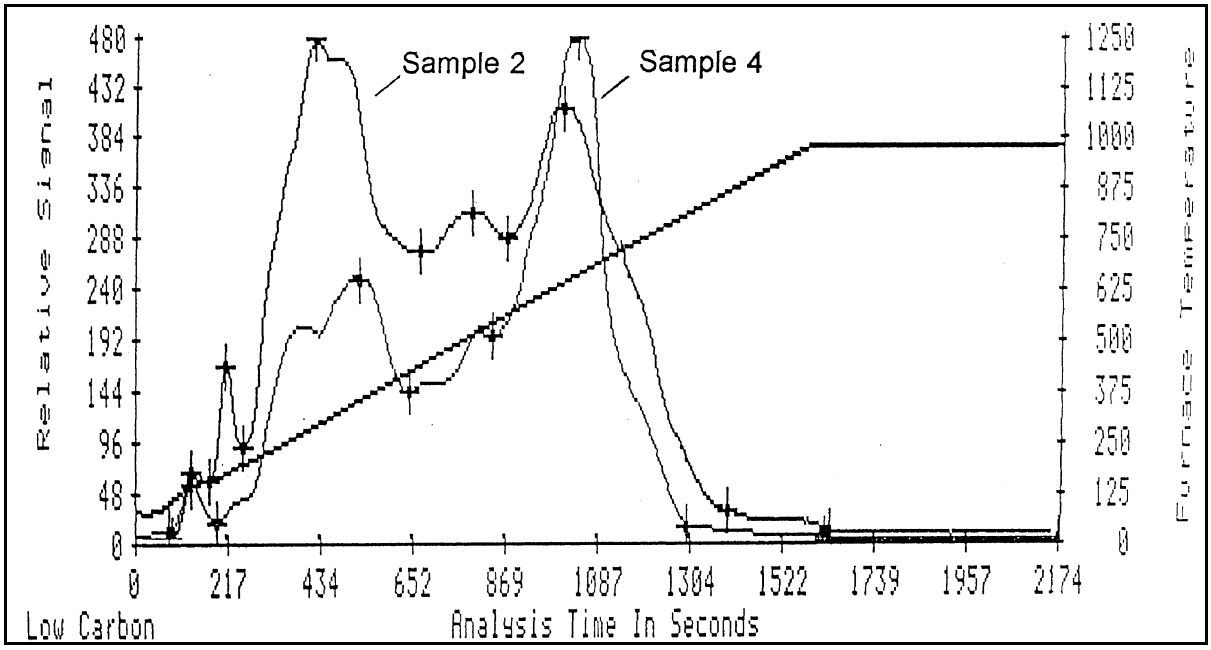

Fig. 2: Thermoanalysis of DOC Fractions

Oxidative thermoanalysis (Fig.2) revealed the predominance of compounds rich in hydrogen and oxygen in the early fractions (first peak at 350 °C) and substances with a more stable carbon structure in the later eluents (high-temperature peak). According to Schnitzer et al. /3/ this should be an indication for the presence of both cellulose material, that can be easily oxidized to more resistant lignins, giving evidence of other sources of organic matter as at the earth surface, underlying the natural degradation, for instance the wood of the mine pit props.

References:

/1/ G.R. Choppin,
Radiochim. Acta 58/59, 113 (1992)

/2/ J.I. Kim, D.S. Rhee, G. Buckau,
Radiochim. Acta 52/53, 49 (1991)

/3/ M. Schnitzer, J. Hoffmann,
Geochim. Cosmochim. Acta 29, 859 (1965)

LASER-INDUCED PHOTO ACOUSTIC SPECTROSCOPY STUDY OF THE INTERACTION OF U(VI) WITH MINE-WATER-DISSOLVED ORGANIC SUBSTANCES

L. Baraniak, G. Geipel, G. Bernhard, H. Nitsche
Forschungszentrum Rossendorf e.V., Institute of Radiochemistry

We investigated the influence of dissolved organic compounds (DOC) from mine drainage water on the chemical species of radionuclides. The DOC was separated from the flood waters of an uranium mine in Schlema, Saxony. The complexation behaviour of the isolated material with U(VI) was studied by laser-induced photoacoustic spectroscopy (LIPAS).

The DOC was isolated by adsorbing the organic material on a hydrophobic resin from the acidified mine water (pH#2) followed by a fractional elution with $NaClO_4$ and NaOH solutions of increasing concentration /1/.

Two different sample series were prepared by mixing a solution of DOC with uranyl perchlorate. Each series had a constant DOC amount of 7.1 ppm and 5.7 ppm, respectively (corrsponding to $1.42 \cdot 10^{-4}$ M and $1.14 \cdot 10^{-4}$ M acidic functional groups) and varying uranyl ion concentrations from $6.5 \cdot 10^{-5}$ M to $1.14 \cdot 10^{-4}$ M. The solutions' pH was adjusted to a constant value between 5.5 and 6.0.

The spectra of the DOC-uranyl-complex species were recorded from 410-445 nm using a stilben laser. The photoacoustic signals were sampled from 100 laser shots at each wave-length point with a resolution 0.1 nm.

The complex formation constant was calculated from the concentration dependency of the U(VI) signal. As a first approximation, no U(VI) hydrolysis was considered /2/.

pH	5.54	5.63	5.68	5.81	5.84	5.94
log K_c	3.415	3.204	3.255	3.230	3.633	4.045

Tab. 1: Mean Conditional Complex Formation Constant of U(VI) with Mine Water DOC in Dependence on the pH

The results given in Tab.1 show a stability constant in the pH range 5.5-5.8 with a log $ß_1$ value of 3.28±0.09. At higher pH values of 5.84 and 5.94, the complex stability increases to 3.63 and 4.05, respectively. The magnitude of the complex stability agrees with the findings of Higgs et al. for uranyl complexation with DOC from the Drigg's aquifer (Cumbria, UK) /3/. They found values for log $, between 3.42 and 3.74 for solutions with a pH from 5.24 to 5.40 (I = 0.01 M).

Acknowledgements

The measurements were carried out at the G.T. Seaborg Institute of Transactinium Science, Lawrence Livermore National Laboratory (LLNL), Livermore, CA. We want to thank R.J. Silva, C. Palmer and D. Wruck for the possibility of measuring our samples at the LLNL photoacoustic spectrometer and for their support during the experiments.

References

/1/ L. Baraniak, G. Schuster, G. Bernhard
Isolation of Mine-Water Dissolved Organic Substances
this report

/2/ D.A. Schurig, G.L. Klunder, M.A. Shannon, R.E. Russo, R.J. Silva
Signal Analysis of Transients in Pulsed Photoacoustic Spectroscopy
Rev. Sci. Instrum. 64, 363 (1993)

/3/ J.J.W. Higgo, D. Kinniburgh, B. Smith, E. Tipping
Radiochim. Acta 61, 91 (1993)

SQUARE-WAVE AND CYCLIC VOLTAMMETRY OF THE U(VI)-HUMATE COMPLEX

M. Schmidt, L. Baraniak, G. Bernhard, H. Nitsche
Forschungszentrum Rossendorf e.V., Institute of Radiochemistry

Environmental radionuclide transport via aquatic pathway is strongly influenced by dissolved organic compounds (DOC), mainly macromolecules, such as humic and fulvic acids, polysaccharides and lignins. In order to investigate the complexation of U(VI) with different DOC fractions, a preliminary examination using square-wave and cyclic voltammetry was carried out to determine the interaction of U(VI) with humic acid.

Square-wave voltammograms of pure humic acid (HA) solution in 0.1 M $NaClO_4$ supporting electrolyte at pH=4 show no reduction peak in the range from 0.05 to -0.8 V vs. SCE. Solutions of uranyl ion at the same conditions show a reduction wave with a maximum at -0.13 V vs. SCE. The signal increases linearly with increasing uranium concentration. Up to 0.2 mmol/l U(VI) the slope amounts to $1.86 \cdot 10^{-3}$ A· l/mol.

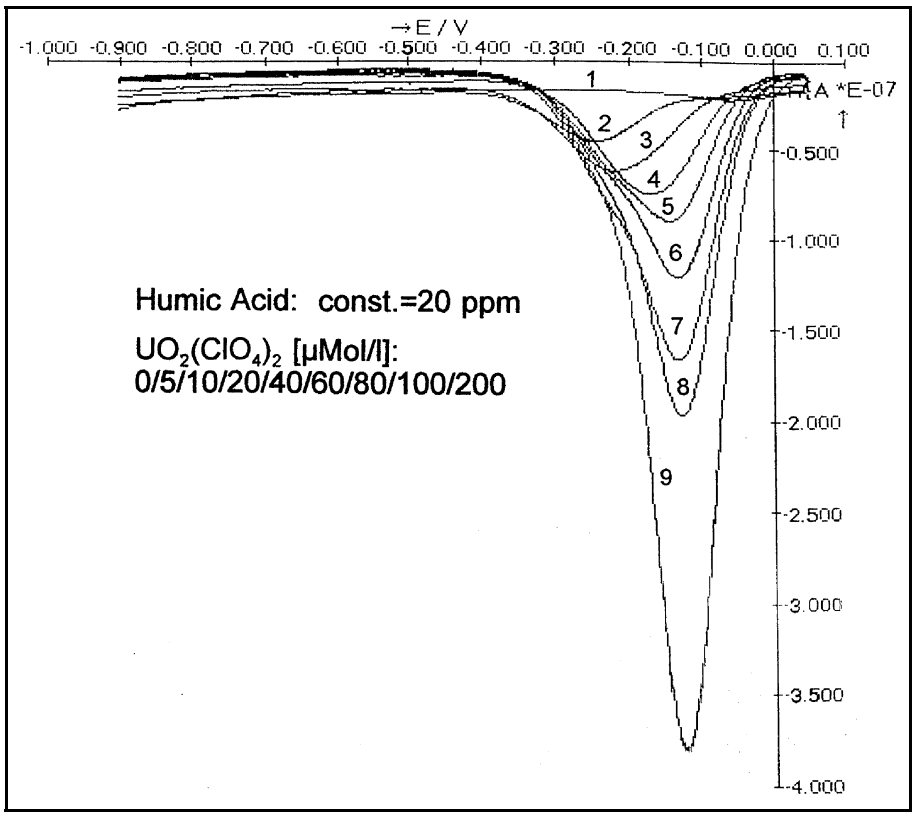

Fig. 1: Square-Wave Voltammograms of humic acid solutions with increasing amounts of U(VI)

When a constant concentration of 20 ppm of humic acid is present, the addition of increasing amounts of U(VI) produces a peak that shifts from about !0.25 V to a constant value of !0.13 V vs. SCE (Fig.1). The resulting current too is also proportional to the U(VI) concentration with a slope of $5.60 \cdot 10^{-3}$ A· l/mol up to about 10 µmol/l.

The sensitivity of determining this complex can be enhanced by a pre-accumulation step on a hanging mercury drop. Using this method Mlakar /1/ determined the complex in the sub-µmolar level (detection limit $5 \cdot 10^{-9}$ mol/l).

From these results, the maximum amount of U(VI) that can be bound to the HA was determined as $(5\text{-}6) \cdot 10^{-2}$ µmol U(VI)/µmol H^+ or to $(0.27\text{-}0.32)\,10^{-3}$ mol/g (using the

proton-exchange capacity /PEC/ of 5.3±0.15 meq/g). This means that only 10-12 % of the HA's PEC was available for the complexation of U(VI). Czerwinski et al. /2/ found 18.5 % in a laser-spectroscopic study.

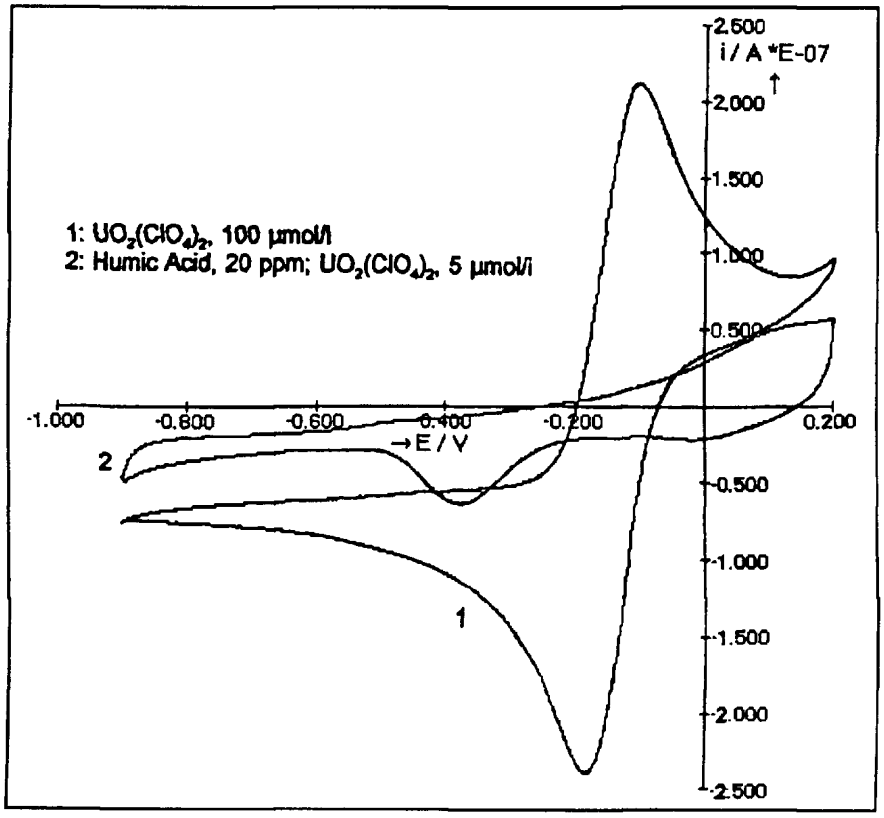

Fig. 2: Cyclic voltammograms of U(VI) solutions (5 µmol/l) in 0.1 m $NaClO_4$ at pH=4

The cyclic voltammograms (Fig.2) are quite different for the U(VI)-humate complex and the uncomplexed U(VI). For free U(VI) we find distinct anodic and cathodic peaks indicating a reversible electrode reaction. Furthermore the peak height increases linearly with the square root of the scan rate /3/. In the curve of the uranyl humate complex, however, only the reduction peak at -0.38 V vs. SCE occurs, indicating a completely irrversible electrode reaction.

Acknowledgements

This study was supported by Sächsisches Ministerium für Wissenschaft und Kunst under contract No. 4-7541.83-FZR/402.

References

/1/ M. Mlakar
Anal. Chim. Acta 276, 367 (1993)
/2/ K.R.Czerwinski, G. Buckau, F. Scherbaum, J.I. Kim
Radiochim. Acta 65, 111 (1994)
/3/ R. Djogic, M. Branica
Anal. Chim. Acta 281, 291 (1993)

CAPILLARY ELECTROPHORESIS FOR A "FINGER-PRINT"-CHARACTERIZATION OF FULVIC AND HUMIC ACIDS

S. Pompe, K.H. Heise, H. Nitsche
Forschungszentrum Rossendorf e.V., Institute of Radiochemistry

Fulvic and humic acids play a key role in the migration and retardation of heavy metals in the environment. Depending on their origins and the conditions prevailing during their formation, fulvic and humic acids have different structural, physical and chemical properties. This opens the possibility for developing a "finger-print"-catalogue for fulvic and humic acids of different origins, based on these features.

The objective of our work is the characterization and separation of fulvic and humic acids by capillary electrophoresis, which is suitable because of the polyelectrolytic properties of humic substances /1,2,3,4/. We use capillary zone electrophoresis for the investigation of fulvic and humic acids. This method is characterized by short analysis times, selectivity to the analytes and high resolution. Separations take place in uncoated capillaries (fused silica).

The sample material investigated consisted of the humic acid standards "Suwannee River" (sample A) and "Laurentian River" (sample B), the commercially available humic acids from FLUKA (sample C) and ALDRICH (sample D), a humic acid extracted from a loess soil /5/, originating in the region near Halle, Germany (sample E) as well as the standard fulvic acids "Suwannee River" (sample F) and "Laurentian River" (sample G). Solutions were prepared by dissolving the solid samples in 10^{-3} M NaOH, p.a. (MERCK). The investigations were carried out with the capillary electrophoresis system P/ACE 2050 from BECKMAN Instruments.

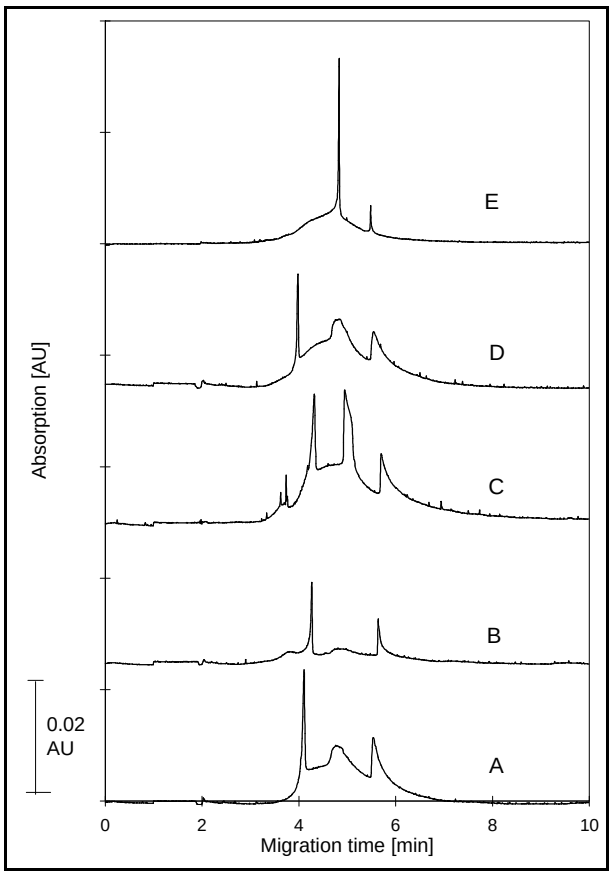

Fig. 1: Electropherograms of the investigated natural humic acids
Capillary: fused-silica 75 µm i.d. x 50 cm; buffer: KH_2PO_4 (3 mM)-$Na_2B_4O_7$ (6 mM), pH 8.9; injection: 70 nl; temperature: 30°C; voltage: 30 kV; detection: 214

The migration behavior of molecules in the capillary zone electrophoresis depends on their charge/size-ratio. If two humic acids exhibit the same behavior in the electric field, then they are likely to have a comparable charge/size-ratio. Differences in the intensity of the background, the electrophoretic mobility and absorption behavior are established by structural and

chemical differences resulting from the differing origins of the humic acids.
Figure 1 shows the electropherograms of the humic acids (samples A to E). All humic acids, except the humic acid from loess soil (sample E), show three sumperimposed peaks on a broad background. These peaks cannot presently be assigned to any substances. The humic acid from loess soil only shows two peaks in its electropherogram. It is remarkable that humic acids A and D exhibit comparable electrophoretic behavior. The first peak of humic acid A is more pronounced than the one in D. A possible reason for this behavior is that humic acid A contains a larger amount of this component. Due to this similar migration behavior, humic acids A and D may posses an approximately similar size as well as a similar number of dissociated carboxylic groups, which are the charge carriers of humic acids under the given conditions.
The electropherograms of humic acids B and C stand in clear contrast to the others and show dissimilarities compared to one another. These observations are caused by differences in the charge/size-ratios of the individual fractions.
The differences in the absorption behavior, visible in the electropherograms of the different humic acids at same concentrations, point to variations in the aromatic carbon content, the presence of a different number of UV-active groups or variations in the concentration of the individual fractions. The cause of these differences are founded in the presence of different precursor substances and/or unequal conditions during the humification, which are characteristic for a specified origin.
The electropherograms of the investigated fulvic acids (sample F and G) are represented in Figure 2. There are marked differences in the migration behavior and in the absorption intensity between fulvic and humic acids having the same origin. It is known that fulvic acids have a higher content of carboxylic groups and a smaller molecular weight than humic acids stemming from the same source /6/. These features are reflected in their migration behavior in the electric field. The smaller absorption intensity of fulvic acids in comparison to that of humic acids signifies their having a smaller aromatic carbon content.

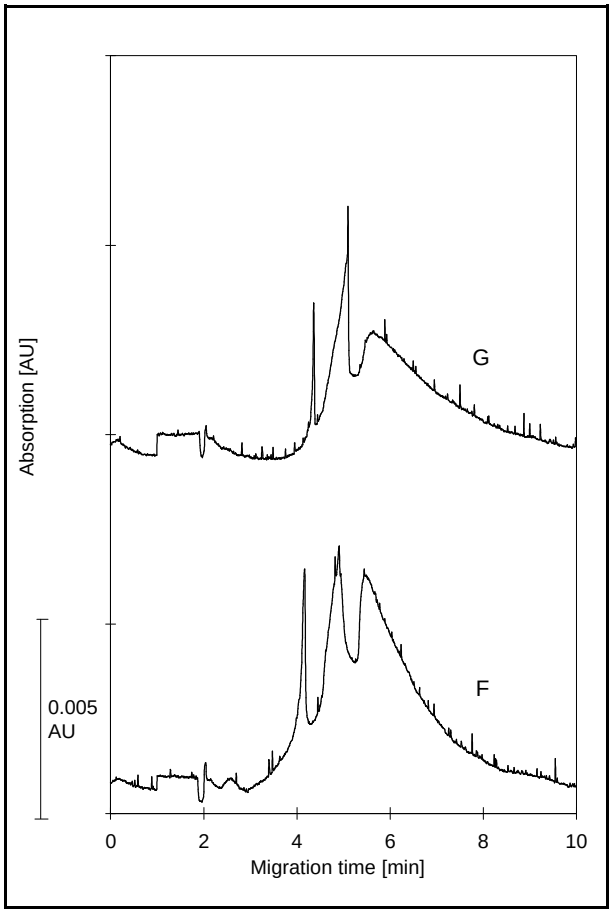

Fig. 2: Electropherograms of the investigated fulvic acids
Conditions: fig. 1

We conclude that the investigated humic and fulvic acids from different origins exhibit

characteristic electropherograms under the applied conditions, which appear suitable for a "finger-print" characterization of these substances based on their functionality (charge/size-ratio). Further investigations are underway to confirm these results and to identify the individual peaks. We also want to study, if the interaction behavior of these acids with radionuclides and heavy metals can be predicted by means of their "finger-print"-electropherograms.

Acknowledgment

We thank Dr. van Loon (PSI Villigen) for providing the fulvic and humic acid standards.

References

/1/ Flaig, W., Beutelspacher, H., Rietz, E.
Soil Compounds Vol.1 "Organic Components"
Ed. J.E. Gieseling, Springer Verlag 1975, p. 31

/2/ Duxbury, J.M.
Humic Substances II
Eds. M.H.B. Hayes, P.M. Carthy, R.L. Malcolm, R.S. Swift
John Wiley&Sons Ltd., 1989, p. 600

/3/ Rigol, A., López-Sánchez, J.F., Rauret, G.
Capillary zone electrophoresis of humic acids
Journal of Chromatography A 664, 301 (1994)

/4/ Kopácek, P., Kániansky, D., Hejzlar, I.
Characterization of humic substances by capillary isotachophoresis
Journal of Chromatography 545, 461 (1991)

/5/ Stevenson, J.F.
Methods of Soil Analysis, Part II
Ed. C.A. Black, 1965, Madison, Wisconsin, p.1409

/6/ Schnitzer, M.
Environmental Biogeochemistry, Vol. 1
Ed. J.O. Nicagu, 1976, Ann Arbor Science, p. 89-92

THERMOANALYTICAL INVESTIGATIONS ON THE CHEMICAL CONSTITUTION AND THE OXYDATIVE DECOMPOSITION OF THE NATURAL HUMIC COMPOUNDS

G. Schuster*, M. Bubner, K. H. Heise
Forschungszentrum Rossendorf e.V., Institute of Radiochemistry
* WIP of TU Dresden

The aim of this thermoanalytical investigations on humic compounds is their qualitative identification (fingerprints) and to find quantitative relations to chemical and structural datas, especially those which are connected with the complex formation with cations of nuclides of the nuclear decay series of uranium.
The measurements were made with a TG, DTA thermoanalyzer (Setaram STA 92) together with a DSC[1)] and a thermoanalytically working ir carbon and water analyzer (Leco RC 412). The sensitivity of the thermobalance is 1µg and of the DSC 15 µWs, that of the Leco is 0.02% for carbon and 0.1% for water. The samples were powdered, the heating rate in the TA was 5 dg/min and in the Leco 25 dg/min, the gas atmosphere was streaming oxygen.
The genesis of humic compounds in the nature is characterized by a stepwise carbonisation and oxidation process /1/.

$$\text{Wood} \xrightarrow[\text{Demethanisation}]{\text{Dehydratisation}} \text{Lignin} \xrightarrow[\text{Demethanisation}]{\text{Oxidation}} \text{Humic Acid} \xrightarrow[\text{Demethanisation}]{\text{Oxidation}} \text{Fulvic Acid}$$

The results of measurements on this substances are shown in table 1. Going from wood to fulvic acid the carbon content arises, the hydrogen content decreases and the oxygen content is first lowered by the loss of many aliphatic OH groups and then increased by the formation of higher oxidyzed groups like carboxylic groups, in agreement with the scheme above. The bonding capacity for metal cations therefore increases in this turn.

Tab.1: Analytical results to the genesis of humic compounds (related to dry pure organic substances, oxygen values as difference to 100%)

Sample	C[%] mass	H[%] mass	O [%] mass	H:C mol	O:C mol	O:C+H mol
Wood (yew)	51.12	5.51	43.37	1.29	0.64	0.28
Lignin (oak)	63.8	6.09	30.1	1.15	0.32	0.16
Hum.ac.(Aldrich)	64.74	4.98	30.3	0.92	0.35	0.18
Fulv. ac.(Laur.)	63.0	3.12	33.9	0.59	0.40	0.25

The DTA curves of the four substances show a principal similar structure. All they have an endothermic peak of drying up to 150 ^{o}C, a first exothermic peak of oxidation from 150-350^{o}C, which represents according to IR measurements /1/ the release of OH groups, the degratation of carboxylic groups and the oxidation of reactive aliphatic and alicyclic groups. That means, that all proton exchanging places like carboxylic

groups and phenolic OH groups are degradated in this first oxidation peak. The second oxidation peak from 350-450°C involves the oxidation of the residual compact carbon structure, which either is a initial part of the substances or is formed during the reaction. The thermoanalytical and analytical values of the single peaks can be used for the estimation of the kind and the amount of the oxidized groups. In table 2 are shown the results of the measurements of the oxidation enthalpies and the mass changes for the humic and fulvic acid Laurentian

Tab. 2: Thermoanalytical comparison of humic and fulvic acid

Sample/Peak	T_i [°C]	T_f [°C]	TG) m/g	) H/g [J/g]	) H/) m[J/g]
Humic ac. Laur. (at all)	171	500,4	1,0	-11234,9	-11234,9
Peak 1	171	313,1	0,465	-4307,3	-9263,0
Peak 2	313,1	500,4	0,535	-7260,5	-13571
Fulv. ac Laur. (at all)	169,9	581,3	1,0	-6471,4	-6471,4
Peak 1	169,9	361,6	0,482	-1857,8	-3858,5
Peak 2	361,6	581,3	0,519	-4613,6	-8897,6

The higher) H values for the the complete oxidation points at a higher oxidation level of the fulvic acid. An approach was made to calculate the difference of the carboxylic groups between Laurentian fulvic and humic acid. From table values was accounted the reaction enthalpy for the oxidation of a methoxylic to a carboxylic group :

$$-CH_2OH + O_2 \text{ -----> } -COOH + H_2O \quad -489 \text{ KJ/mol= -489 J/mequ} \qquad (1)$$

The difference between the measured values for the first peak of oxydation of Laurentian humic and fulvic acid is:

$$)H^*_{\text{Hum. ac.}} -)H^*_{\text{Fulv. ac}} = -2449.5 \text{ J/g} \quad * = \text{value for the first peak} \qquad (2)$$

(for this approach unchanged were taken the) H, measured at peak temperature)

Tab. 3: Analytical results of the Aldrich humic acid and its Na-humate (values of the dry organic substance, without Na)

Sample	C[%] mass	H [%] mass	O [%] mass	res.% mass	H:C mol	O:C mass	Na^+ mequ/g
Na-humate	79.1	6.6	14.3	26.2	0.99	0.14	5
Humic acid	64.7	5.0	30.3	0	0.92	0.35	-

From the equ. 1 and equ. 2 a difference of 5 carboxylic groups results according this estimation. In /1/ a value of 6 was determined by IR measurements for the difference of carboxylic groups of humic and fulvic acid.
Further investigation dealt with the influence of chemical treatment on humic substances. Already in /2/ was written that the usual treatment of the humic acids with NaOH and HCl essentially changes the thermoanalytical curves. This was also found by light absorption spectrometry in /3/. To check this thermoanalytically, measurements were made on Aldrich humic acid and its Na salt.

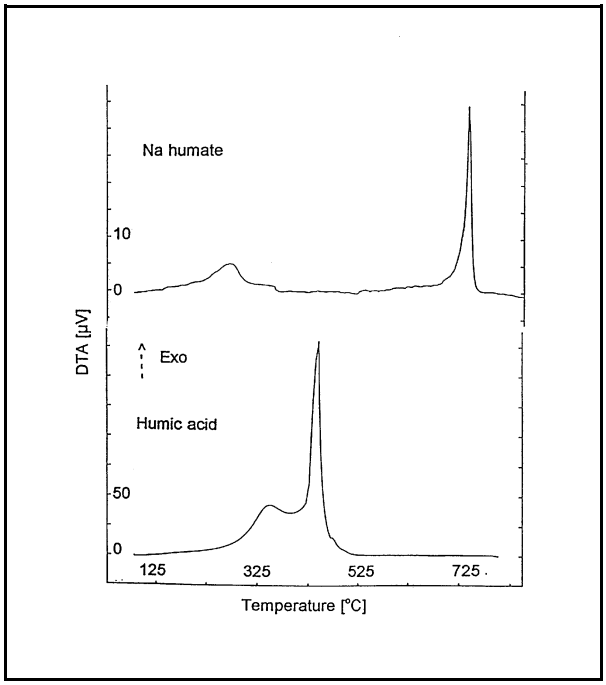

Fig. 1: DTA curves of Aldrich humic acid and its Na-humate

The thermoanalytical curves for this acid and his Na-salt, shown in fig 1; demonstrate a big difference. For the salt the difference between the two oxidation peaks is much larcher and the temperature for the second peak is much higher. From 26.2% unoxidable residue (table 3), the number of the bonded Na^{+} ions was accounted to 5 mequ/g humic acid. In /1/ the content of proton exchanging places was determined by IR to 5 for a huimic acid. That in the Na-humate the hydrogen content is not lowered and the carbon content is increased can be caused by the fragmentation by NaOH [3]. Such changes of the thermoanalytical characteristics are also reported in /4/ for Al^{+++}, Fe^{+++} and some mono- and divalent metall ions. It is to see there, that the differences in the thermoanalytic curves are bigger for higher valent ions.

[1)] Thermoanalytical shortenings: TG - Thermogravimetry, DTG - Differential thermogravimetry, DTA - Differential thermoanalysis, DSC - Differential scanningcalorimetry

References

/1/ M. Schnitzer, J. Hoffmann
Termogravimetry of Soil Humic Compounds
Geochimica and Cosmochimica Acta 29, 859 (1965)

/2/ G. Schuster, M. Bubner, K.H. Heise
Thermoanalytical Investigations on Humic Compounds
Report FZR 43, 25, (1994)

/3/ A. H. Khairy, W. Ziechmann
Influence of the Conc. of the Hu. Ac. on their Fragmentation in Alcaline Solutions
Z. Pflanzenernähr. Bodenk. 145, 600 (1982)

/4/ M. Schnitzer
Reactions betw. Fulv. Ac., a Soil Hum. Comp. and Inorg. Soil Constituents
Soil Science Soc. Am. Proceedings 33, 75 (1969)

THERMOANALYTICAL INVESTIGATIONS ON THE SYNTHESIS, CHEMICAL CONSTITUTION AND OXYDATIVE DEGRATATION OF HUMIC COMPOUNDS

G. Schuster*, S. Pompe, R. Jander, K.H. Heise
Forschungszentrum Rossendorf e.V., Institute of Radiochemistry, *WIP of TU Dresden

Because of the large variety of natural humic compounds there is a need for the development of synthetic model substances for humic materials. Their structure and chemical constitution can be controlled via synthesis thus allowing more reproducible results when used for investigation on the formation and migration of complexes of cations of the decay series of Uranium with humic compounds. One way for this synthesis is the condensation of amino acids with sugars /1/ like phenylalanine with glucose (JM-) and Xylose (POM series), which were investigated in the present work. The subject of this work is the thermoanalytical control of the synthesis products to ascertain the preparation of an analytical reproducible substance with thermoanalytical similarities to the natural humic compounds. The experimental details are described in /2/. The DTA curve of the reaction product shows, that the characteristic of phenylalanin was completely lost in contrary to that of the glucose. Already the original picture of the glucose DTA curve shows similarities to that of the humic compounds, and that is also the case for the reaction product. Obviously the carboxylic group of the reactive phenylalanin is bound at the resulting macromolecule whose structure is strongly influenced by the saccharid structure of the glucose. How it is to see in tab. 1 at the same time the hydrogen and oxygen content are decreased and the carbon content is increased. That means, that the reaction represents a accelerated carbonisation process.

Tab. 1: Comparison of the measured analytical values of the synthesized humic acids with those of the natural humic compounds*

Sample	C[%] mass	H[%] mass	O[%] mass	H:C mol	O:C mol	O:C+H mol
Synth.POM 2	69.5	6.73	23.8	1.16	0.25	0.12
Synth.POM 4	68.3	6.55	25.1	1.15	0.28	0.13
Synth.JM 3	64.3	5.82	29.9	1.09	0.35	0.17
Synth.JM 4	66.5	5.48	28.1	0.99	0.32	0.16
Hu.ac. Aldrich	64.7	4.98	30.3	0.92	0.35	0.18
Hu.ac.from peat	68.8	5.72	25.5	1.0	0.32	0.14
Lignin (oak)	63.8	6.09	30.1	1.15	0.35	0.16
Fulv.ac. Laur.	63.0	3.12	33.9	0.59	0.40	0.25
Glucose	42.5	7.18	50.3	2.03	0.89	3.41

* Values of dry, pure organic substance; oxygen is accounted as difference to 100 %

The analytical values, represented in table 1, show a distinct relations between the

samples of the synthetic JM series and the lignin oak, and between the synthetic Pom series and the humic acid extracted from peat. The humic acid Aldrich and the fulvic acid Laurentian are more carbonized and have a lower hydrogen and a higher oxygen content. This simularities are also found in the thermoanalytical curves shown in fig. 1 as DSC curves. Clearly similar are the additional exotherm peaks of the Pom samples and the humic acid from peat. That peak is caused by a more compact carbon structure, which either is in this substances from the beginning or is formed during the oxydation reaction. Like it is explained in /1/ in table 2 is given a comparison of the H:C values of single peaks of some synthetic and natural humic compounds. The synthetic humic substances of the Pom series have a relative low H:C value in the low temperature oxydation peak and a relative high in the second oxydation peak. That means, that the content of reactive hydrogenrich aliphatic groups is low and of more resistent alicyclic groups is higher. At the JM series the latter fact is not relevant. Here the H:C value of the second oxydation peak is much lower and is in the region of the natural humic compounds, for which a low hydrogen content is typically for the atomic groups, oxidized at higher temperatures.

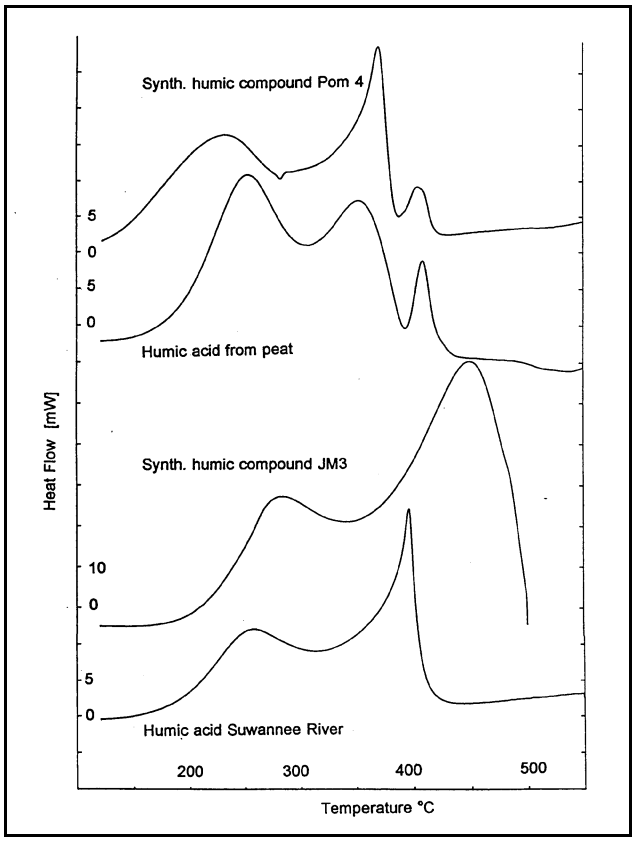

Fig. 1: Comparision of DSC curves of synthetic and natural humic compounds

Tab. 2: Hydrogen - carbon relations of the peaks in the thermoanalytical oxydation curves

Peak	H:C POM 4	H:C JM 4	H:C Hu.ac. Aldrich	H:C Hu.ac Torf	H:C Laur. Fulv. ac.
Moisture	10.5	75	50,4	57.7	68.5
1.Oxyd. Peak	1,17	1,68	0,51	2.0	1,33
2.Oxyd. Peak	0,75	0,35	0,88	0,34	0,41

References

/1/ L.C. Maillard
Annales de Chimie (Paris) 5, 258 (1916)

/2/ G. Schuster, M. Bubner, K.H. Heise
this report

OPTIMIZATION OF THE CONDITIONS OF THE [^{14}C]BENZIDINE CHLORINATION FOR [^{14}C]POLYCHLORINATED BIPHENYLS (PCB) SYNTHESIS AND GASCHROMATOGRAPHIC ANALYSIS

M. Bubner, M. Meyer, R. Jander, K.H. Heise, M. Matucha[1]
A. Pacakova-Kubatova[2]
Forschungszentrum Rossendorf e.V., Institute of Radiochemistry
[1] Academy of Sciences of the Czech Republic, Institute of Experimental Botany
[2] Academy of Sciences of the Czech Republic, Institute of Microbiology

Our synthesis strategy /1/ for the synthesis of selected uniformly ^{14}C-labelled PCB-congeners, starting from [U-^{14}C]benzidine (1), has been examined. The focus of this work was on the the chlorination of acetylated [U-^{14}C]benzidine (2) leading to the intermediate key product for [^{14}C]PCB synthesis and the identification and quantitative determination of the congeners. Since the synthesized congeners are only slightly soluble inl solvents, measuring the chlorinated derivatives of 2 by TLC or HPLC is difficult. The analysis of the intermediate and final products of our synthesis route can be considered to be representative for chlorinated diacetylbenzidines. The PCB´s have been identified and determined quantitatively by capillary gas chromatography with mass detector (GC-MS) and electron capture detector (GC-ECD), respectively.

1. Synthetic approach of [^{14}C]PCB

To optimize conditions for selected PCB-syntheses, the concentration of precursor 2 was 1 mmol of 2 in 10 mL acetic acid. With chlorsuccinimide as the reagent, the reaction temperature was 115°C and the reaction time 1h. Using elemental chlorine the temperature was 130°C with a time of 1 to 3 h. The amount of chlorosuccinimide and the reaction time of chlorination with elemental chlorine were varied.
After deacetylation and diazotation, the chloro substituted 2 was converted to [^{14}C]PCB by the Sandmeyer reaction with chloride and the elimination of the diazonium group. ´The relationships between the chloroderivatives of 2 and the corresponding PCB-congeners are presented in Tab 1.

Tab. 1: Synthesis of PCB-congeners from chlorinated N,N'-diacetylbenzidine

Chlorinated Benzidine	Resulting PCB´s	
	by Sandmeyer-Reaction No.*)	by Elimination No.*)
benzidine	15	biphenyl
3-chloro-benzidine	37	2
3,3'-dichloro-benzidine	77	11
3,3',5-trichloro-benzidine	126	36
3,3',5,5'-tetrachlorobenzidine	169	80

*) Ballschmiter Number

Table 2 shows the results from the variation of conditions for the chlorination of 2.

Tab. 2: Variation of the conditions for chlorination of 1mmol diacetylbenzidine and the resulting PCB Composition

Chlorinating Reagent	mmol	Resulting PCB´s by Sandmeyer Reaction		by Elimination	
		No.*)	%	No.*)	%
Chlorosuccinimide	2,4	77	70	11	30
		37	30	2	60
				biphenyl	10
Chlorosuccinimide	5	77	100	11	96
				36	4
Chlorosuccinimide	8	77	100	11	90
				36	10
Chlorosuccinimide	16	77	70	11	65
		126	20	36	18
		169	5	80	16
Elemental Chlorine (reflux for 1 hour)	excess	37	30	2	30
		126	50	36	50
		169	10	80	20
Elemental Chlorine (reflux for 3 hours)	excess	126	20	36	30
		169	80	80	70

*) Ballschmiter number

The PCB yield obtained by the two methods (Sandmeyer reaction and elimination) is qualitatively equivalent However, the composition of the PCB-congeners from chlorinated diacetylbenzidine is reaction dependent. This may be due to the PCB isolation technique.

The results indicate monochlorination of 2 in acetic acid with chlorosuccinimide on the aromatic ring at 3 - and 3' - position is favoured over further chlorination at the 5 - position. Neither PCB No. 81 (chlorine in the 3,4,4',5-position) nor PCB No.14 (chlorine in the 3,5-position) has been recovered. PCB No.11 and 77 may be obtained under definite chlorination conditions with chlorosuccinimide in relatively pure form. In order to obtain PCB No. 2 and 37 in pure form, one must apply isolation and separation procedures.

Chlorination with elemental chlorine preferentially yields 3,3',5-trichloro- and 3,3',5,5'-tetrachlorobenzidine. This method is useful for the synthesis of PCB No. 36 and 126 and No. 80 and 169, respectively.

2. Congener-specific analysis of PCB-mixtures by capillary gaschromatography

Compared with the industrial produced PCB-mixtures with high congener yield such as Arochlor, Clophen, and Delor, the ^{14}C-labelled products obtained by previously described routes contain only a few congeners. No more than 3 congeners are to be expected. The products from our syntheses do not contain any position-isomers simplifying analytical approaches. We have correlated retention data published /2/ for all 209 congeners and retention data obtained using a limited number of standards and the same type of GC-MS column /3, 4/.
For selective ion monitoring with GC-MS the mass numbers 188 and 190 for mono-, 222 and 224 for di-, 256 an 258 for tri-, 290 and 294 for tetra-, 324 and 328 for penta-, 360 and 362 for hexa-, 394 and 396 for hepta-, 426 and 428 for octa-, 464 and 466 for nona- and 498 and 500 for deca-chlorobiphenyl were chosen.

References

/1/ M. Bubner, K.H. Heise
Report FZR - 43, 36 - 38 (1993)
/2/ M.D. Mullin et al.
Environm. Sci. Technol. 18, 468 - 476 (1984)
/3/ A. Pacakova - Kubatova
Diploma - thesis, Charles University Prague (1994)
/4/ J. Krupcik et al.
Chromatographia 35, 410 - 418 (1993)

^{3}H,^{14}C-DOUBLE-LABELLING OF POLYCHLORINATED BIPHENYLS (PCB)-CONGENERS

M. Bubner, M. Meyer, K. H. Heise, K. Fuksova[1], M. Matucha[2]
Forschungszentrum Rossendorf e.V., Institute of Radiochemistry
[1]Charles University, Prague, Medical Faculty
[2]Academy of Sciences of the Czech Republic, Institute of Experimental Botany

Our research on the behaviour of PCB has two aspects. One is the investigation of PCB in actual ecosystems and the natural degradation of this xenobioticum, including parameters influencing its microbiological decline /1,2,9,12,13/. The other is the uptake, accumulation, biotransformation and the toxic impact of PCB on plants and animals via the food chain /3,7,8,10/.

In both cases it is essential to observe the qualitative and quantitative changes of this organic chemical in very complex organic systems. This is only possible with the aid of isotopic labelled substrates. An established method is the examination using ^{14}C-labelled PCB- congeners /3,5, 6,15/.

The identification of the biotransformation products is difficult due to the diversity of degradation products /3,4,5,11/, their complexation behaviour, and the biological speciation. Double-labelling of the PCB-molecule with a uniform distribution of ^{14}C, specific position substitution by ^{3}H, and determining the transformation products $^{3}H/^{14}C$ ratio may provide information about the primary oxidative enzymatic attack at the PCB-molecule. Time consuming reference material isolation and identification can therefore be eliminated. The aim of the synthetic work was the double labelling (^{3}H, ^{14}C) of PCB by selective dehalogenation of bromo-chloro-[^{14}C]biphenyls (Fig. 1).

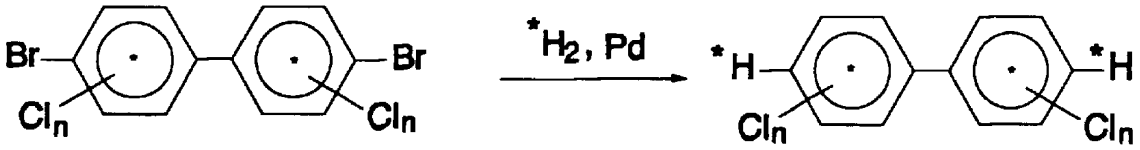

Fig. 1: Selective debromination of bromo-chloro-biphenyls

The double labelling work presents two problems. The first is the development of a method for selective substitution of Br by ^{3}H in bromo-chloro-aromatics (o-, m-and p-bromo-chloro-benzene). The second is the synthesis of bromo-chloro substituted biphenyls (3,3'-dichloro-4,4'-dibromo-biphenyl, 4-bromo-4'chloro-biphenyl).

The simultaneous debromination and hydrogenation of o-, m- and p-bromo-chlorobenzene by 10% Pd on $BaSO_4$ as catalyst resulted in 90% yield. The conversion reaction times were 40 min for p-bromo-chlorobenzene and 60 min for o- and m-bromo-chlorobenzene. The products were analysed by GC-MS (Tab. 1).

Tab. 1: Synthesis of chlorobenzene by hydrogenation of bromo-chlorobenzene

precursor bromochlorobenzene	chlorobenzene[%]	benzene[%]	remaining precursor[%]
ortho	99	<<1	<<1
meta	95	<5	<1
para	90	<5	<5

The Sandmeyer-reaction with bromide /14/, using chlorinated benzidines and chlorinated aminobiphenyls, was successful for the synthesis of bromo-chloro-biphenyls as precursors for the specific ^{3}H-labelling of PCB-congeners. The purity of the bromo-chloro-biphenyls substantially depends upon the purity of the precursor. The product purity was examined by GC-MS. The relationship of chlorinated benzidine-derivative to the ^{3}H-labelled final product ([^{3}H]PCB) is given in Tab. 2.

Tab. 2: Synthesis of precursors for ^{3}H-labelling of PCB in 4-position

Precursor amine	Product of the Sandmeyer-reaction with bromide	^{3}H-labelled final product
benzidine	4,4'-dibromo-biphenyl	[4,4'-^{3}H]biphenyl
3-chloro-benzidine	3-chloro-4,4'-dibromo-biphenyl	3-chloro-[4,4'-^{3}H]biphenyl (PCB No. 2)
3,3'-dichloro-benzidin	3,3'-dichloro-4,4'-dibromo-biphenyl	3,3'-dichloro-[4,4'-^{3}H]biphenyl (PCB No. 11)
4-chloro-4'-amino-biphenyl	4-chloro-4'bromo-biphenyl	4-chloro-[4-^{3}H]biphenyl (PCB No. 3)

References

/1/ K. Ballschmiter et al.
Chemosphere 5, 367 - 372 (1976)
/2/ R. Baxter, D. Sutherland
Environ. Sci. Technol. 18, 608 - 610 (1984)

/3/ C. Bock
Diplomarbeit, TU Braunschweig, 8 - 15 (1994)
/4/ J.M. Butler et al.
Bull. Environ. Contam. Toxicol. 49, 821 - 826 (1992)
/5/ M. Goto et al.
Chemosphere 4, 177 - 180 (1975)
/6/ W. Greb et al.
Bull. Environ. Contam. Toxicol. 13, 424 - 432 (1975)
/7/ W. Heeschen, A. Blüthgen
Schriftenreihe des Bundesministerium für Ernährung, Landwirtschaft und Forsten, Reihe A: Heft 418
Landwirtschaftsverlag GmbH, Münster, 15 - 43 (1993)
/8/ O. Hutzinger et al.
J. Assoc. Offic. Anal. Chem. 57, 5 (1974)
/9/ W. Klein, I. Weisberger
Bull. Environ. Contam. Toxicol. 12, 237 - 250
/10/ F. Korte
Lehrbuch der Ökologischen Chemie
Thieme Verlag (1992)
/11/ I. Lee, J. Fletcher
Plant Cell Reports 11, 97 - 100 (1992)
/12/ D. Pal et al.
Res. Rev. 74, 45 -98 (1980)
/13/ B. Streit
Lexikon der Ökotoxikologie
VCH Verlag, Weinheim, 1. Aufl.
/14/ M. Bubner, K.H. Heise
Report FZR - 43, 36 - 38 (1993)
/15/ P. Moza et al.
J. Agric. Food Chem. 27, 1120 - 1125 (1979)

Application of X-Ray Absorption Spectroscopy

STRUCTURAL ANALYSIS OF $(UO_2)_2SiO_4 \cdot 2H_2O$ BY XRD AND EXAFS

H. Moll, T. Reich, W. Matz[1], G. Bernhard, H. Nitsche, D. K. Shuh[2], J. J. Bucher[2], N. Kaltsoyannis[2], N. M. Edelstein[2], A. Scholz[1]
Forschungszentrum Rossendorf e.V., Institute of Radiochemistry
[1] Institute of Ion-Beam Physics and Material Research
[2] Chemical Sciences Division, Lawrence Berkeley Laboratory, Berkeley, USA

The aim of this work was to determine the structural parameters of hydrous uranyl silicate by X-ray powder diffraction (XRD) and extended X-ray absorption fine structure analysis (EXAFS).

Samples of $(UO_2)_2SiO_4 \cdot 2H_2O$ were synthesized according to Ref. /1/. XRD measurements were performed with the Universal-Röntgen-Diffraktometer (URD 6, Freiberger Präzisionsmechanik) in Bragg-Brentano geometry with CuK" radiation (0.1542 nm). Diffractograms were recorded in the 22 range from 8° to 60°. Indexing of all peaks of the diffraction pattern was possible according to the orthorhombic structure of uranyl silicate reported in the literature /2-6/. The space group is Fddd.
Uranium L_{III}-edge EXAFS spectra were recorded in transmission mode in the energy range from 16.9 - 18.2 keV at the Stanford Synchrotron Radiation Laboratory (SSRL, BL 4-3). The energy scale was calibrated relative to the first inflection point of the L_{III} absorption edge (17.166 keV) of a 0.2 M UO_2Cl_2 solution. E_0 was assumed to be 17.185 keV.
The smallest contributions from additional phases were detected in samples synthesized with 0.1M solution of Na_2SiO_3. The largest contributions were observed in samples synthesized with 1M solution of Na_2SiO_3 (see also /1/). The main component of all samples is uranyl silicate. In the pattern of all samples, peaks appear that can not be assigned to the crystal lattice. Samples of the highest purity show only one clear additional Bragg peak at 22 . 10.2° (d . 0.88 nm), as well as some indication of peaks just above the background level. The unidentified reflections can not be assigned to ingredient chemical reagents or to other compounds containing U, Si, and/or O compiled in the JCPDS data base /6/. It can be seen from Fig. 1

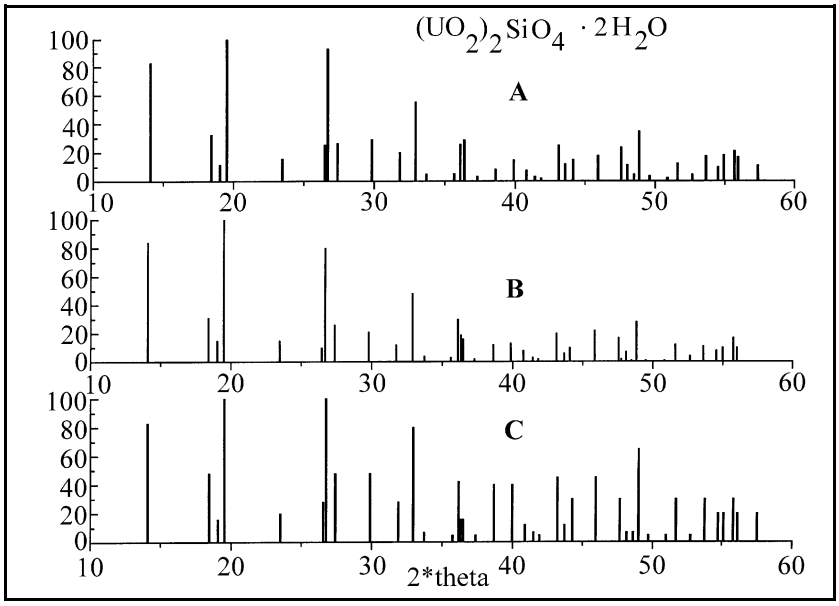

Fig. 1: X-ray diffraction pattern of synthetic soddyite by different authors; A: this work; B: Legros et al. /2/; C: Kuznetsov et al. /4/.

that our XRD data agree well with values published in the literature. Most of our integral intensities are in the range of literature values /2, 4/, coming closest to the results of Ref. /2/. The calculation of lattice constants of our sample yielded the following values:

a = 0.8306(3) nm b = 1.1245(6) nm c = 1.8622(8) nm V = 1.7393(23) nm^3

Our a- and b-values obtained in the routine analysis of all samples vary in the range of ±0.0025 nm and the c-values in the range of ±0.002 nm. There was no clear correlation between lattice constants and sample purity. In general, the lattice constants agree with the values published in Refs. /2, 4, 7/. After twelve months, a sample showed no change in its XRD pattern, indicating that the compound remains stable under ordinary conditions for long periods of time.

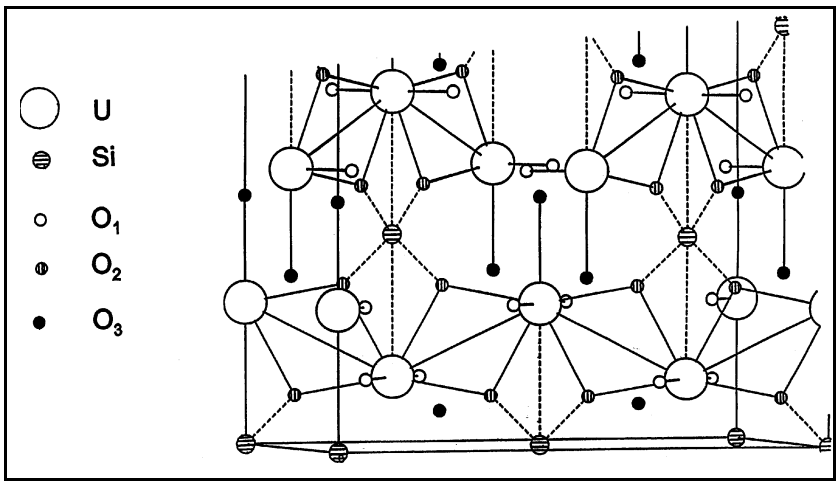

Fig. 2: Fragment of the cell of $(UO_2)_2SiO_4 \cdot 2H_2O$

According to the XRD measurements, the uranium atom in $(UO_2)_2SiO_4 \cdot 2H_2O$ is surrounded by two axial oxygen atoms, O_1, and five oxygen atoms in the equatorial plane, O_2 and O_3 (Fig. 2). The atoms O_2 are part of SiO_4-tetrahedra which are bound to the uranium. O_3 is the oxygen atom of the crystal water.

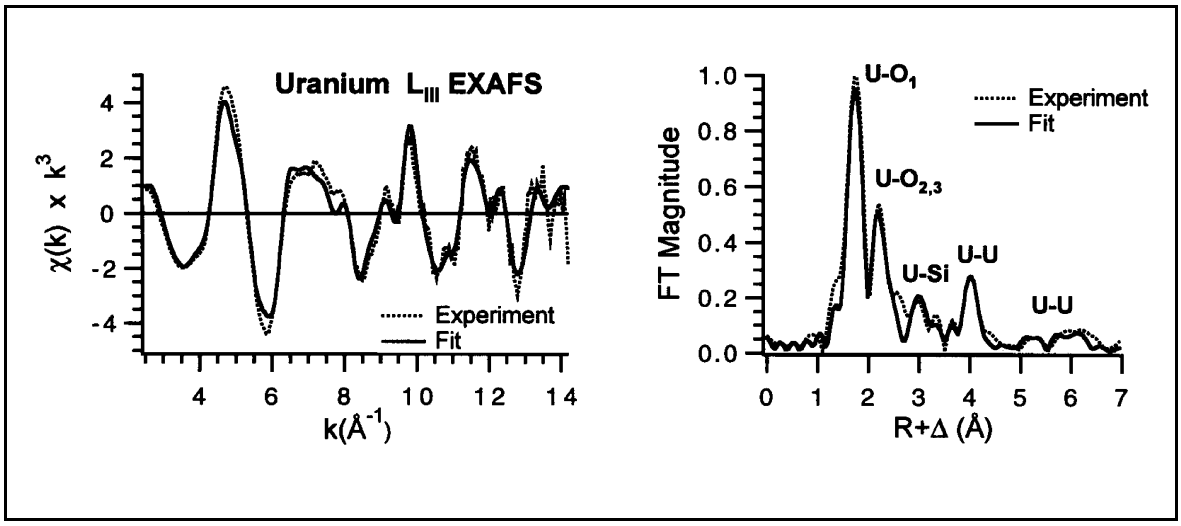

Fig. 3: Left panel: EXAFS spectrum of $(UO_2)_2SiO_4 \cdot 2H_2O$, right panel: Fouriertransform (magnitude) over the k-range of 2.5 - 14.2 Å

This local structure of the uranium atoms give rise to the observed oscillations in the U L_{III} EXAFS and to the peaks in its Fourier transform (Fig. 3). The main peaks centered at 1.8, 2.4, 3.1, and 3.9 Å in the Fourier transform correspond to the U-O_1, U-$O_{2,3}$, U-Si, and U-U absorber-backscatterer pairs, respectively. To fit the EXAFS curve, the absorber-backscatterer distance, R_i, and the mean square deviation in $_iR$, $_iF$, were varied. The coordination number, N_i, was fixed according to the results of the XRD analysis. Scattering amplitudes and scattering phases were calculated with the code FEFF /8/ in the single-scattering approximation. The results of the fit are given in Tab. 1. All features of the experimental EXAFS curve are reproduced well by the fit (see Fig. 3). The backscatterers Si and O at R_i > 3.5 Å (coordination shells 4,6, and 8) contribute less than 1% to the EXAFS. Structural parameters for these light elements in higher coordination shells cannot be determined without a priori knowledge of their presence. It is interesting to note that in a well-ordered structure, U scatterers can be determined up to R = 5.8 Å at room temperature. It was impossible to obtain a good fit by including only lighter elements like Si or O in the 5th coordination shell instead of U. The values of F_i given in Tab. 1 correlate well with the distribution of the elements over a distance range as measured by XRD. For example, the 5 equatorial atoms O_2 (2.31, 2.40 Å) and O_3 (2.34 Å) cannot be resolved by EXAFS and appear in the Fourier transform as one peak at 2.36 Å with a larger F_i than for the first O_1 shell. Based on the agreement of the R_i values determined by EXAFS and XRD measurements, we conclude that the theoretical scattering amplitudes and scattering phases calculated by FEFF can be used for an accurate R_i determination. This is especially important when experimental scattering amplitudes and scattering phases are unavailable.

Tab. 1: Summary of EXAFS and XRD results on uranyl silicate.

Shell	Absorber-backscatterer	N_i *)	EXAFS		XRD
			F^2_i (Å^2)	R_i (Å)	R_i (Å)
1	U-O_1	2	0.003	1.79	1.79
2	U-$O_{2,3}$	5	0.009	2.36	2.31, 2.34, 2.40
3	U-Si	1	0.002	3.13	3.15
4	U-Si	2	0.02	3.88	3.80
5	U-U	2	0.002	3.89	3.86
6	U-$O_{1,2,3}$	20	0.04	4.37	4.12 - 5.05
7	U-U	2	0.01	5.13	5.13
8	U-$O_{1,3}$	10	0.01	5.66	5.30 - 5.71
9	U-U	4	0.008	5.82	5.82

*) Kept constant during the fit.
k-range for Fourier transformation: 2.5 - 14.2 Å^{-1}, ΔE_0 = -14.23 eV.

In the future the speciation of UO_2^{2+} sorbed on Si-containing minerals in the environment will be studied by EXAFS. The hydrous uranyl silicate can be used as a reference for the EXAFS data analysis of similar but non-crystalline samples and as model substance for speciation investigations studying the environmental behavior of uranium in laboratory experiments.

Acknowledgments

The EXAFS measurements were performed at the SSRL which is operated by the US Department of Energy, Office of Basic Energy Sciences, Divisions of Chemical Sciences and Materials Science.

References

/1/ H. Moll, G. Schuster, G. Bernhard
A new hydrothermal synthesis and characterization of hydrous uranyl silicate, $(UO_2)_2SiO_4 \cdot 2H_2O$
this report.

/2/ J.P. Legros, R. Legros, E. Masdupuy
Sur un Silicate d'Uranyl Isomere du Germanate d'Uranyl
Bull. Soc. Chim. France 8, 3051 (1972).

/3/ F. Demartin, C.M. Gramaccioli, T. Pilati
The importance of accurate crystal structure determination of uranium minerals. II. Soddyite
Acta Cryst. C48, 1 (1992).

/4/ L.M. Kuznetsov, A.N. Tsvigunov, E.S. Makarov
Hydrothermal synthesis and physics-chemical study of the synthetic analog of soddyite
Geochimiya 10, 1493 (1981).

/5/ E.L. Belokoneva, V.I. Mokeeva, L.M. Kuznetsov, M.A. Simonov, E.S. Makarov, N.V. Belov
Crystal structure of the synthetic soddyite
Dokl. Akad. Nauk SSSR 246, 93 (1979).

/6/ Powder Diffraction File
International Centre of Diffraction Data, Newtown Square, PA 19073.

/7/ Yu.Z. Nozik, L.M. Kuznetsov
Neutron diffraction study of synthetic soddyite by the full-profile analysis technique
Kristallografiya 35, 1563 (1990).

/8/ J.J. Rehr, R.C. Albers, S.I. Zabinsky
High-Order Multiple-Scattering Calculations of X-Ray-Absorption Fine Structure
Phys. Rev. Lett. 69 3397 (1992)

A XANES AND EXAFS INVESTIGATION OF THE SPECIATION OF SELENITE FOLLOWING BACTERIAL METABOLIZATION

B. B. Buchanan,[a] J. J. Bucher,[b] D. E. Carlson,[a] N. M. Edelstein,[b] E. A. Hudson,[c] N. Kaltsoyannis,[b] T. Leighton,[d] W. Lukens,[b] H. Nitsche,[e] T. Reich,[e] K. Roberts,[f] D. K. Shuh,[b] P. Torretto,[f] J. Woicik,[g] W-S. Yang,[h] A. Yee[f] and B. C. Yee[a]

[a] Department of Plant Biology, University of California, Berkeley, CA 94720, USA
[b] Chemical Sciences Division, Lawrence Berkeley Laboratory, Berkeley, CA 94720, USA
[c] G. T. Seaborg Institute for Transactinium Science, Lawrence Livermore National Laboratory, Livermore, CA 94551, USA
[d] Department of Molecular and Cell Biology, University of California, Berkeley, CA 94720, USA
[e] Forschungszentrum Rossendorf e. V., Institute of Radiochemistry
[f] Earth Sciences Division, Lawrence Berkeley Laboratory, Berkeley, CA 94720, USA
[g] National Institute of Standards and Technology, Gaithersburg, MD 20899, USA
[h] Department of Biology, Jackson State University, Jackson, MS 39217, USA

Abstract

The common soil bacterium, *Bacillus subtilis*, can reductively metabolize selenite Se(IV). X-ray Absorption Near Edge Structure (XANES) spectroscopy demonstrates that both *B. subtilis* and an unidentified bacillus isolated from selenium contaminated soil reduce selenite to the red allotrope of elemental selenium. The red and grey forms of selenium are distinguished by their XANES spectra (Fig. 1). Extended X-ray Absorption Fine Structure spectroscopy shows only one absorber-backscatter distance in both red and grey selenium, at 2.43 Å and 2.44 Å respectively.

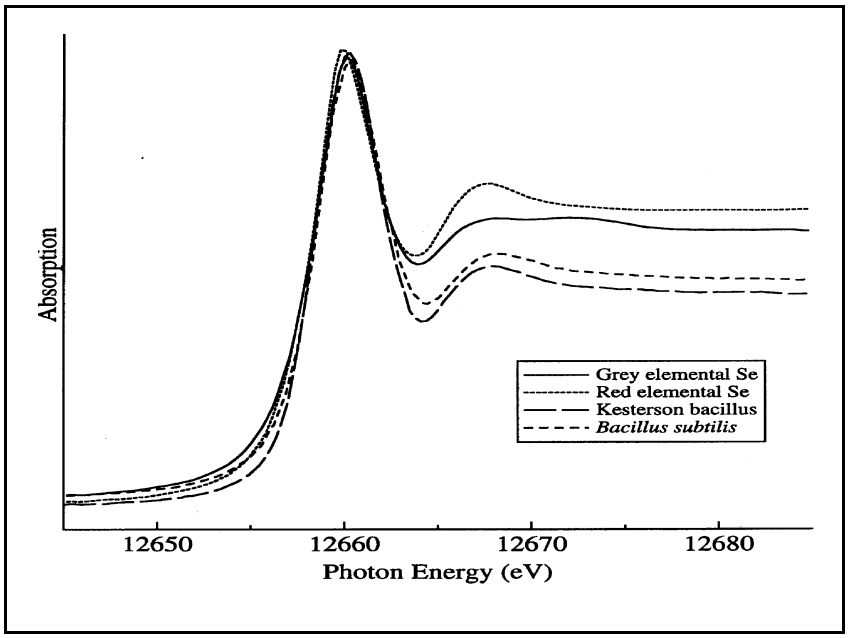

Fig. 1: The selenium K edge XANES spectra of amorphous red and grey selenium and from *B. subtilis* and the Kesterson bacillus after growth in a selenite medium. The spectra have been normalized to equivalent peak heights. Grey selenium was employed as a reference in all cases, and the energy scales have been aligned with respect to its absorption edge at 12658 eV.

ELECTRONIC AND STRUCTURAL INVESTIGATIONS OF TECHNETIUM COMPOUNDS BY X-RAY ABSORPTION SPECTROSCOPY

I. Almahamid,[a] J. C. Bryan,[b] J. J. Bucher,[c] A. K. Burrell,[b] N. M. Edelstein,[c]
E. A. Hudson,[d] N. Kaltsoyannis,[c] W. W. Lukens,[c] H. Nitsche,[e] T. Reich,[e] D. K. Shuh[c]

[a] Earth Sciences Division, Lawrence Berkeley Laboratory, Berkeley, CA 94720, USA
[b] Inorganic and Structural Chemistry Group, Los Alamos National Laboratory, Los Alamos, NM 87545, USA
[c] Chemical Sciences Division, Lawrence Berkeley Laboratory, Berkeley, CA 94720, USA
[d] G.T. Seaborg Institute for Transactinium Science, Lawrence Livermore National Laboratory, Livermore, CA 94551, USA
[e] Forschungszentrum Rossendorf e.V., Institute of Radiochemistry

Abstract

X-ray Absorption Near Edge Structure spectroscopy has been used to establish the chemical shifts of the technetium K edge in a range of compounds containing Tc in a variety of formal oxidation states. The edge positions span 19.9 eV from Tc metal to NH_4TcO_4. Strong correlation between chemical shift and formal oxidation state is observed (Fig. 1). Extended X-ray Absorption Fine Structure (EXAFS) spectroscopy of $Tc_2(CO)_{10}$ indicates that multiple scattering along the Tc-C-O vector is more important than direct Tc••O scattering. TcO_2 is shown by EXAFS to possess a distorted rutile structure with a closest Tc-Tc distance of 2.61 Å. This is rationalized in terms of the Goodenough model for bonding in transition metal dioxides.

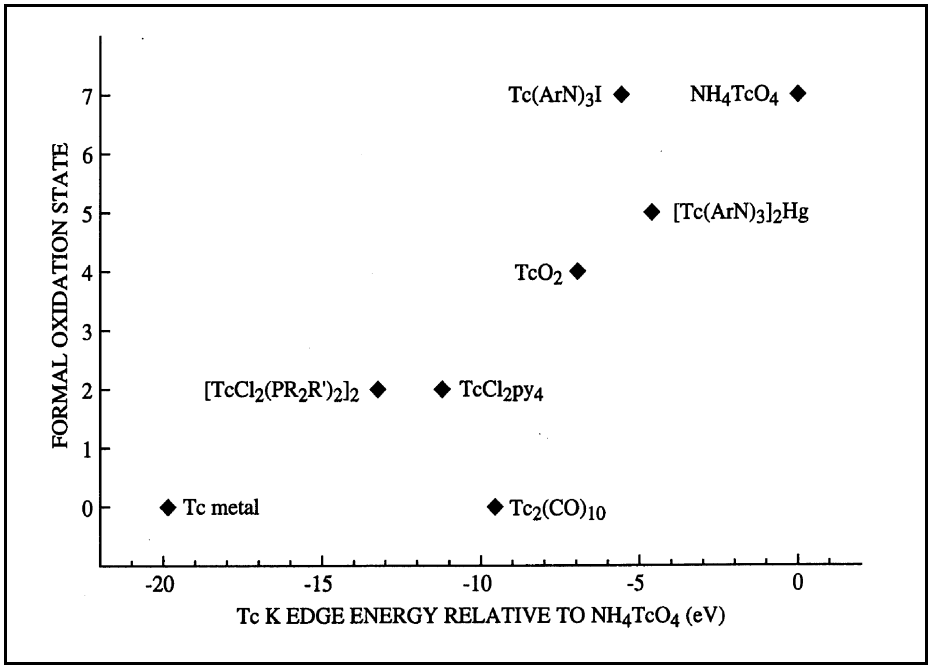

Fig. 1: Chemical shifts of the Tc K edge versus formal oxidation state.

All XANES spectra were acquired with NH_4TcO_4 as a reference, and the chemical shifts are therefore reported relative to NH_4TcO_4.

PROPOSED CONCEPTUAL DESIGN OF THE RADIOCHEMISTRY END STATION FOR THE ROSSENDORF BEAM LINE AT THE ESRF

H. Nitsche, G. Bernhard, T. Reich
Forschungszentrum Rossendorf e.V., Institute of Radiochemistry

In March 1994, the Forschungszentrum Rossendorf e.V. submitted a proposal for 'A Beam Line for Radiochemistry and Ion Beam Physics on a Bending Magnet Source at the ESRF' (Project ROBL) /1/ to the European Synchrotron Radiation Facility (ESRF) at Grenoble, France. This project is carried out in colaboration with the Institute of Ion Beam Physics and Materials Research. The aim is to build a hard X-ray beam line with the following experimental end stations:

- radiochemistry hutch for X-ray absorption measurements (XAS),
- materials research hutch for in situ studies with ion beam assisted deposition (IBAD),
- materials research hutch with a multipurpose goniometer.

In the following paragraphs the conceptual design of the radiochemistry end station for the ROBL project will be presented in detail.

The proposed radiochemistry end station at the ESRF will be used for X-ray absorption near-edge structure spectroscopy (XANES) and extended X-ray absorption fine structure spectroscopy (EXAFS) of lanthanide and actinides elements and other radionuclides /2,3/. The aim is to study the speciation and complexation of these elements in aqueous and non-aqueous solutions, the adsorption processes at the solid-water interface of these solutions with soils, minerals, mineral assemblies and uranium mill tailings, and the adsorption and incorporation of these elements in biological materials.
The radiochemistry hutch will be part of the Rossendorf Beam Line (ROBL) installed at the high-field section of a bending magnet at the ESRF. The double-crystal monochromator system will have an usable energy range of about 5-35 keV, with an energy resolution of $)E/E \# 10^{-4}$. An unfocused and a focused beam are planed with an intensity of approximately 10^{13} photons s^{-1} and bw^{-1}. The dimension of the focused beam will be 0.1 x 0.1 mm^2.
The end station for XAS measurements of radioactive samples requires a special design to satisfy the radiation protection requirements at the ESRF. It is planned to measure the following radioactive elements: uranium, thorium, technetium, polonium, protactinium, radium, neptunium, plutonium, and americium. The maximum activity of radioactive samples that will be measured will not exceed 5 mCi. Therefore the samples will generate a very weak exterior radiation field at best. Because of the "-activity and the potential heavy metal toxicity in case of ingestion, samples must be handled in a special containment.
This containment can be a simple plastic enclosure for some samples or a sophisticated glove box for other samples. The glove box is operated under slightly negative pressure with a double high-efficiency filter system on the vented side. There is the possibility that the regulations may demand a double containment. This redundancy will guarantee that, in the unlikely event of failure of one containment, the

radioactive sample is still safely contained in the other. Such a double-containment system can be a plastic-sealed sample in a negative-pressure glove box, or a negative-pressure glove box in a slightly negative-pressure room. Such containment technology is common worldwide for laboratories working with radioactive "-samples. It is planned to have the possibility of some sample handling within the glove box at the beam line, e.g. for applying an electrical potential to a solution in order to follow the in-situ change of solution species, etc. For some cases, a special sample holder will allow sample cooling down to 90 K and thermostating in the range from -20° to 90° C.

For relatively concentrated samples, standard XAS equipment for transmission measurements will be used. Fig. 1 shows the layout of the experimental station. It consists of three ionization chambers mounted on an optical rail and a remote-controlled sample positioning system. Dilute samples will be measured in fluorescence mode using Stern-Heald type gas ionization chambers (Lytle detectors) or multielement solid state detector systems. A non-radioactive reference sample for calibration of the energy scale and the monochromator resolution will be placed inside the Lytle detector for measurements either in transmission or fluorescence mode. All detectors are mounted outside the glove box and only the sample-positioning system must be placed inside. The glove box itself is mounted on a precision rail system, so that it can be moved in and out the X-ray beam. For XAS measurements of non-radioactive samples, the glove box will be out of the X-ray beam.

The photon beam and the detectors are connected to the glove box *via* transmissive windows of Mylar or any other suitable material. These windows can have an additional renewable protection which can be exchanged in case of a low-level contamination from inside the glove box.

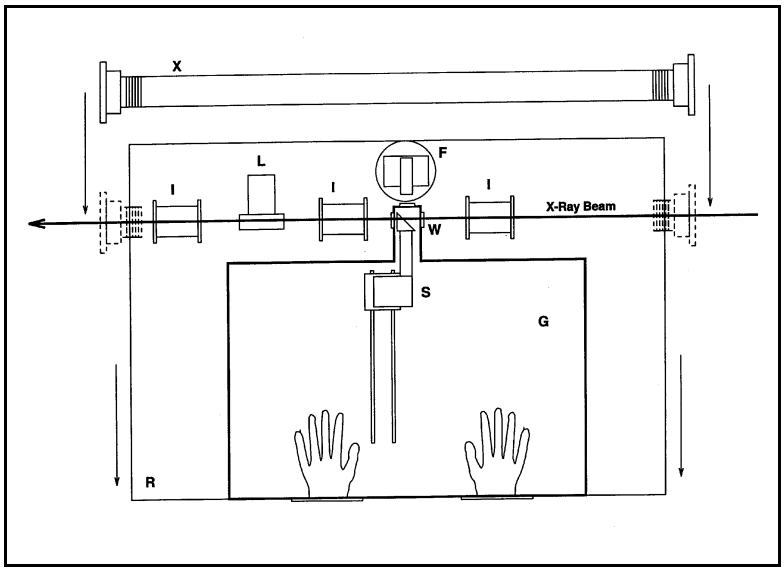

Fig. 1. Layout of the experimental station: F, multielement solid state fluorescence detector; G, glove box; I, ionization chamber; L, Lytle fluorescence detector, R, table on rail system; S, sample-positioning system; W, Mylar windows; X, X-ray beam tube.

References

/1/ Matz, W., Nitsche, H., Baraniak, L., Bernhard, G., Betzl, M., Brendler, V., Eichhorn, F., Hüttig, G., Leege, K., Merker, P., Möller, W., Pröhl, D., Prokert, F., Reichel, P., Schlenk, R., Stephan, J.

Proposal for ‘A Beam Line for Radiochemistry and Ion Beam Physics on a Bending Magnet Source at the ESRF’
Forschungszentrum Rossendorf e.V., March 1994.

/2/ Almahamid, I., Bryan, J.C., Bucher, J.J., Burrell, A.K., Edelstein, N.M., Hudson, E.A., Kaltsoyannis, N., Lukens, W.W., Shuh, D.K., Nitsche, H., Reich, T.
Electronic and Structural Investigation of Technetium Compounds by X-ray Absorption Spectroscopy
Inorg. Chem. 34 193 (1995).

/3/ Buchanan, B.B., Bucher, J.J., Carlson, D.E., Edelstein, N.M., Hudson, E.A., Kaltsoyannis, N., Leighton, T., Lukens, W.W., Nitsche, H., Reich, T., Roberts, K., Shuh, D.K., Torretto, P., Woicik, J., Yang, W.S., Yee, A., Yee, B.C.
A XANES and EXAFS Investigation of the Speciation of Selenite Following Bacterial Metabolization
Inorg. Chem. 34 1617 (1995).

Chemistry of the Heaviest Elements

CONTRIBUTION TO THE EVALUATION OF THERMOCHROMATOGRAPHIC STUDIES OF TUNGSTEN

H. Funke, A. Vahle, S. Hübener
Forschungszentrum Rossendorf e.V., Institute of Radiochemistry

The importance of thermochromatographic investigations of the lighter homologues of element 106 is widely described. In this note, experiments of Ross et al. /1/ are evaluated with the program TECRAD /2/ not containing approximations like a linear temperature profile within the gradient tube.
The differential enthalpy of the adsorption process is determined from the zero of the equation:

$$t_{exp} = \int_{T_A}^{T_S} \frac{1}{u(T)} \cdot \frac{dz(T)}{dT}\, dT = 0. \qquad (1)$$

The temperature-dependend function u(T) = $u_0 \cdot T/T_O$ means the velocity, z(T) the inverse function of the (monotone) temperature profile of the tube T(z) and q(T) the corrected partition coefficient /3/ including the more complex dissociative reactions /4/:[1]

$$q(T) = a \cdot \frac{c^0_{ads}}{c_{H_2O}} \cdot \exp\left(\frac{\Delta S^0_{diss.ads}}{R}\right) \exp\left(\frac{\Delta H^0_{diss.ads}}{RT}\right). \qquad (2)$$

Figure 1 shows a typical example for a thermochromatographic measurement from which the adsorption enthalpy is determined:

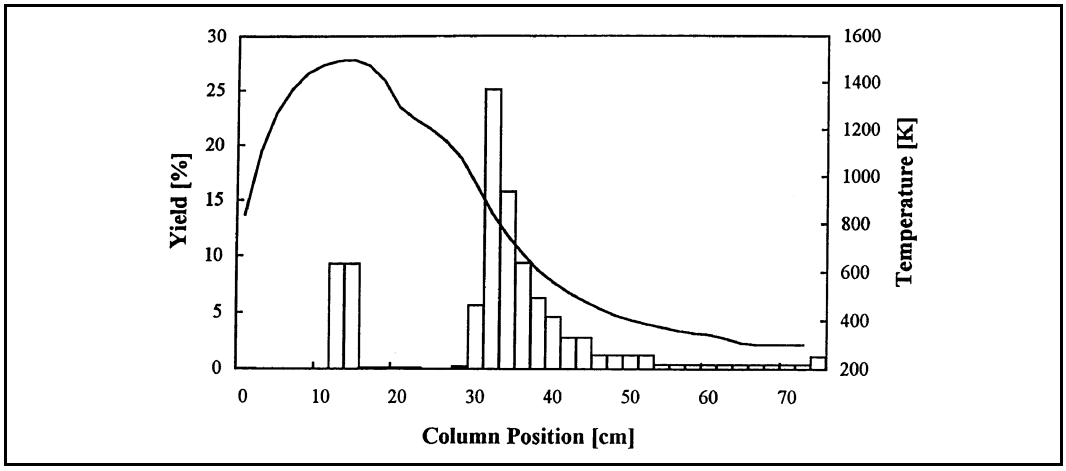

Fig. 1: Typical thermochromatogram of Tungsten (^{176}W) in humid oxygen (exposure time: 30 min, $v_0(Ar)$ = 500 ml/min, $v_0(O_2)$ = 250 ml/min, $p(H_2O)$ = 160 Pa, starting position/quartz wool plug: 12-16 cm, for experimental arrangement see /5/)

[1] The meaning of the symbols are : z-length coordinate of the tube, t-time, T-temperature, $\Delta S^0_{diss.ads}$-dissociative adsorption-entropy, $\Delta H^0_{diss.ads}$-dissociation-adsorption-enthalpy, t_{exp}-time of the experiment, T_S- starting temperature, T_A-adsorption temperature, a-surface area per unit of column length, u_0-initial velocity, T_0-standard temperature, g-temperature gradient, c_{H2O}-concentration of H_2O, c^0-standard concentration.

The confirmation for a dissociative adsorption as the underlying chemical process that can also be derived from equation (1). Little changes in TECRAD allow to calculate the dependence of the H_2O concentration from the deposition temperature for fixed enthalpy values and to compare the resulting curves with the curve corresponding to the theoretical estimation /6/ of ΔH = -55 kJ/mol for a dissociative adsorption process. The estimated value of ΔH without inclusion of dissociative effects is: $\Delta H_{ads}(WO_2(OH)_2)$ = -172 ±18 kJ/mol.
Figure 2 shows the plot of the H_2O concentration depending on the deposition temperature for isoenthalpies corresponding to the measured enthalpy values in kJ/mol: ΔH = -69.6, -66.1, -64.8, -58.7 (twice), -53.8 (downwards), the mean - and the estimated value.

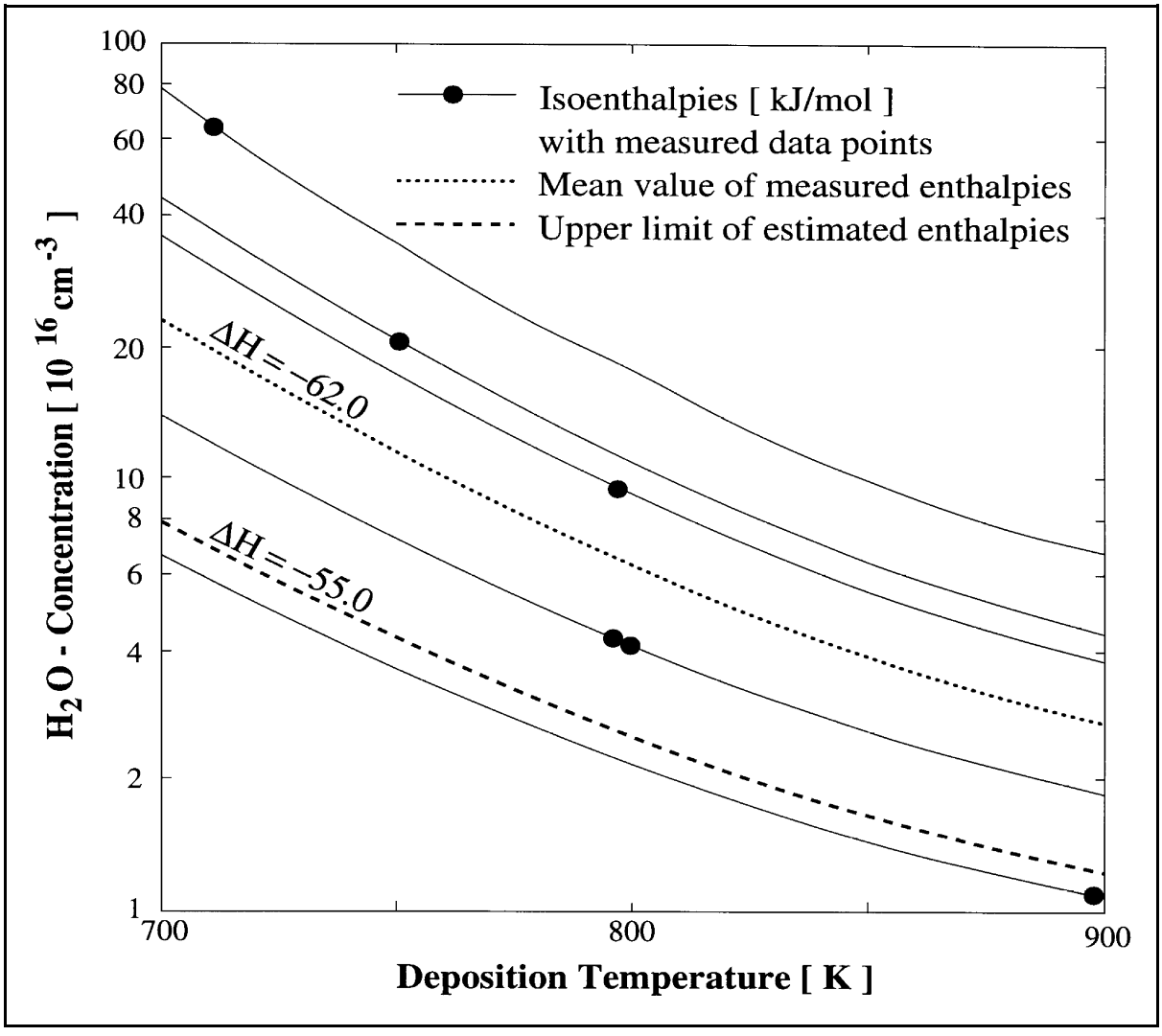

Fig. 2: H_2O concentration as a function of deposition temperature for some fixed enthalpies

The comparison of measured and estimated data gives strong evidence for a dissociative adsorption according to equation (1).

Acknowledgment

These studies were supported by the Bundesminister für Forschung und Technologie of the Federal Republic of Germany under contract 06 DR 101 D.

References

/1/ A. Ross et al.,
Gas Chromatographic Studies of Tungsten in Humic Oxygen,
Report FZR 94-43, 60,(1994)

/2/ H. Funke et al.,
Contribution to the Evaluation of Thermochromatographic Experiments
Report FZR 94-43, 53,(1994)

/3/ B. Eichler, I. Zvara,
Evaluation of the Enthalpy of Adsorption from Thermochromatographical Data
Radiochimica Acta 30, 233 (1982)

/4/ B. Eichler et al.,
Complex Transport Reactions in a Temperature Gradient Tube: Radiochemical Study of Volatization and Deposition of Iridium Oxides and Hydroxydes
Radiochimica Acta 61, 81 (1993)

/5/ S. Hübener et al.,
Gas Chromatic Studies of Molybdenum Oxides and Hydroxydes
Report FZR 93-15, 41,(1993)

/6/ B. Eichler, V. Domanov,
Verflüchtigung von Radionukliden im Luftstrom und ihre Abscheidung im Thermogradientrohr
J. Radioanal. Chem. 28, 143 (1975)

TRANSPORT BEHAVIOUR OF MACROSCOPIC MOLYBDENUM AMOUNTS IN THE O_2-$H_2O_{(g)}$/$SiO_{2(s)}$-SYSTEM

A. Vahle, S. Hübener
Forschungszentrum Rossendorf e. V., Institute of Radiochemistry

K. Eberhardt
University Mainz, Institute of Nuclear Chemistry

In addition to gas chromatographic studies of trace amounts of molybdenum /1,2/ the volatilization, transport, and deposition of macroamounts of molybdenum were studied by thermochromatographic techniques.
The transport of molybdenum in the presence of oxygen and water vapour in the temperature range of 600 - 1450 K may be governed by the following reactions:

$(MoO_3)_{n\,(g)}$	:	n	$MoO_{3\,(s)}$	(1)
$MoO_2(OH)_{2\,(g)}$	:		$MoO_2(OH)_{2\,(s)}$	(2)
$MoO_2(OH)_{2\,(g)}$	:		$MoO_{3\,(s)} + H_2O_{(g)}$	(3)

Thermodynamic functions and experimental variables in the temperature gradient tube are connected as follows /5/:
for a simple desublimation

$$R \ln \frac{m R T_0}{M v_0 t_r} = \frac{\Delta H^E_{des}}{T_D} - \Delta S^E_{des} + R \ln p_0 \qquad (4)$$

for a dissociative desublimation without change of the oxidation state of molybdenum

$$R \ln \frac{m R T_0}{M v_0 t_r} = \frac{\Delta H^E_{des,des}}{T_D} - \Delta S^E_{des,des} + R \ln p(H_2O) \qquad (5)$$

From a plot of the left-hand side of Equation (4) or (5) versus $1/T_D$ the thermodynamic functions ΔH^E and ΔS^E can be derived from experimental data. Vice versa, from the thermodynamic data given in literature /3,4/ deposition temperatures can be calculated for different molybdenum species in order to interpret experimental data.

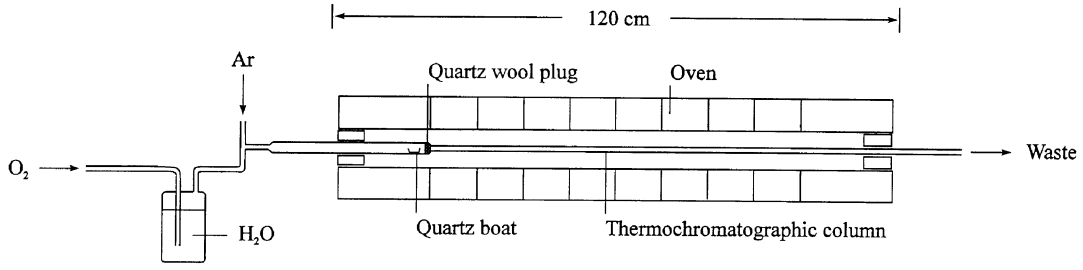

Fig. 1: Experimental arrangement

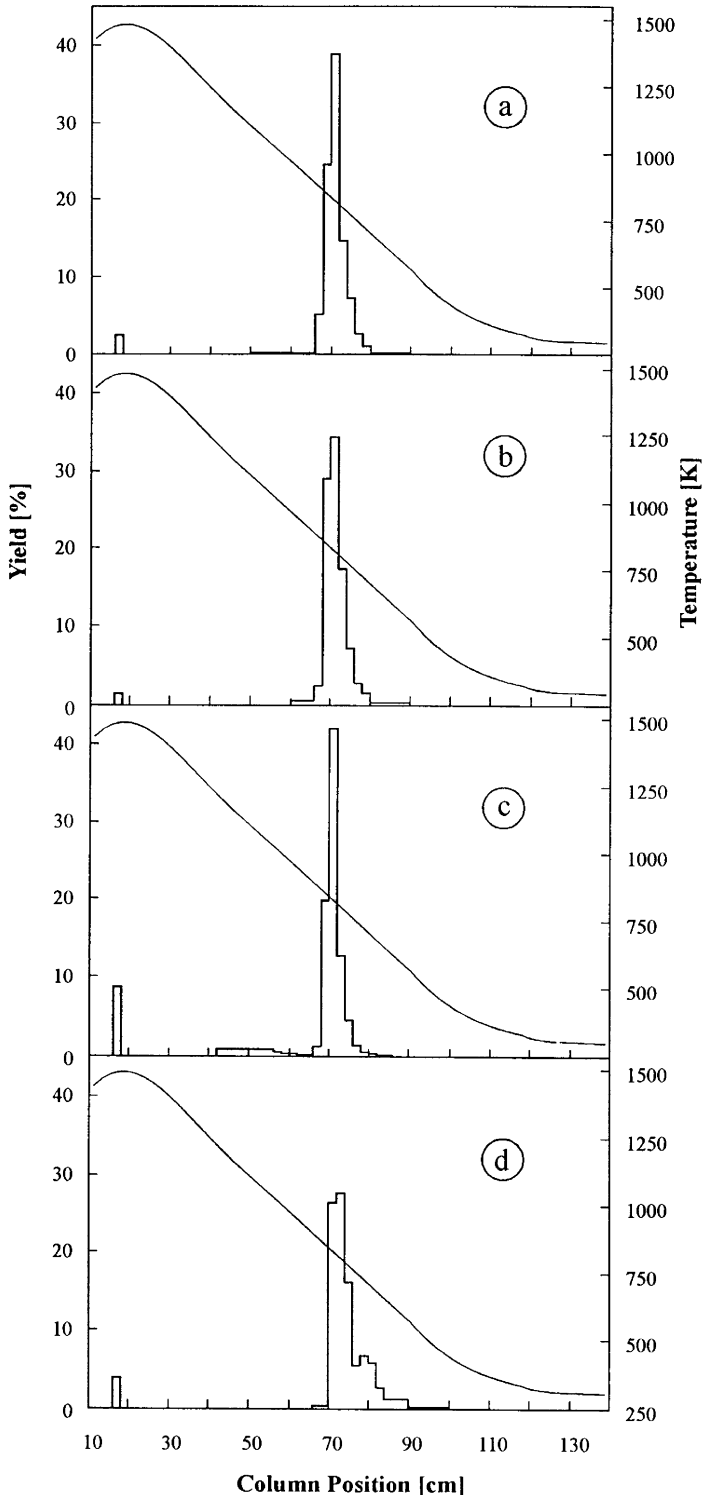

Fig. 2: Thermochromatograms of molybdenum in macroscopic amounts at different water vapour pressures: (a) dry, (b) 400 Pa, (c) 900 Pa, (d) 2300 Pa
m(Mo) = 100 Fg, exposure time 30 min
starting position: 16-18 cm, quartz wool: 18-20 cm

Figure 1 shows the experimental arrangement for the thermochromatographic studies. The 120 cm long oven consists of 10 separate heating sections. Empty quartz tubes were used as chromatographic columns. A mixture of argon and oxygen in the ratio 2:1 was used as the carrier gas at a total flow rate of 150 $ml \cdot min^{-1}$.

The oxygen was moistened by bubbling through water. The partial pressure of water varied in the range 2300 Pa $ $p(H_2O)$ $ 400 Pa. In dry carrier gas the remaining water vapour pressure was << 3 Pa, but could not be measured exactly.

Isotopes of molybdenum (^{93m}Mo, ^{99}Mo) were produced in ^{nat}Zr (", xn) reactions at the U-120 cyclotron of the Forschungszentrum Rossendorf and processed as described earlier in detail /6/. The molybdenum isotopes deposited in a small region of a quartz column were dissolved in diluted ammonia. A mixture of this solution and a solution of natural molybdenum with known concentration was evaporated in a quartz boat which then was inserted into the thermochromatographic column in front of a quartz wool plug. The total molybdenum amount was in the range of 10 Fg to 10 mg.

The distribution of molybdenum was measured off-line in 2 cm sections by (-ray spectroscopy with a HPGe detector. The distribution of the radioactive molybdenum isotopes and the inactive carrier was found to be identical, as proven by neutron activation analysis.

Typical thermochromatograms obtained in a dry and a moist oxygen atmosphere are shown in Figure 2.

The behaviour of molybdenum in the system under study is as follows: More than 90 % of the molybdenum are volatilized and deposited as a single peak at the same position regardless whether dry or moist oxygen was used.
A plot of experimental retention data versus $1000/T_D$ is shown in Figure 3. Results of model calculations for the transport reactions (1 - 3) are plotted for comparison.

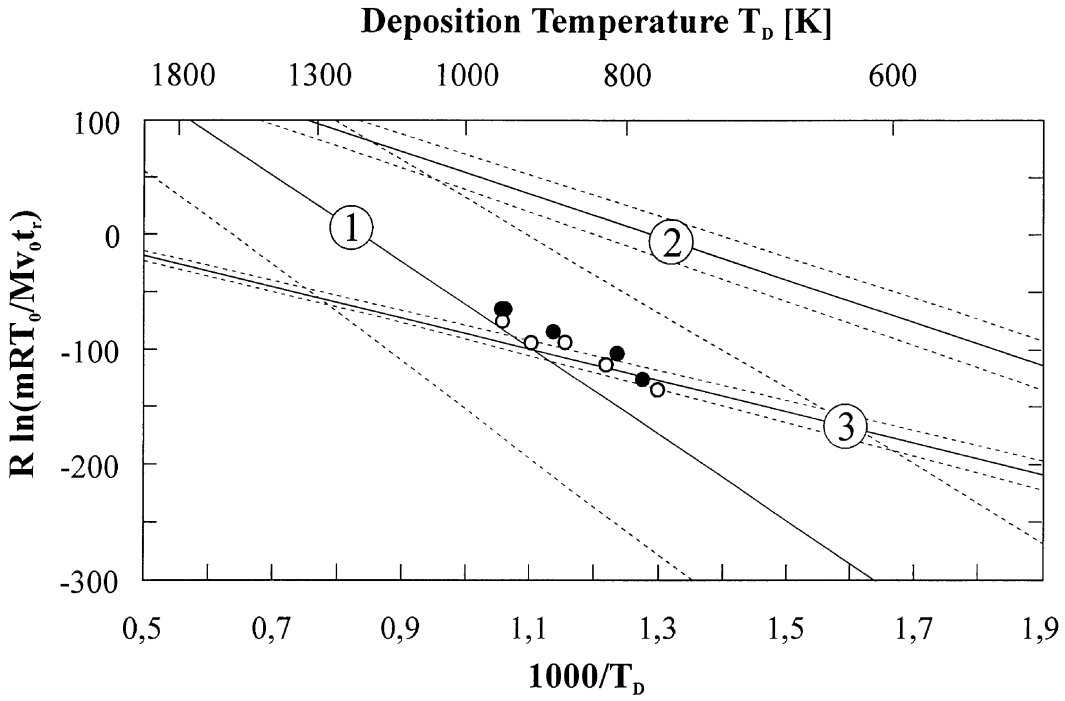

Fig. 3: Retention data for molybdenum in macroscopic amounts in dependence on $1000/T_D$, the reciprocal deposition temperature
Exposure time 30 min, dry (dots) or with 900 Pa water vapour pressure (circles).
The solid straight lines show calculated equilibrium data for the reactions:
(1) $(MoO_3)_{3\,(g)}$: $3\ MoO_{3\,(s)}$, (2) $MoO_2(OH)_{2\,(g)}$: $MoO_2(OH)_{2\,(s)}$,
(3) $MoO_2(OH)_{2\,(g)}$: $MoO_{3(s)} + H_2O_{(g)}$

$MoO_2(OH)_{2\,(g)}$ cannot be formed with dry carrier gas. A contribution of MoO_2 or MoO_3 as volatile species can be excluded because their sublimation enthalpies are very high. Hence, the transport is most likely governed by reaction (1):

$$(MoO_3)_{n\,(g)} \quad : \quad n \quad MoO_{3\,(s)}$$

There is a good agreement with the calculated temperature function. The correspondence of the deposition temperatures suggest that the same species is transported with both, dry and moist oxygen. However, as shown in Figure 3, the calculated temperature function of reaction (1) is similar to that of reaction (3), the dissociative desublimation of $MoO_2(OH)_2$:

$$MoO_2(OH)_{2\,(g)} \quad : \quad MoO_{3\,(s)} + H_2O_{\,(g)}$$

Both functions intersect at about 900 K where the partial pressures of gaseous $(MoO_3)_n$ and $MoO_2(OH)_2$ above the solid MoO_3 become equal in moist oxygen. Therefore it is

impossible to assign the experimental data unambiguously to one of the possible reactions. However, in case of reaction (3) a significant dependence on the water vapour pressure has to be expected but by thermochromatography we could not found any evidence for it. Possibly the two reactions overlap and in case of a high molybdenum amount and/or a low water vapour pressure reaction (1) dominates and otherwise reaction (3) prevails.
The high resolution sector field mass spectrometer Finnigan MAT 95 was used to characterize the chemical state of the molybdenum species deposited on the quartz surface. A suspension of some crystals in n-hexane was applied to a tungsten wire which could be heated up to 1850 K. Negative ions received by chemical ionization were proved. Regardless whether dry or moist oxygen was used in the experiment only $(MoO_3)_n$ with mainly n = 3, 4 could be proved in the gaseous phase indicating a deposition as MoO_3. Neither the mass peak of $MoO_2(OH)_2$ nor that of H_2O, possibly indicating the dissociation of $MoO_2(OH)_2$, could be found. Therefore a simple desublimation of $MoO_2(OH)_2$ (reaction 2) can be ruled out. Further evidence for this interpretation comes from the deviation between the calculated temperature function (2) and the experimental data.

Acknowledgements

These studies were supported by the Bundesministerium für Forschung und Technologie of the Federal Republic of Germany under contract 06 DR 101 D.

References

/1/ S. Hübener, A. Roß, B. Eichler, H. W. Gäggeler, J. Kovacs, S. N. Timokhin, A. B. Yakushev
Gas Chromatographic Studies of Molybdenum Oxides and Hydroxides
Report FZR 93-15, p. 41 (1993)

/2/ A. Roß, S. Hübener, B. Eichler, H. W. Gäggeler, A. Türler, D. T. Jost
Gas Chromatographic Studies of Molybdenum in Humid Oxygen
Report FZR-43, p. 63 (1994)

/3/ E. H. P. Cordfunke, R. J. M. Konings
Thermochemical Data for Reactor Materials and Fission Products
North-Holland, Amsterdam 1990

/4/ O. Knacke, O. Kubaschewski, K. Hesselmann
Thermochemical Properties of Inorganic Substances
Springer-Verlag, 2nd Ed., Berlin 1991

/5/ B. Eichler, F. Zude, W. Fan, N. Trautmann, G. Herrmann
Complex Transport Reactions in a Temperature Gradient Tube:
Radiochemical Study of Volatilization and Deposition of Iridium Oxides and Hydroxides
Radiochim. Acta 61, 81 (1993)

/6/ A. Roß, S. Hübener
Separation of Carrier-"free" Molybdenum from Zirconium
Report FZR 93-15, p. 43 (1993)

ON-LINE HIGH TEMPERATURE GAS CHROMATOGRAPHY OF GROUP 6 ELEMENTS IN HUMID OXYGEN - TEST EXPERIMENTS WITH OLGA II

S. Hübener, A. Vahle, M. Böttger, K. Eberhardt[1], M. Mendel[1], N. Trautmann[1], A. Türler[2], B. Eichler[2], D.T. Jost[2], D. Piquet[2], H.W. Gäggeler[2]

Forschungszentrum Rossendorf e.V., Institute of Radiochemistry
[1] University Mainz, Institute of Nuclear Chemistry
[2] Paul Scherrer Institut, CH-5232 Villigen PSI

On the way to develop an apparatus well suited to study element 106 in the O_2-$H_2O_{(g)}$/$SiO_{2(s)}$-system by the on-line isothermal gas chromatography technique the On-Line Gas Chemistry Apparatus OLGA II /1/ was tested in experiments with short-lived molybdenum and tungsten isotopes.
In experiments at the TRIGA Mainz Reactor the fission products produced by thermal neutron-induced fission of ^{235}U were transported by an Ar/MoO_3 gas-jet to the gas chemistry arrangement. Humid oxygen was added as a reactive gas. A breakthrough of aerosol particles of about 3 % was observed when the quartz wool plug for destroying aerosols was positioned in the first section of the chromatography furnace at 1320 K. This is the maximum permissible temperature of the furnace. A complete aerosol retention was achieved if the quartz wool plug was positioned in the middle of the furnace at 1320 K and the preceding sections were kept at the same temperature. But under these conditions the isothermal part of the open tubular column is with 20 cm rather short for chromatography.
To collect the species passing through the column both the reclustering mode and the direct condensation on metal foils were tested.
The recluster unit of OLGA II was operated with an Ar/KCl aerosol. The KCl clusters loaded with volatile species were collected on glass fibre filters. At a column temperature of 1070 K the collection yield of ^{101}Mo as determined by (-spectrometry was approx. 40 %.
On stainless steel and gold (deposited on copper) foils which were arranged in face of the column exit on a cooling finger ^{101}Mo was collected to approx. 50 %. Over the foil temperature range 0 ^{o}C # T # 100 ^{o} C the collection yield on both metals was nearly constant.
The complete OLGA II device was tested in experiments with tungsten. Carrier free, short-lived isotopes of W were produced by bombarding gadolinium enriched in ^{152}Gd with 155 MeV ^{20}Ne at the PSI PHILIPS cyclotron. The reaction products were transported to the gas chemistry arrangement with a He/MoO_3 gas-jet. In order to study the transport reaction

$$WO_2(OH)_{2(g)} \quad : \quad WO_{3(ads)} + H_2O_{(g)}$$

by on-line isothermal gas chromatography the quartz wool was placed in the first section of the furnace taking into the bargain a breakthrough of aerosols. The quartz wool was kept at 1320 K and the temperature of the 50 cm long isothermal part of the column was varied between 870 and 1170 K. The recluster unit was operated with an Ar/KCl aerosol. The moving tape system equipped with a HPGe detector was used as the detection unit.

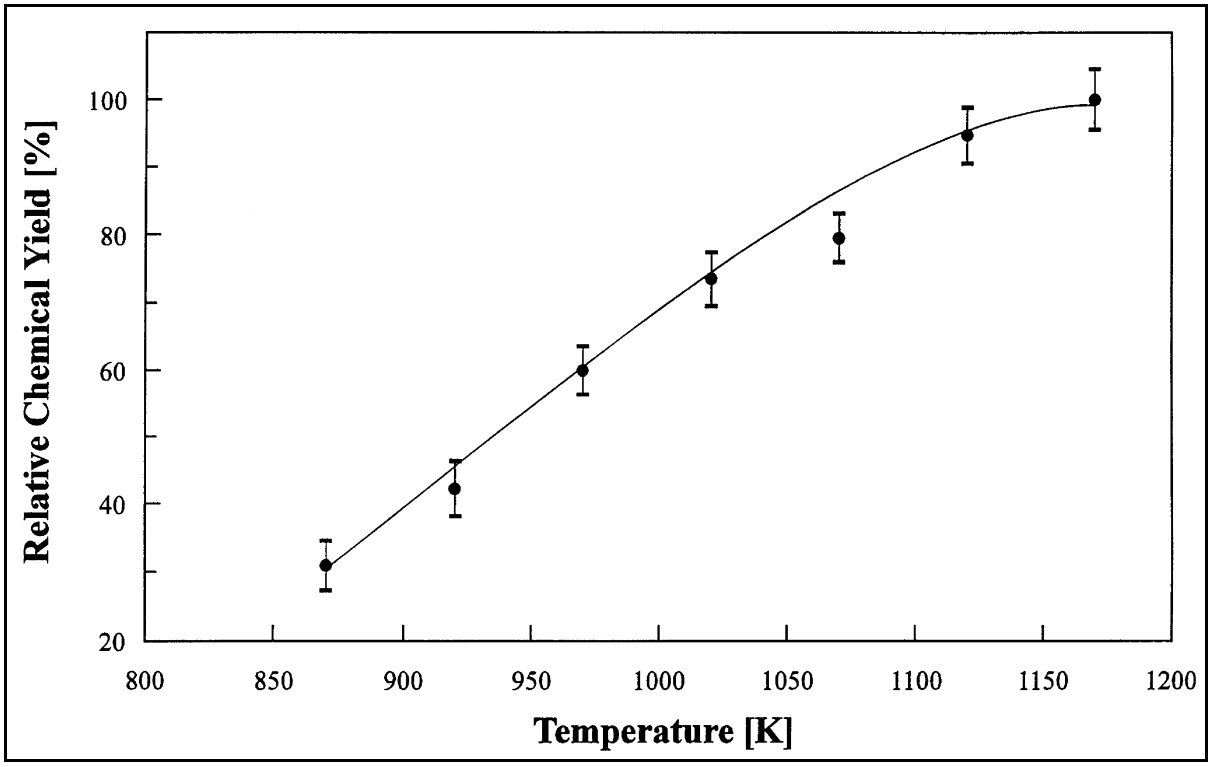

Fig. 1: Relative gas chemistry yield of ^{168}W as a function of the temperature in the isothermal part of the OLGA II furnace. The He carrier gas flow amounted to 1.0 l/min. Humid oxygen (0.5 l/min) with a water partial pressure of about 2300 Pa was added as the reactive gas. Empty quartz tubes with an inner diameter of 3.5 mm were used as chromatography columns.

In Fig. 1 the chemical yield measured for the 53 s ^{168}W is shown as a function of the isothermal temperature. The flat increase of the yield curve indicates a poor chromatographic resolution due to the slow kinetics of the chemical transport reactions involved. To the relatively long retention time of about 120 s as evaluated from the yields of ^{168}W, ^{169}W and ^{171}W both the slow kinetics of the chromatographic process and the residence time in the recluster unit contribute. Under optimal conditions the residence time in the recluster unit of OLGA II amounts to about 20 s /1/. Attempts to apply alternatively a rotating wheel detection system for the fast direct condensation of group 6 hydroxides on metal foils were started only.

For the detection of ^{166}W and ^{167}W with $t_{1/2}$ = 19 s and 20 s, respectively, the total retention time was to long. To study ^{265}106 and ^{266}106 whose half life is estimated to be in the same order of magnitude the total retention time has to be shortened.

In conclusion, the features of a device for isothermal on-line gas chromatography studies of element 106 in the O_2-$H_2O_{(g)}$/$SiO_{2(s)}$-system should include a preheating section prior to the quartz wool filter and a chromatography column longer than 1 m. In order to achieve shorter retention times the maximal permissible column temperature should be increased to 1400 K at least. The fast collection of the species under study by direct condensation on metal foils has to be studied further.

Acknowledgement

The support of these studies by the Bundesminister für Forschung und Technologie of the Federal Republic of Germany under contract 06 DR 101 D is gratefully acknowledged.

References

/1/ H.W. Gäggeler
On-Line Gas Chemistry Experiments with Transactinide Elements
J. Radioanal. Nucl. Chem. 183, 261 (1994)

II. PUBLICATIONS, LECTURES AND POSTERS

PUBLICATIONS

L. Baraniak, A. Mende
Radiological Characterization of Saxon Coal Mining Area around Freital
Proceedings of International Symposium on Remediation and Restoration of Radioactive-contaminated Sites in Europe; Antwerp, (NL), Oct. 11-15, 1993
EC-Document: Radiation Protection-74, XI-5027/1994, Vol. II, p. 911

G. Bernhard
Separation of Radionuclides from a fission product solution by ionexchange on alumina
Journal of Radioanalytical and Nuclear Chemistry 177, 321 (1994)

G. Bernhard, H. Friedrich, W. Boeßert, A. Eckardt
Operating and strategy for the decommissioning of the radiochemical plant AMOR-I
Kerntechnik 59, 135 (1994)

T. Ebert, L. Havlicek, Z. Wimmer, M. Bubner
Synthesis of the ^{14}C-labelled juwenoid W 328
J. Labelled Compounds Radiopharm. XXXIV, 377 (1994)

G. Geipel, M. Thieme
Determination of inorganic species in seepage water of uranium-mining rockpiles and in related media
Journal of Radioanalytical and Nuclear Chemistry 183, 139 (1994)

G. Geipel, M. Thieme, G. Bernhard, H. Nitsche
Distribution of uranium and radionuclides in a uranium-mining rockpile in Schlema, Saxony, Germany
Radiochimica Acta 66/67, 305 (1994)

M. Große, G. Schuster, K. Teske, W. Anwand, K. Henkel
Neutron and X-Ray Investigations on the Oxygen Bonding in $YBa_2Cu_3O_{7-x}$ combined with Physico-chemical Methods
Fresenius J. Anal. Chem. 349, 231 (1994)

M.R. Howells, K. Frank, Z. Hussain, E.J. Moler, T. Reich, D. Möller, D.A. Shirley
Toward a soft x-ray fourier-transform spectrometer
Nucl. Instr. and Meth. A 347, 182 (1994)

S. Hübener, B. Eichler, H.W. Gäggeler
Thermochromatographic studies of heavy actinides in metal columns
Journal of Alloys and Compounds 213/214, 429 (1994)

H.P. Martin, G. Irmer, G. Schuster, E. Müller
Structural Investigations on Pyrolysed Polycarbosilanes
Fresenius J. Anal. Chem. 349, 160 (1994)

M.P. Neu, D.C. Hoffman, K.E. Roberts, H. Nitsche, R.J. Silva
Comparison of chemical extractions and laser photoacoustic spectroscopy for the determination of plutonium species in carbonate solution
Radiochimica Acta 66/67, 251 (1994)

H. Nitsche, R.C. Gatti, S.A. Carpenter, K.E. Roberts, K.A. Becraft, T.G. Prussin
Determining plutonium concentration in solution using a germanium crystal and a new *L* x-ray/(-ray spectrographic method
Proc. 5th International Conference on High Level Radioactive Waste Management
Las Vegas, Nevada, USA, May 1994.

H. Nitsche, K.E. Roberts, R. Xi, T.G. Prussin, K.A. Becraft, I. Al Mahamid, H.B. Silber, S.A. Carpenter, R.C. Gatti
Long term plutonium solubility and speciation studies in a synthetic brine
Radiochimica Acta 66/67, 3 (1994)

T. Reich, P.A. Heimann, B.L. Petersen, E. Hudson, Z. Hussain, D.A. Shirley
Near-threshold behavior of the K-shell satellites in CO
Phys. Rev. A 49, 4570 (1994)

H.B. Silber, H. Nitsche, R.C. Gatti, H. Gehmecker, G. Feige, J.J. Bucher, N.M. Edelstein
The effects of radiolysis upon speciation and solubility of neptunium in brine solutions
Radiochimica Acta 66/67, 15 (1994)

B.R.M. Vyas, V. Sasek, M. Matucha, M. Bubner
Degradation of 3,3',4,4'-Tetrachlorobiphenyl by selected white rot fungi
Chemosphere 28, 1127 (1994)

LECTURES

H. Ullmann, G. Schuster, K. Teske
Materials for a Quasi Monolythic SOFC: Investigation on the Sr-Ce-O System
6th IEA Workshop
Rom, Italy, Febr. 1994

G. Bernhard, G. Geipel, M. Thieme, H. Nitsche
Mobilisierung von radioaktiven Wasserschadstoffen aus Uranbergbauhalden
GDCh-Chemiedozententagung 1994
Universität GH Siegen, Siegen, Germany, 06.-09.03.1994

H. Nitsche
Investigation of the Distribution and Speciation of U and Decay Products in a Mill Tailings Pile in the Erzgebirge, Germany
G.T. Seaborg Institute, Lawrence Livermore National Laboratory
Livermore, CA, USA, 24.03.1994

G. Geipel, M. Thieme, G. Bernhard, H. Nitsche
Uranium Mining in the former Eastern Germany - Problems of Mill Tailings piles
G.T. Seaborg Institute, Lawrence Livermore National Laboratory
Livermore, CA, USA, 01.04.1994

H. Nitsche
Speziation technogener Radionuklide in natürlichen aquatischen Systemen.
Analytica ' 94
München, Germany, 19.-22.04.1994

G. Bernhard, S. Hübener, C. Nebelung
Methodenentwicklung zur Freimessung von Bauschutt auf alpha-aktive Nuklide
Arbeitskreis "Freimessung von Anlagenteilen und Bauschutt aus dem Abbau kerntechnischer Anlagen des Brennstoffkreislaufes", 2. Sitzung
Karlsruhe, Germany, 05.05.1994

T. Reich
Experimental study of electron-correlation processes in small molecules with synchrotron radiation
Universität Leipzig, Inst. f. Physikalische und Theoretische Chemie
Leipzig, Germany, 13.06.1994

B.R.M. Vyas, V. Sasek, M. Matucha, M. Bubner
Investigation into the degradation of PCB 77 by white rot fungi using radiolabelled substrate
7th. Internat. Congr. of Bact. and Appl. Microbiol. and Mycol. Div.; MS - 12/25
Prague, CS, 03.-08.07.1994

H. Nitsche
Synchrotron X-Ray Absorption Spectroscopy:
A New Tool for Actinide and Lanthanide Speciation in Solids and Solution
First Workshop on “Comparative Science of the f-Elements"
Bühlerhöhe, Germany, Juli 1994

G. Geipel, M. Thieme, G. Bernhard, H. Nitsche, J. Einax
Bergbauhalden des Uranbergbaus im Erzgebirge: Radionuklidinventar und Radionuklidemission
GDCh-Fachgruppe Nuklearchemie, Vortragstagung
Berlin, Germany, 05.-07.09.1994

H. Friedrich, G. Bernhard, W. Boeßert
Dekontaminationsuntersuchungen an Bauteilen der Anlage "AMOR-I"
GDCh-Fachgruppe Nuklearchemie, Vortragstagung
Berlin, Germany, 05.-07.09.1994

H. Nitsche
Konzeption einer Synchrotron Beam Line zur Untersuchung radioaktiver

Substanzen
GDCh-Fachgruppe Nuklearchemie, Vortragstagung
Berlin, Germany, 05.-07.09.1994

A. Roß, S. Hübener, B. Eichler
Transportreaktionen der Elemente der 6. Gruppe im O_2-$H_2O_{(g)}$/$SiO_{2(s)}$-System
GDCh-Fachgruppe Nuklearchemie, Vortragstagung
Berlin, Germany, 05.-07.09.1994

I. Almahamid, J.C. Bryan, J.J. Bucher, A.K. Burrell, D. Clark, S. Clark, N.M. Edelstein, E.A. Hudson, N. Kaltsoyannis, C. Langdon, W.W. Lukens, M. Neu, H. Nitsche, T. Reich, D.K. Shuh
XAS of technetium and uranium materials relevant to environmental concerns
Stanford Synchrotron Radiation Laboratory (SSRL) User's Meeting
Stanford, USA, Oct. 1994

H. Nitsche
The Proposed FZR-Radiochemistry Environmental Beam Line at ESRF
Workshop on “Analytical Applications of Synchrotron Radiation: Environmental and Materials Sciences”
Menlo Park, CA, USA, October 1994

C. Nebelung, S. Hübener, G. Bernhard
Bestimmung von Actiniden im Bauschutt
Arbeitskreis "Freimessung von Anlagenteilen und Bauschutt aus dem Abbau kerntechnischer Anlagen des Brennstoffkreislaufes", 3. Sitzung
Salzgitter, Germany, 22.11.1994

H. Nitsche, L. Baraniak, G. Bernhard
Radioecological Aspects of the Interaction of Radionuclides and Heavy Metals with Biomass: Methods for Speciation and Structural Information
NATO Advanced Research Workshop "Biotechnologies for Radioactive and Toxic Waste Management and Site Restoration: Scientific, Educational, Social, Economical and Buissiness Aspects"
Mol, Belgium, 28.11.-02.12.1994

H. Nitsche
Grundlagenforschung für die Nukleare Umweltsanierung
Johannes-Gutenberg-Universität, Institut für Kernchemie
Mainz, Germany, Dez. 1994

H. Nitsche
Das Institut für Radiochemie des Forschungszentrum Rossendorf:
Ein Wissenschaftliches Profil
Kernforschungszentrum Karlsruhe, Institut für Nukleare Entsorgungstechnik
Karlsruhe, Germany, Dez. 1994

POSTERS

M. Thieme, G. Geipel, G. Bernhard, H. Nitsche
Elektroanalytische In-situ-Verfolgung von Schwermetallretentions- und Auslaugungsprozessen an Gesteinsmaterial
Analytica ' 94
München, Germany, 19.-22.04.1994

W. Anwand, G. Brauer, P.G. Colman, K. Teske, K. Rudolph, G. Schuster
Positron Implantation Studies of $YBa_2Cu_3O_{7-x}$
10th International Conference on Positron Annihilation
Beijing, China, May 1994

W. Anwand, G. Brauer, P.G. Colman, A.P. Knights, K. Teske, G. Schuster, K. Rudolph
Positron Implantation Studies of YBaCuO
26th Polish Seminar on Positron Annihilation
Pokrzywna, Poland, Sept. 1994

S. Hübener, C. Nebelung, G. Bernhard
Bestimmung von Actiniden im Bauschutt
GDCh-Fachgruppe Nuklearchemie, Vortragstagung
Berlin, Germany, 05.-07.09.1994

S. Hübener, A. Roß, H. Funke, B. Eichler, H.W. Gäggeler, D.T. Jost, M. Schädel, E. Schimpf, N. Trautmann, K. Eberhardt
Modellexperimente zur physikochemischen Charakterisierung des Elements 106 als Oxid
GDCh-Fachgruppe Nuklearchemie, Vortragstagung
Berlin, Germany, 05.-07.09.1994

G. Schuster, M. Bubner, K.-H. Heise, H. Nitsche
Thermoanalytical Investigations on Humic Substances
Annual Meeting of the Society for Thermoanalysis (GEFTA)
Leipzig, Germany, Sept. 1994

W. Richter, K. Künstler, H.-J. Lang, G. Schuster, H. Zitzmann
Preparation and Measurement of the Electrical Conductivity of Solid Electrolyte Oxides for an Application in Sensores working at Low Temperatures
Annual Meeting of the Society for Applied Elektrochemistry
Dresden, Germany, Sept. 1994

E.A. Hudson, L.J. Terminello, B.E. Viani, J.J. Bucher, D.K. Shuh, N.M. Edelstein, T. Reich
X-ray absorption studies of uranium and thorium sorption on mineral substrates
Stanford Synchrotron Radiation Laboratory (SSRL) User's Meeting
Stanford, USA, Oct. 1994

T. Reich, P.A. Heimann, W.R.E. Huff, B.L. Petersen, E.A. Hudson, Z. Hussain, D.A. Shirley
Near-threshold behavior of the K-shell satellites in $N_2$and CO
International Workshop on Photoionization-IWP94,
San Francisco, USA, 24.-27.10.1994

G. Geipel, M. Thieme, G. Bernhard, H. Nitsche
Bergbauhalden des Uranerzbergbaues im Erzgebirge: Quelle und Rückhalt natürlicher Radioaktivität
GDCh-Fachgruppe Umweltchemie und Ökotoxikologie, Jahrestagung
Heidelberg, Germany, 03.-05.11.1994

A. Brachmann, G. Geipel, G. Bernhard, H. Nitsche
Untersuchungen zur Speziation des Elementes Bismut
GDCh-Fachgruppe Umweltchemie und Ökotoxikologie, Jahrestagung
Heidelberg, Germany, 03.-05.11.1994

III. SEMINARS

TALKS OF VISITORS

Prof. J.H. Wissler, Dr. M.K. Otto
Frauenhoferinstitut für Grenzflächen- und Bioverfahrenstechnik, Stuttgart
Biohydrometallurgie und Umwelt
26.01.1994

Prof. Schmidt
Bergakademie Freiberg
Geologische Entwicklung und Lagerstättenbildung im Erzgebirge
03.03.1994

Dr. S.M. Benson
Earth Sciences Division, Lawrence Berkeley Laboratory, (USA)
Environmental Remediation and Restoration Research in Lawrence Berkeley Laboratory
28.03.1994

Dr. V. Pershina
Universität Kassel, Institut für Theoretische Physik
Regularities in the Electronic Structure and Properties of the Transition Elements and their Compounds, and Influence of Relativistic Effects on them
29.03.1994

Dr. G. Buckau
TU München, Institut für Radiochemie
Komplexierung von Actiniden mit natürlichen Huminstoffen
08.04.1994

Dr. D. Read
WS Atkins Consultants Ltd., Epsom (GB)
The Mobilisation and Fixation of Uranium Series Elements in Natural Systems
14.04.1994

Dr. M. Ivanowich
AEA Technology, Analytical Science Centre, Harwell (GB)
U/Th series studies of rock/water interaction and studies of natural colloids and groundwater
21.04.1994

Dr. A. Harworth
AEA Technology, Analytical Science Centre, Harwell (GB)
Geochemical transport modelling, remediation/clean up and relevant to decomissioning and waste work
21.04.1994

Prof. I. Zvara
Flerov Laboratory of Nuclear Reactions, JINR Dubna (Russia)
Problems of the Chemical Investigation of Transactinide Elements
28.04.1994

Dr. A. Jakuschew
Flerov Laboratory of Nuclear Reactions, JINR Dubna (Russia)
Die chemische Identifizierung des Elements 106 als Eka-Wolfram
28.04.1994

Dr. Urs Baltensperger
Paul-Scherrer-Institut Villigen (Schweiz)
Atmosphärische Aerosole
29.04.1994

Dr. Luc van Loon
Paul-Scherrer-Institut Villigen (Schweiz)
Der alkalische Abbau von Zellulose: Einfluß auf die Metallspeziierung
10.05.1994

Dr. W. Hummel
Paul-Scherrer-Institut Villigen (Schweiz)
Komplexierung von Metallionen mit Huminstoffen
10.05.1994

Dr. H.-G. Löhmannsröben
TU Braunschweig
PAK, Huminstoffe, Böden - Fluoreszenzspektroskopie für die Umweltanalytik
17.06.1994

Prof. K. Fischer
TU Dresden
Die Rolle der Sauerstoffradikale in der Pflanzen- und Holzchemie
24.06.1994

Prof. H.W. Gäggeler
Paul-Scherrer-Institut Villigen (Schweiz)
Oberflächenchemische Studien mit einzelnen Atomen kurzlebiger Radionuklide
05.07.1994

Dr. Ken Czerwinski
TU München, Institut für Radiochemie
Complexation of Actinide Ions with Humic Acid
06.07.1994

Prof. D.C. Hoffman
University of California Berkeley and Glenn T. Seaborg Institute for Transactinium

Science, Lawrence Livermore National Laboratory (USA)
Naming of the Heavy Elements
08.09.1994

Dr. E. Hudson
University of California, Glenn T. Seaborg Institute for Transactinium Science, Berkeley (USA)
Uranium XANES: Theory and Application to Mineral Sorption
09.09.1994

Prof. O.Yu. Bitchaeva
Center for Biotechnologies for Nuclear and Industrial Power, St. Petersburg (Russia)
Biotechnologies for Nuclear and Toxic Waste Management and Site restoration (INTAS Program)
10.10.1994

Dr. I.N. Ryasov
Svertsov Institute of Evolutionary Morphology and Ecology of Animals, Russian Academy of Sciences, Moscow (Russia)
Radionuclide Distribution from the Chernobyl Accident in Plants and Fish
22.11.1994

Dr. Mats Skalberg
Chalmers University of Technology, Department of Nuclear Chemistry (Sweden)
Nuclear Chemistry Research at Chalmers University of Technology
02.12.1994

Prof. G. Marx
TU Berlin
Elektrochemische und radiochemische Unersuchungen der Korrosion an UO_2 und der Adsorption von Actiniden an Zementkorrosionsprodukten in Salzlaugen
07.12.1994

IV. PERSONNEL

Director

Prof. Dr. H. Nitsche

Administrative Staff

H. Pospischil
K. Wünsche

Scientific Staff

Dr. L. Baraniak
Dr. G. Bernhard
Dr. V. Brendler
Dr. M. Böttger*
Dr. M. Bubner
Dr. M. Denecke
Dr. H.-J. Engelmann
Dr. E. Förster*
Dr. H. Funke
Dr. G. Geipel
Dr. K.H. Heise
Dr. S. Hübener
Dr. P. Merker
DC C. Nebelung
Dr. T. Reich
Dr. D. Rettig
Dr. S. Taut*
Dr. M. Thieme*
Dr. H. Zänker

Technical Staff

B. Eisold
J. Falkenberg
DI(FH) H. Friedrich
Ch. Fröhlich
G. Grambole
G. Heinz
H. Heyne
B. Hiller
DI(FH) G. Hüttig
DI(FH) R. Jander
P. Kluge
DI(FH) M. Meyer
Ch. Müller
H. Neubert
A. Rumpel
R. Ruske
K. Wolf*

Graduate Students

DMin. A. Brachmann
DC A. Vahle
DC H. Moll
DC(FH) A. Otto
DC S. Pompe
DC M. Schmidt

* term contract

V. ACKNOWLEDGEMENTS

Acknowledgements for financial and material support

The Institute is part of the Forschungszentrum Rossendorf e.V., which is financed in equal parts by the Federal Republic of Germany and the Free State of Saxony.

Four projects are supported by the Bundesministerium für Bildung, Wissenschaft, Forschung und Technologie (BMBF):

- Behavior of radiotoxic pollutants in rock piles of uranium mining for the development of remediation concepts
  BMBF 02 S 7533

- Chemistry of heaviest elements
  BMBF 06 DR 101

- Development of methods for the determination of alpha active nuclides in concrete
  BMBF 02 S 7422

- Chemistry of element 106
  BMBF 06 DR 666 I (4)/1

One project was supported by Commission of the European Communities:

- An assessment of the status of activities for decommissioning of old uranium ore extraction and treatment installations, and site remediation in europe
  Contract No. FI2D-CT93-0083
  In collaboration with:
  Compagnie Générale des Matiéres Nucléaires (COGEMA), France
  Empress Nacional del Uranio, S.A. (ENUSA), Spain

In addition, the Free State of Saxony provided support for the projects:

- Chemical conversion of ^{14}C-labeled products to [^{14}C]Barium carbonate for long time disposal
  SMWK 4-7581.312/20

- Behavior of the natural daughter nuclides of radon-222 in surface relics of uranium milling and mining
  SMWK 4-7541.83-FZR/303

- Mine-water induced wood decomposition and influence of the degradation products on radionuclide speciation, sorption and migration
  SMWK 4-7541.83-FZR/402

The project:

- Migration of ^{226}Ra in sediments of the Königstein uranium mine.

  was supported in part by a contract with the WISMUT GmbH.